UNIVERSITA' VITA-SALUTE SAN RAFFAELE

CORSO DI DOTTORATO DI RICERCA

IN MEDICINA MOLECOLARE

Curriculum in Neuroscienze e Neurologia Sperimentale

EXPLOITING CELLULAR IMMUNOTHERAPY STRATEGIES FOR PARKINSON'S DISEASE

Supervisore: Vania Broccoli, PhD

Co-supervisore: Adrian Liston, Professor

Tesi di DOTTORATO di RICERCA di Alice Calderoni

matr. 022222

Ciclo di dottorato XXXVIII

SSD BIO/13 - BIOLOGIA APPLICATA

Anno Accademico 2024/2025

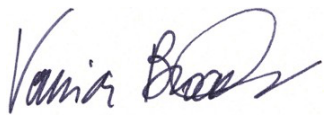

CONSULTAZIONE TESI DI DOTTORATO DI RICERCA

La sottoscritta	Alice Calderoni
Matricola	22222
nata a	Verbania (VB)
il	01/01/1997

autore della Tesi di Dottorato di Ricerca dal titolo:
Exploiting Cellular Immunotherapy Strategies for Parkinson's Disease

☒ AUTORIZZA la Consultazione della Tesi

☐ NON AUTORIZZA la Consultazione della Tesi per …… mesi a partire dalla data di sottomissione della domanda di conseguimento titolo

Poiché:

□ l'intera ricerca o parti di essa sono potenzialmente soggette a brevettabilità*;*

□ ci sono parti di Tesi che sono già state sottoposte a un editore o sono in attesa di pubblicazione*;*

□ la Tesi è finanziata da enti esterni che vantano dei diritti su di esse e sulla loro pubblicazione*.*

È fatto divieto di riprodurre, in tutto o in parte, quanto in essa contenuto

Data 27.11.2025 *Firma* Alice Calderoni

DECLARATION

Questa Tesi è stata:

- Redatta da me e non è mai stata utilizzata in alcuna precedente richiesta di laurea. Nel testo si utilizza sia il pronome "io" che "noi" in modo intercambiabile.
- Scritta in conformità alle linee guida editoriali approvate dall'Università.

È stata richiesta e ottenuta l'autorizzazione all'uso di immagini e altro materiale coperto da copyright. Per le immagini riportate nella figura 3.21 A, non è stato possibile ottenere il permesso e pertanto, sono incluse nella Tesi in base all'eccezione di "fair use" (Decreto Legislativo italiano n. 633/1941 e successive modifiche).

Tutti i risultati qui presentati sono stati ottenuti da me, ad eccezione di:

1) Le fibrille preformate di α-sinucleina sono state prodotte e fornite nell'ambito della collaborazione con il laboratorio del Professor Ronald Melki, presso l'Istituto di Biologia François Jacob.
2) Gli oligomeri e i monomeri di α-sinucleina sono stati prodotti e forniti dal laboratorio del Professor Alfonso De Simone, presso l'Università degli Studi di Napoli Federico II.
3) In collaborazione con il laboratorio della Dottoressa Monica Casucci dell'Istituto Scientifico San Raffaele di Milano, sono stati ottenuti e monitorati i topi umanizzati NSG-SGM3 utilizzati negli esperimenti *in vivo*.
4) Il gruppo della Professoressa Chiara Bonini dell'Istituto Scientifico San Raffaele di Milano ha gentilmente fornito il costrutto LV FOXP3_CD19-CAR impiegato nello studio, che è stato utilizzato come CAR di controllo contro antigene non correlato e come costrutto di partenza per clonare CAR contro la α-sinucleina.

Tutte le fonti di informazione sono state riconosciute tramite citazioni bibliografiche.

Acknowledgments

I would like to express my gratitude to my supervisor and Principal Investigator Vania Broccoli, who welcomed me into the laboratory and guided me throughout my doctoral journey.

A special thanks to the Parkinson's team, who worked closely with me and provided invaluable support. I am particularly grateful to Sharon for her critical guidance in experimental decision-making, and to Giorgia and Melania for their dedicated help and training in the *in vivo* techniques. I would also like to thank the other members of the lab for their support and collaboration.

I would like to thank my co-supervisor Professor Adrian Liston for following and advising the progression of this work.

A key collaboration was recently established with Professor Chiara Bonini's group, that kindly provided the LV FOXP3_CD19-CAR construct employed in this study. I am especially grateful to Matteo Doglio whose valuable advice and insights greatly supported the development of this work.

I also want to acknowledge the collaborators who generously provided key materials and support for the first experiments with humanized mice: Professor Ronald Melki's laboratory that produced and supplied the preformed α-synuclein fibrils; Professor Alfonso De Simone's lab that provided α-synuclein monomers and oligomers; and Dr. Monica Casucci's lab that obtained the humanized NSG-SGM3 mice used in the *in vivo* studies.

I would also like to thank animal house and Charles River staff for support on animal work, the staff of FRACTAL facility for the help in performing flow cytometry, and the staff of ALEMBIC facility for support on imaging techniques.

Furthermore, I would like to acknowledge the joint funding of my PhD fellowship from the Italian Ministry of University and Research and Università Vita-Salute San Raffaele, as well as the ongoing ERC Advanced Grant 2024 (project "CARgiver") to Dr. Vania Broccoli.

Abstract

English

Parkinson's disease (PD) is characterized by progressive neurodegeneration and chronic neuroinflammation driven by pathological α-synuclein (αSyn) accumulation. Regulatory T cells (Tregs) represent a promising therapeutic tool to restore immune homeostasis, however, their stability and antigen specificity are critical limitations. This study aimed to engineer αSyn-specific chimeric antigen receptor (CAR) Tregs for targeted immunomodulation in PD.

Initially, retroviral transduction of murine $CD4^+$ T cells to express CAR and FOXP3 transgenes was optimized. CAR transduction achieved high efficiency and determined activation and proliferation in response to αSyn *in vitro*, while FOXP3 expression levels remained unsuited for Treg reprogramming. Furthermore, due to poor murine Treg survival *in vitro* and *in vivo*, we revised our strategy and shifted to using human cells.

Human $CD4^+$ T cells were efficiently transduced with CAR and FOXP3, achieving stable generation of reprogrammed CAR Tregs. These engineered cells exhibited antigen-dependent activation and IL-10 secretion upon αSyn exposure. Polyclonal and antigen-specific suppression assays confirmed the functional suppressive phenotype of reprogrammed CAR Tregs.

To evaluate in vivo efficacy, an immunodeficient NSG mouse model overexpressing αSyn was established. This model demonstrated dopaminergic neuron loss and neuroinflammation consistent with PD pathology. Infusion of human CAR Tregs led to detectable persistence in peripheral blood but limited brain detection, highlighting challenges in either visualization or central nervous system (CNS) trafficking.

Overall, the study demonstrates the feasibility of generating functional αSyn-targeted CAR Tregs and establishes a relevant preclinical PD model for investigating their therapeutic potential. Future work will focus on improving CAR Treg CNS homing and persistence to harness their immunomodulatory capacity against neuroinflammation in PD.

Italiano

La malattia di Parkinson (MP) è caratterizzata da neurodegenerazione progressiva e neuroinfiammazione cronica guidata dall'accumulo patologico di α-sinucleina (αSyn). Le cellule T regolatorie (Treg) rappresentano una promettente strategia

terapeutica per ristabilire l'omeostasi immunitaria, tuttavia, la loro stabilità e specificità antigenica costituiscono limiti critici. Questo studio ha avuto l'obbiettivo di ingegnerizzare Treg con recettore chimerico per l'antigene (CAR) specifico per αSyn, per un'immunomodulazione mirata nella MP.

Inizialmente, è stata ottimizzata la trasduzione retrovirale di cellule T $CD4^+$ murine per l'espressione di CAR e FOXP3. La trasduzione del CAR ha raggiunto elevata efficienza e ha determinato attivazione e proliferazione in risposta ad αSyn *in vitro*, mentre i livelli di espressione di FOXP3 sono rimasti inadatti alla riprogrammazione a Treg. Oltretutto, la limitata sopravvivenza delle Treg murine *in vitro* e *in vivo* ci ha portati a cambiare il nostro approccio, utilizzando cellule umane.

Le cellule T $CD4^+$ umane sono state efficientemente trasdotte sia con CAR che FOXP3, determinando una stabile produzione di CAR Treg riprogrammate. Queste cellule ingegnerizzate hanno mostrato attivazione dipendente dall'antigene e secrezione di IL-10 a seguito di esposizione ad αSyn. Test di soppressione policlonale e antigene specifica hanno confermato la funzionalità soppressiva delle CAR Treg riprogrammate.

Per valutare l'efficacia *in vivo* è stato sviluppato un modello murino NSG immunodeficiente con sovraespressione di αSyn. Il modello ha mostrato perdita di neuroni dopaminergici e neuroinfiammazione, coerentemente con la MP. L'infusione di CAR Treg umane ha evidenziato persistenza nel sangue periferico ma limitato rilevamento a livello cerebrale, indicando difficoltà nella visualizzazione oppure nel traffico al sistema nervoso centrale (SNC).

In sintesi, lo studio dimostra la fattibilità di generare CAR Treg funzionali specifiche per l'indirizzamento verso αSyn e stabilisce un modello preclinico adeguato a indagare il loro potenziale terapeutico. Studi futuri mireranno a migliorare la migrazione al SNC e la persistenza delle CAR Treg per sfruttare la loro capacità immunomodulatoria contro la neuroinfiammazione nella MP.

Table of contents

Abbreviations

αCD3/28	anti-CD3 and anti-CD28
αSyn	α-synuclein
BBB	blood-brain barrier
BLI	bioluminescence imaging
BSA	bovine serum albumin
CAR	chimeric antigen receptor
CMV	Cytomegalovirus
CNS	central nervous system
DBS	deep brain stimulation
ELISA	enzyme-linked immunosorbent assay
FOXP3	Forkhead Box P3
GWAS	genome-wide association study
GFP	green fluorescent protein
HEK293T	human embryonic kidney 293T cells
HLA	Human leukocyte antigen
Fc	fragment crystallizable region
GFAP	Glial fibrillary acidic protein
GM-CSF	granulocyte-macrophage colony-stimulating factor
hHSCs	human hematopoietic stem cells
HRP	horseradish peroxidase
i.c.	intracerebral
i.v.	intravenous
IBA1	Ionized calcium-binding adapter molecule 1
IL	Interleukin
iPSCs	induced pluripotent stem cells
IVIS	*in vivo* imaging system
LF-LTX	Lipofectamine® LTX/PLUS™
LV	lentiviral vector
LTR	long terminal repeat
$SNCA^{A53T}$	mutant human $SNCA^{A53T}$
MAO-B	Monoamine oxidase B
MESV	murine embryonic stem cell virus
MPTP	1-methyl-4-phenyl-1,2,3,6-tetrahydropyridine
NB	nanobody
NGFR	Nerve growth factor receptor

NSG	NOD-scid IL2Rg^{null}
NSG-SGM3	NSG expressing human IL-3, GM-CSF and SCF
P-αSyn	αSyn phosphorylated on serine 129 (aggregated form)
P2A	porcine teschovirus-1 2A self-cleaving peptide
PBS	Dulbecco's Phosphate Buffered Saline
PD	Parkinson's Disease
PFFs	αSyn preformed fibrils
PGK	Phosphoglycerate kinase
PINK1	PTEN-induced kinase 1
Plat-E	Platinum-E Retroviral Packaging Cell Line
PRKN	Parkin
REM	rapid eye movement sleep
RBD	REM sleep behavior disorder
RV	retroviral vector
SCF	stem cell factor
scFv	single chain variable fragment
SN	substantia nigra
SNpc	substantia nigra pars compacta
T2A	thosea asigna virus 2A self-cleaving peptide
Tconvs	conventional CD4+ T cells
TCR-KO	T cell receptor knockout
Th1	T helper cell subset 1
Th17	T helper cell subset 17
TLR	toll-like receptor
TMB	tetramethylbenzidine
Tregs	regulatory T cells
TNF-α	tumor necrosis factor α
V_H	variable heavy domain
V_L	variable light domain

1. Introduction

1.1 Parkinson's Disease

Epidemiology

Parkinson's Disease (PD) is the second most common neurodegenerative disorder and is estimated to affect more than 10 million people worldwide, with 572 cases per 100'000 persons aged 45 years or older and an impact on 2-3% of the population older than 65 years of age (Poewe et al., 2017; Tanner & Ostrem, 2024). The incidence increases with age, reaching approximately 62 per 100'000 persons aged 45 years or older and 160 per 100'000 persons aged 65 years or older. The prevalence is higher in males than females, with a 2:1 ratio (Luo et al., 2024; Tanner & Ostrem, 2024). The number of global PD cases has been growing and is predicted to reach 25,2 million in 2050, with a 112% increase (Bloem et al., 2021; Su et al., 2025). This is suggested to be due to the increased longevity of the population together with the reduced risk of mortality from other diseases. In particular, The World Health Organization estimated that neurodegenerative disorders such as Alzheimer's Disease and PD will be the second leading cause of death by 2040, following cardiovascular disorders and surpassing cancer-related deaths. With PD being reported as the neurological disorder with the fastest growing prevalence and disability by the Global Burden of Disease Study 2015, this pathology is gaining a high priority in the research field (Bloem et al., 2021; Su et al., 2025).

Clinical manifestations

PD is a progressive degenerative pathology associated with motor symptoms typical of parkinsonism and non-motor symptoms. The non-motor symptoms are the first to arise during the prodromal phase and can precede the motor manifestations by many years (Poewe et al., 2017). These symptoms include olfactory impairment (anosmia), sleep disturbances, autonomic dysfunction, mood alterations and cognitive impairment. In particular, having idiopathic rapid eye movement (REM)-sleep behavior disorder (RBD) is a risk factor to developing PD or other α-synucleinopathies, with a conversion rate of 15-40% after 2-5 years and a striking 90% after 10 years (Poewe et al., 2017). The autonomic dysfunction includes constipation as a very early onset symptom while the mood alterations concern anxiety and depression. Cognitive impairment can arise in early-stages PD, but dementia is more common in the later stages. In presence of medication, hallucinations and paranoid behavior also occur (Poewe et al., 2017). Although the first symptoms are often non-motor, the initial step in the diagnosis of PD is the

identification of parkinsonism, defined by the presence of bradykinesia and at least one other cardinal motor feature, either rigidity or rest tremor. As the disease progresses, these symptoms significantly contribute to patient disability, with dyskinesia, gait disorders, and postural instability possibly emerging, ultimately leading to loss of independence (Hayes, 2019; Poewe et al., 2017).

Etiology

The etiology of PD is multifactorial, involving a complex interplay between genetic susceptibility, environmental exposures and aging-related cellular vulnerability. Most PD cases are sporadic, however, 10–15% of cases show a clear familial link and numerous genetic risk factors have been identified, highlighting molecular pathways involved in disease initiation (Tansey et al., 2022; Tanner & Ostrem, 2024). Mutations in the α-synuclein (αSyn) gene SNCA were among the first identified in familial PD and directly link the protein aggregation to pathogenesis. Duplications and triplications of SNCA increase αSyn expression and determine a more aggressive disease progression, supporting the central role of overproduction and misfolding of αSyn, that are central drivers of neuronal degeneration (Poewe et al., 2017; Tanner & Ostrem, 2024). Other monogenic forms implicate pathways involved in mitochondrial homeostasis and proteostasis. Mutations in Leucin-rich repeat kinase 2 (LRRK2), the G2019S variant in particular, represent the most common autosomal dominant cause of PD and are implicated in aberrant kinase activity that modulates immune signalling and autophagy (Rocha et al., 2022; Tansey et al., 2022). In recessive forms, PINK1 and PRKN (parkin) gene defects impair mitophagy, leading to accumulation of dysfunctional mitochondria and increased oxidative stress (Tansey et al., 2022). Together, these genetic insights highlight how mitochondrial integrity, protein degradation and immune regulation converge in the vulnerability of dopaminergic neurons.

Beyond monogenic causes, genome-wide association studies (GWAS) have identified dozens of common risk loci, implicating genes associated with lysosomal trafficking, lipid metabolism and immune function. For example, variants in Human leucocyte antigen (HLA), in particular HLA-DR, are linked to altered antigen presentation and microglial activation, implicating immune dysregulation in PD susceptibility (Harms et al., 2023; Tansey et al., 2022). Similarly, mutations in glucocerebrosidase (GBA) significantly elevate PD risk: reduced enzyme activity impairs lysosomal clearance of αSyn and promotes its aggregation, while secondary effects include inflammation and neuronal stress (Tansey et al., 2022). These

associations emphasize how inherited susceptibility can interface with immune pathways, proteostasis and mitochondrial dysfunction.

Environmental influences further shape PD risk. Exposure to pesticides, heavy metals and solvent has been consistently associated with higher PD incidence, likely through mitochondrial inhibition and microglial activation (Tanner & Ostrem, 2024). Age remains the most significant risk factor: aging contributes to declining mitochondrial performance, accumulation of misfolded proteins and immunosenescence — creating a permissive environment for αSyn pathology and chronic neuroinflammation (Tanner & Ostrem, 2024; Tansey et al., 2022; Terkelsen et al., 2022). Altogether, PD etiology reflects the convergence of genetic mutations, environmental exposures and age-related decline, which collectively disrupt mitochondrial function, protein clearance pathways and immune regulation.

Pathophysiology

The primary neuropathological hallmarks of PD are the neurodegeneration of dopaminergic neurons of the substantia nigra (SN) and the accumulation of aggregates of αSyn that lead to the formation of Lewi bodies. The interaction between αSyn aggregation, propagation of pathology and intrinsic neuronal vulnerability is now considered central to PD pathogenesis (Srinivasan et al., 2021; Morris et al., 2024; Watanabe et al., 2024)

αSyn is a presynaptic protein implicated in vesicle trafficking and neurotransmitter release. Under pathological conditions, it can misfold into β-sheet–rich aggregates that seed further misfolding of native αSyn (Srinivasan et al., 2021). Experimental work demonstrates that these aggregates can transfer between neurons in a prion-like manner, producing progressive pathology along anatomically connected networks (Visanji et al., 2013). Braak and colleagues proposed that αSyn pathology begins in the olfactory bulb and dorsal motor nucleus of the vagus, spreading upward to midbrain, limbic structures and cortex (Braak et al., 2003) (fig. 1.1). This model links early peripheral and brainstem involvement to prodromal non-motor features such as anosmia, constipation and REM sleep behavior disorder, while later cortical spread correlates with cognitive decline. Although many autopsy studies support this general pattern, individual variability indicates that αSyn propagation interacts with region-specific susceptibility rather than following a rigid sequence (Rietdijk et al., 2017).

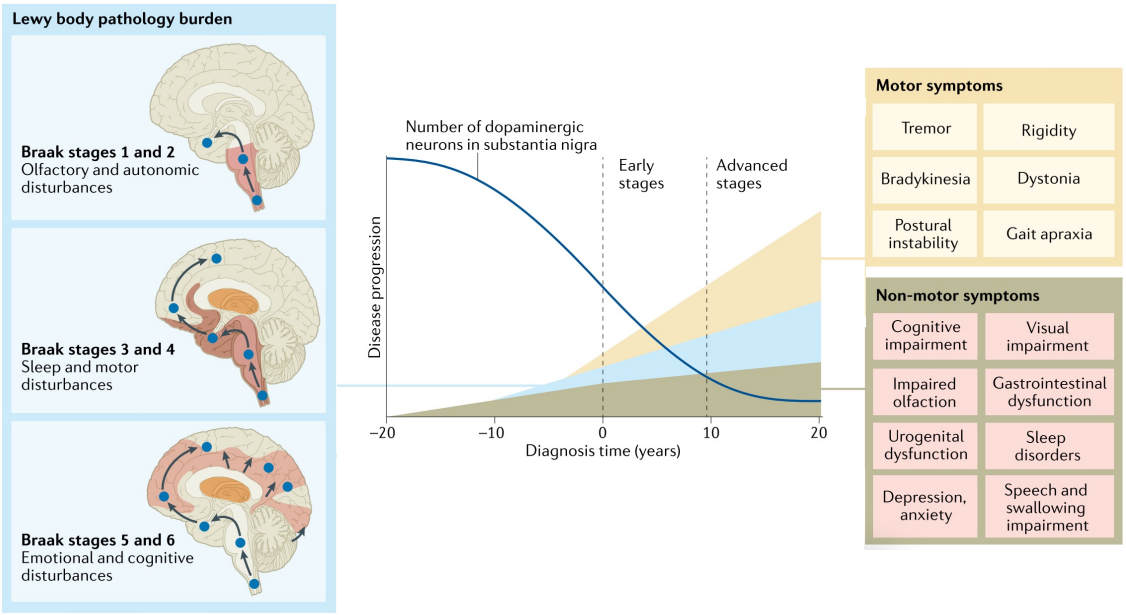

Figure 1.1. PD progression. *Schematic representation of time course of PD αSyn accumulation and symptomatic events. Adapted from Tansey et al., 2022.*

αSyn pathology can arise in different regions and consequently spread, but a common denominator for the PD development is the neurodegeneration of dopaminergic neurons of the SN, in particular in the neuromelanin-rich A9 area (Watanabe et al., 2024). For this reason, the SN is the brain region that is widely taken into consideration for the study of the pathology. SN is located in the ventral midbrain and comprises the pars compacta (SNpc) and pars reticulata. SNpc neurons produce dopamine and project to the dorsal striatum, forming the nigrostriatal pathway that modulates basal ganglia circuits governing movement control. Dopamine release facilitates the direct pathway and suppresses the indirect pathway, promoting voluntary motion (Young et al., 2023). Motor symptoms emerge only after substantial dopaminergic loss, as compensatory mechanisms initially preserve striatal function. Postmortem and imaging studies suggest that motor signs appear once about 50% of SNpc neurons and 70–80% of striatal dopamine content are lost (Srinivasan et al., 2021; Watanabe et al., 2024). PD likely arises from the combination of αSyn propagation and intrinsic neuronal fragility. Misfolded αSyn may originate in peripheral or central regions, spread trans-neuronally and induce degeneration preferentially in neurons with high metabolic and calcium stress. Aging, genetics and environmental exposures further modulate both misfolding and resilience (Rietdijk et al., 2017; Watanabe et al., 2024).

1.2 Neuroinflammation in PD

Neuroinflammation is now recognized as a central and active component of PD pathogenesis, bridging the gap between genetic predisposition, environmental exposure and progressive neuronal degeneration. Far from being a secondary reaction to dopaminergic cell death, immune dysregulation in PD represents an early and sustained pathological driver that affects both the central nervous system (CNS) and the periphery (Tansey et al., 2022). A growing body of clinical and experimental evidence reveals that PD is characterized by a systemic immune imbalance involving the interplay between innate and adaptive immunity, which correlates closely with disease severity, rate of progression and disability scores (Terkelsen et al., 2022).

Among the innate immune components, microglia play a key role in both the initiation and propagation of neuroinflammation. In healthy brains, microglia maintain homeostasis by clearing debris and monitoring neuronal activity. In PD, however, they adopt a chronically activated and pro-inflammatory phenotype driven by multiple stimuli, including aggregated αSyn, mitochondrial dysfunction and systemic inflammatory cues. Pathological αSyn can engage Toll-like receptors (TLR2 and TLR4) and other pattern recognition receptors on microglia, activating the NF-κB and NLRP3 inflammasome pathways and leading to increased production of TNF-α, IL-1β, IL-6 and reactive oxygen and nitrogen species (Tansey et al., 2022). Previous work from our laboratory using experimental models of αSyn accumulation interestingly showed that microglia exposed to prolonged αSyn burden develop phagocytic exhaustion, accumulate intracellular αSyn aggregates and undergo oxidative and mitochondrial stress, ultimately shifting into a toxic, self-sustaining pro-inflammatory state (Bido et al., 2021). Furthermore, microglial dysfunction emerges before dopaminergic neuron loss and attempts to restore microglial homeostasis further highlight their central role: targeted delivery of IL-10 to microglia significantly reduces neuroinflammation and neurodegeneration in αSyn-driven pathology (Bido et al., 2024). These findings parallel human observations in which microglia containing αSyn inclusions show lysosomal impairment and heightened oxidative stress, indicating that microglial dysregulation is a mechanistic driver of disease progression (Lee et al., 2009; Terkelsen et al., 2022).

Astrocytes also contribute to the neuroinflammatory landscape. Under chronic inflammatory stress, astrocytes adopt a reactive A1 phenotype, characterized by the release of pro-inflammatory cytokines and loss of neurotrophic support. This reactive transformation further compromises synaptic function and may perpetuate neuronal vulnerability (Lee et al., 2009; Wang et al., 2023). Meanwhile, alterations in the blood–brain barrier (BBB), detected in both animal models and patient imaging

studies, suggest that systemic inflammation can penetrate the CNS and exacerbate local immune activation (Lee et al., 2009).

Together, sustained glial activation, oxidative stress and BBB perturbation create a chemokine-rich environment that favors early recruitment of peripheral immune cells into the nigrostriatal region, providing the mechanistic link between innate and adaptive immune activation in PD (fig.1.2).

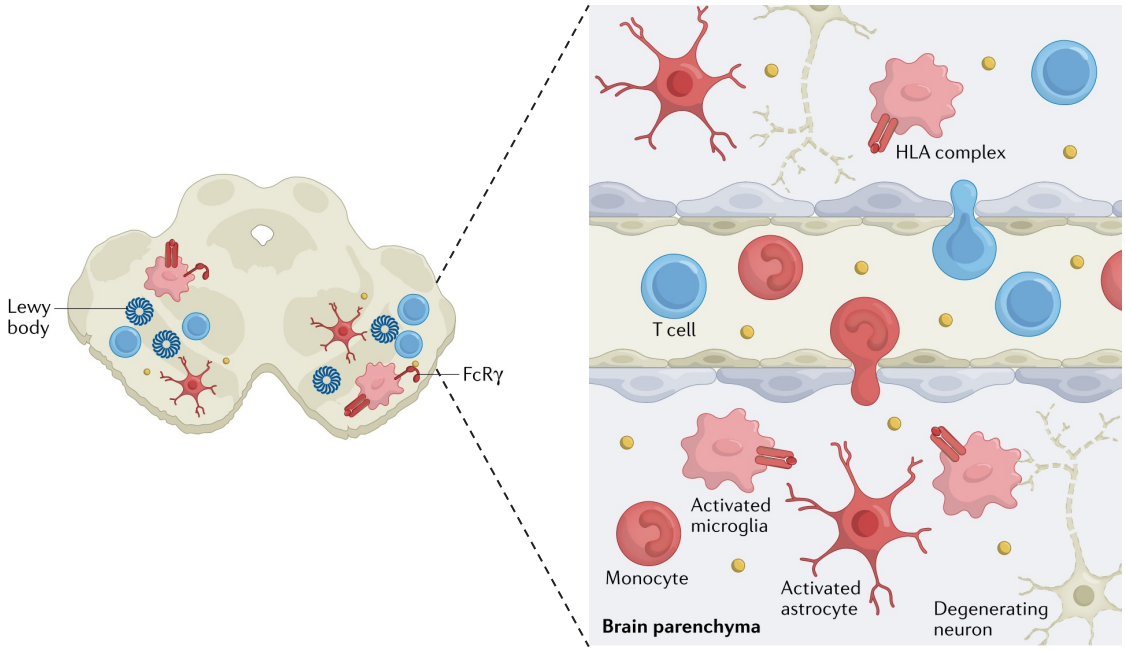

Figure 1.2. Inflammatory milieu in PD. *Schematic representation depicting activated glial cells, recruitment of peripheral immune cells and neurodegeneration into the SN. Adapted from Tansey et al., 2022.*

Peripheral immune profiling of PD patients consistently reveals alterations in circulating lymphocyte populations, with expansion of pro-inflammatory T cell subsets and reduced regulatory control. Specifically, $CD4^+$ T-helper cells exhibit a shift toward Th1 and Th17 phenotypes, producing IFN-γ and IL-17, cytokines that potentiate microglial activation and neuronal injury (Tansey et al., 2022). $CD8^+$ T cells have been detected in the substantia nigra in early stages of PD and are thought to contribute to direct cytotoxicity against dopaminergic neurons (Jordi Galiano-Landeira et al., 2020; Tansey et al., 2022). Longitudinal analyses demonstrate that these adaptive immune alterations correlate with higher pathological scores and faster motor decline, suggesting that peripheral immune imbalance mirrors and possibly drives CNS pathology (Terkelsen et al., 2022).

Regulatory T cells (Tregs), which play a crucial role in maintaining immune tolerance and suppressing excessive inflammation, appear quantitatively and

functionally compromised in PD. Several studies report reduced circulating Tregs frequencies and impaired suppressive function, leading to diminished control over effector T cell activity and heightened inflammatory tone (Harms et al., 2023). Experimental data further suggest that restoring Tregs function, either through ex vivo expansion or pharmacological enhancement, can attenuate neuroinflammatory markers and provide neuroprotection in preclinical PD models (Tansey et al., 2022). This evidence positions Tregs dysfunction not as a bystander effect but as a pivotal element of the immunopathogenic cascade in PD.

Overall, neuroinflammation in PD is best conceptualized as a multidimensional immune imbalance that involves both innate and adaptive arms of the immune system. Microglial overactivation initiates a self-reinforcing inflammatory loop, while the loss of Tregs-mediated regulation and expansion of pro-inflammatory T cell subsets sustain chronic immune stress. These immune perturbations are not only correlated with neurodegeneration but may also serve as biomarkers of disease activity and potential targets for therapeutic intervention. Understanding how immune imbalance evolves from early prodromal stages to advanced disease offers critical insight for the development of precision immunomodulatory therapies aimed at restoring immune homeostasis and protecting dopaminergic neurons (Harms et al., 2023; Tansey et al., 2022; Terkelsen et al., 2022).

Although neuroinflammation is recognized as a central contributor to PD pathogenesis, existing pharmacological approaches lack antigen specificity and long-term efficacy in modulating the immune milieu. This unmet need underscores the potential of engineered cellular therapies that can selectively suppress pathological immune responses, supporting the rationale for this research on αSyn–specific CAR Tregs.

Immunomodulatory and Anti-inflammatory Therapeutic Strategies in Parkinson's Disease

To date, there are no disease-modifying therapies for PD. Current treatments such as levodopa, dopamine agonists, MAO-B inhibitors, and deep brain stimulation (DBS) are primarily aimed at symptomatic relief rather than halting neurodegeneration (Poewe et al., 2017). Levodopa remains the gold-standard pharmacological treatment for motor symptoms, while DBS is used in advanced stages to improve motor fluctuations, but neither approach impacts the underlying pathological processes including neuroinflammation (Poewe et al., 2017; Tansey et al., 2022).

Recent advances in understanding PD pathophysiology have identified neuroinflammation as a key driver of disease progression, with microglial activation,

pro-inflammatory cytokine release, and adaptive immune dysregulation playing central roles (Tansey et al., 2022). This has stimulated the development of immunomodulatory and anti-inflammatory strategies aimed at targeting these mechanisms. Several clinical trials have investigated therapeutic interventions that specifically modulate immune responses in PD. Active immunization approaches using vaccines targeting αSyn have been tested for safety and immunogenicity, like AFFITOPE PD01A and PD03A vaccines in Phase I trials, showing induction of antibody responses capable of reducing αSyn oligomers present in the cerebrospinal fluid, with an acceptable safety profile (Alfaidi et al., 2025). Monoclonal antibodies such as Prasinezumab have undergone Phase II trials (PASADENA study) in early PD patients, demonstrating favorable safety and some exploratory slowing of motor decline in subgroups, although they did not meet primary efficacy endpoints (Xiao & Tan, 2025). Other immunomodulatory agents explored include NSAIDs and biologics targeting pro-inflammatory cytokines such as TNF-α, although results have been mixed and larger trials are underway to rigorously assess their efficacy (Vega-Angeles et al., 2024).

Moreover, approaches aiming to Tregs function show promise, with early-phase trials investigating the expansion and reinfusion of autologous Tregs in PD patients (Thome et al., 2021). These strategies aim to restore immune tolerance and limit pathological immune activation while preserving overall immune competence.

Ongoing clinical trials are increasingly focused on early intervention with biomarker-guided patient selection to maximize potential benefits. Although no immunomodulatory therapy has yet achieved definitive disease modification in PD, these approaches represent an important frontier for altering disease trajectory by targeting neuroinflammation and immune dysfunction.

1.3 Treg cell therapies for Parkinson's Disease

Treg cells have attracted substantial interest as therapeutic tool to rebalance the immune system in PD, because they have the potential to suppress excessive inflammation and promote tissue homeostasis in contrast to chronic immune activation. In particular, Treg cells exert their suppressive activity through several non-redundant mechanisms, including the secretion of immunomodulatory cytokines (IL-10, TGF-β and IL-35), metabolic disruption through IL-2 consumption and cAMP transfer, modulation of antigen-presenting cells via CTLA-4-dependent mechanisms and cytolysis of target immune cells (Vignali et al., 2008).

Recent immunological studies have revealed that subsets of PD patients exhibit αSyn–specific T cell responses, suggesting a breakdown of immune tolerance to this neuronal antigen. Circulating αSyn reactive $CD4^+$ and $CD8^+$ T cells have been detected in early and prodromal PD, producing IFN-γ and IL-17 upon exposure to α-synuclein peptides, particularly those phosphorylated at Ser129 (Sulzer et al., 2017). These antigen-specific responses are strongest in recently diagnosed patients and decline as the disease progresses, suggesting they may contribute to early pathogenic mechanisms rather than representing secondary phenomena (Lindestam Arlehamn et al., 2020). This evidence provides a strong immunological rationale for the development of αSyn–specific Treg-based therapies, aimed at restoring antigen-specific tolerance and selectively suppressing pathogenic T cell responses while preserving systemic immunity.

Preclinical studies have provided mechanistic support for the neuroprotective role of Tregs. Depletion of Tregs in PD models accelerates neurodegeneration, confirming their key role in maintaining CNS immune homeostasis (Li et al., 2021). Adoptive transfer of $CD4^+CD25^+$ Tregs mitigates dopaminergic neuron loss and decreases microglial activation and lymphocyte infiltration in MPTP toxin-based models (Reynolds et al., 2007, 2010; Huang et al., 2020; Li et al., 2021;) and in a mouse model of αSyn accumulation (Badr et al., 2022), indicating that Tregs can reduce both innate immune effector functions and downstream neuronal injury. More recent work has shown that antigen-specific Tregs can be effective: αSyn-specific Tregs decreased αSyn aggregation, suppressed pro-inflammatory microglial states and improved motor outcomes in transgenic mouse models, supporting the rationale for targeted Treg strategies (S. Y. Park et al., 2023).

Translationally, approaches to harness Tregs include pharmacologic expansion of endogenous Tregs (Markovic et al., 2022), *ex vivo* expansion and autologous reinfusion of Tregs (Thome et al., 2021) and the engineering of stabilized or antigen-specific Treg products (Olson et al., 2023). Notably, Thome and colleagues demonstrated that *ex vivo* expansion of Tregs derived from PD patients restores their suppressive phenotype, providing proof of concept that autologous cell therapy is feasible and capable of correcting intrinsic Treg defects observed in PD patients (Thome et al., 2021).

Early clinical explorations of Treg-based interventions in PD have so far been limited to adjunctive combination approaches rather than stand-alone Treg therapies. A pilot study evaluated the co-transplantation of autologous Tregs with mesenchymal stem cells (MSCs) in PD patients undergoing intracerebral MSC grafting (T. Y. Park et al., 2023). In this setting, Tregs were administered not as a long-term

immunomodulatory therapy but rather as a short-term adjuvant to dampen needle injury–induced neuroinflammation and to transiently promote a more tolerogenic environment at the graft site. The study confirmed feasibility and safety, furthermore peripheral immune profiling indicated transient modulation consistent with Treg activation and reduced inflammatory markers.

These strategies are attractive because they aim to re-establish immune regulation without broadly suppressing host defense. However, several practical and biological challenges remain: (I) maintaining FOXP3 stability and suppressive function after reinfusion, particularly within the pro-oxidant, cytokine-rich milieu of the PD brain; (II) achieving efficient trafficking and retention of therapeutic Tregs at inflamed nigrostriatal sites across the BBB; and (III) defining antigenic specificity that maximizes on-target benefit while minimizing off-target immune effects. These issues are underscored by mechanistic studies showing plasticity of Tregs under inflammatory conditions and by the variable results of Treg-boosting interventions across neurologic diseases (Olson et al., 2023).

In summary, preclinical data strongly support the concept that restoring Treg number or function can attenuate neuroinflammation and protect dopaminergic neurons, while early translational studies demonstrate the feasibility of ex-vivo correction of patient-derived Tregs. Moving forward, combining antigen specificity, engineering for phenotypic stability and delivery strategies that enhance CNS homing will be pivotal to translate Treg therapy from promising preclinical results into effective clinical interventions for PD.

1.4 Chimeric Antigen Receptor (CAR) and CAR Treg Cell Therapies

Building upon evidence that Tregs are central modulators of neuroinflammation, engineered Treg platforms seek to combine antigen specificity with durable suppressive function to deliver localized immunoregulation within inflamed tissues. The chimeric antigen receptor (CAR) concept originally developed for cytotoxic T cells in oncology has been adapted for Tregs, allowing the generation of Tregs that recognize a chosen antigen and concentrate suppressive activity at disease sites rather than systemically. Compared with polyclonal Treg infusion, CAR Tregs offer the theoretical advantages of higher on-target potency, reduced off-target immunosuppression and prolonged residence at antigen-expressing loci (Arjomandnejad et al., 2022). At the molecular level, CARs comprise an extracellular antigen-binding domain, a hinge element, a transmembrane region and intracellular signaling modules. For CAR Tregs in particular, CD28 and CD3ζ are the most

commonly used signaling domains, since the use of CD28 signaling domain had been shown to be optimal for Treg phenotype and function (Boroughs et al., 2019).

Preclinical work focusing on CSN pathologies provides proof of principle that engineered Tregs can reach the desired compartment and modulate brain inflammation. In particular, various studies focused on the employment of CAR Tregs in multiple sclerosis (MS) using experimental autoimmune encephalomyelitis (EAE) mouse models (De et al., 2020; Fransson et al., 2012; Frikeche et al., 2024; Moorman et al., 2023). These studies have shown the potential of CAR Tregs to reach the CNS and determine immunomodulation in the site of pathology, with consequent protection from neurodegeneration and disease amelioration. These studies confirm that CAR Tregs can re-establish local tolerance in neuroinflammatory contexts, though the CNS presents specific obstacles, regarding in particular trafficking to the tissue, across the BBB.

A primary translational challenge is phenotypic stability of Tregs within the pro-inflammatory milieu characteristic of neurodegeneration. FOXP3 is the master transcription factor of Treg identity and loss or instability of FOXP3 expression is associated with loss of suppressive capacity and, in some contexts, conversion to inflammatory effector cells. Several engineering strategies have been developed to address this issue. In particular, co-expression of FOXP3 together with CAR constructs can stabilize CAR Treg products: FOXP3-coexpressing CAR Tregs retain FOXP3 expression and suppressive function under IL-2-deficient and inflammatory conditions and demonstrate improved efficacy and safety in preclinical models (Doglio et al., 2024; Henschel et al., 2023; McGovern et al., 2022). Furthermore, it has been shown that overexpression of FOXP3 through lentiviral vectors (LV) can not only stabilize Treg phenotype, but also reprogram conventional $CD4^+$ T cells (Tconvs) producing potent and stable suppressive cells, expanding to the possibility to use this more abundant population for translational purposes (Aarts-Riemens et al., 2008; Allan et al., 2008; Bacchetta et al., 2020). Collectively, these data support two complementary translational approaches: incorporate FOXP3 stabilization into CAR Treg constructs to preserve lineage fidelity after infusion into an inflammatory niche and convert bulk $CD4^+$ populations into stable regulatory cells to increase starting material and manufacturing yield.

Building upon the evidence that PD involves chronic and self-sustaining immune dysregulation, innovative strategies are now focusing on targeted immunomodulation rather than broad immunosuppression. Among these, CAR Treg therapy emerges as a rational evolution of cellular engineering technologies. By combining the antigen specificity of chimeric receptors with the suppressive function of regulatory T cells,

CAR Tregs have the potential to deliver localized, sustained and antigen-directed immunoregulation within the inflamed nigrostriatal environment. In PD, where αSyn aggregation acts as both a trigger and a perpetuator of neuroinflammation, targeting this antigen represents a particularly compelling strategy.

In healthy individuals, αSyn predominantly exists as monomers or low-level oligomers localized intracellularly, notably within presynaptic terminals in the brain, the enteric nervous system, and peripheral nerve fibers in skin (Srinivasan et al., 2021). Soluble monomeric αSyn is also detectable in blood plasma and erythrocytes (Jiménez-Jiménez et al., 2023).

In PD, pathological αSyn aggregates like oligomers and fibrils accumulate intracellularly within neurons forming Lewy bodies and Lewy neurites, especially in the substantia nigra and related brain regions (Kalia et al., 2013). These aggregated species can be released extracellularly following neuronal injury or death, creating extracellular pools of fibrillary αSyn in brain interstitial fluid and cerebrospinal fluid that contribute both to prion-like propagation of pathology and to immune activation (Kalia et al., 2013). Peripheral fibrillary αSyn deposits have also been identified intracellularly in autonomic nerve fibers of the gut and skin in PD patients, though extracellular release appears less prevalent than in the brain (Domingues et al., 2022).

Targeting these extracellular αSyn species with CAR Tregs offers a precision immunotherapy approach. By focusing on fibrillary and aggregated conformations concentrated in inflamed, neurodegenerating brain regions, CAR Tregs engineered to recognize αSyn pathological accumulation could theoretically home to sites of protein aggregation, suppress local inflammatory circuits and protect dopaminergic neurons by re-establishing immune tolerance. Furthermore, FOXP3 overexpression strategies and dual CAR–*FOXP3* constructs can reinforce Treg lineage stability, overcoming one of the key obstacles that limits Treg-based interventions. The intersection of synthetic biology, antigen engineering and neuroimmunology therefore defines a new translational direction for PD treatment, one that addresses the root immunopathology rather than its downstream consequences.

Taken together, these insights position CAR Treg therapy as a highly innovative and mechanistically grounded approach to modulate the neuroimmune environment in PD. The experimental work described in this thesis aims to explore the feasibility of generating stable and antigen-specific CAR Treg cells directed against αSyn, laying the foundation for a new class of precision immunotherapies for this neurodegenerative disorder.

2. Aim of the Project

The overarching goal of this project is to develop and functionally validate a CAR Treg-based immunotherapy targeting αSyn in PD. This work aims to establish a translational platform for antigen-specific, durable and localized immunomodulation of neuroinflammation, which is a key pathogenic component of PD.

Parkinson's disease is now understood not merely as a disorder of dopaminergic loss but as a condition involving chronic dysregulation of both the innate and adaptive immune systems. Microglial activation, persistent cytokine release and infiltration of αSyn-reactive T cells sustain a self-perpetuating cycle of neuroinflammation that accelerates neuronal degeneration. While conventional pharmacologic and cellular interventions can transiently dampen inflammation, they lack antigen specificity, show limited persistence and fail to achieve long-term immune tolerance. Similarly, adoptive transfer of ex vivo–expanded Tregs has shown neuroprotective potential in preclinical PD models, yet their clinical translation can be limited by major challenges, including FOXP3 instability in inflammatory environments, loss of suppressive capacity and limitations based on lack of antigen specificity. Therefore, developing a strategy that stabilizes Treg lineage identity and enhances their precision in recognizing disease-specific antigens is a critical next step toward durable immune modulation in PD.

Engineering αSyn-specific CAR Tregs provides a rational solution to these challenges. By combining the antigen-recognition capability of a CAR with stabilized FOXP3 expression, this approach enables the generation of regulatory cells that are both disease-targeted and functionally stable, capable of exerting localized immune suppression within the inflamed nigrostriatal microenvironment with the final goal to exert neuroprotection (fig. 2.1). Conceptually, this strategy aligns with the ongoing evolution of precision immunotherapy, which has revolutionized cancer treatment and is now being adapted to immune-mediated neurological diseases.

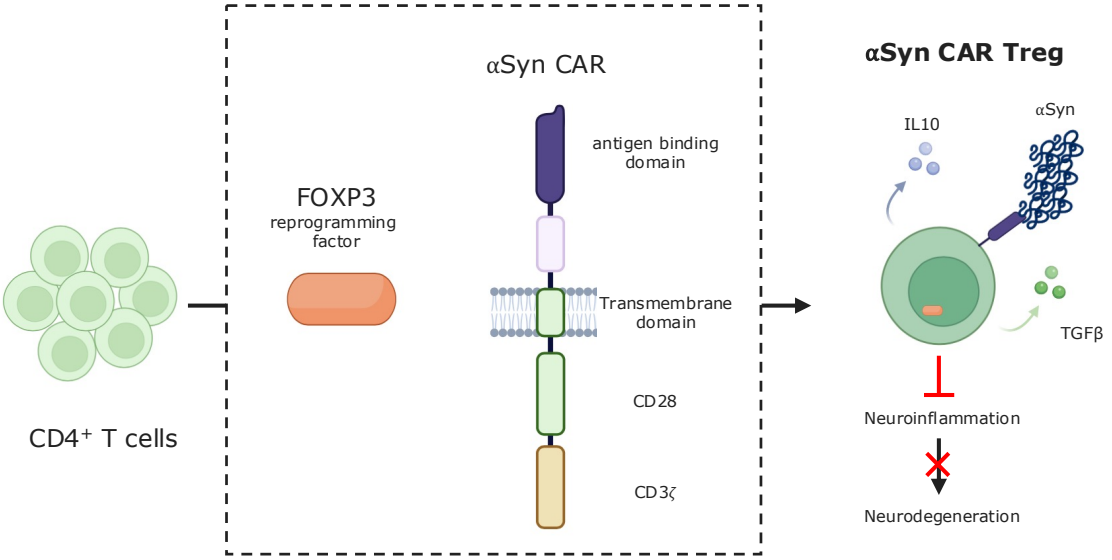

***Figure 2.1. Rationale of the αSyn CAR Treg approach in PD**. Schematic representation of bulk CD4⁺cells reprogramming by FOXP3 and αSyn directed CAR in order to target neuroinflammation in the site of pathology where αSyn is accumulated. Image created using Biorender.*

The specific objectives of this project are to:

1. Efficiently generate and characterize αSyn-specific CAR Tregs by genetic engineering of CD4⁺ T cells.
2. Assess their antigen-dependent activation and suppressive function *in vitro* to confirm dual CAR and FOXP3 activity.
3. Establish and optimize a preclinical model suitable for *in vivo* testing of human CAR Tregs, enabling the evaluation of their trafficking, persistence and neuroprotective capacity in the context of αSyn-driven pathology.

Ultimately, this work seeks to provide proof of concept that CAR Tregs can be rationally engineered to target pathological immune responses in PD, paving the way for the development of next-generation, antigen-specific cellular immunotherapies for neurodegenerative diseases.

2.1 Engineering CD4⁺ T Cells into αSyn-specific CAR Tregs

To achieve antigen-specific immune regulation, we employed a dual genetic engineering strategy to reprogram total CD4⁺ cells into αSyn-specific CAR Tregs.

In particular, we used newly designed CAR molecules based on a second-generation CAR structure with CD28 and CD3ζ signaling domains. Two different αSyn binding domains were used: the NbSyn87 nanobody (NB)(Guilliams et al., 2013), and a newly designed scFv derived from the 306C7B3 antibody (Düchs et al., 2023). We engineered cells with both the anti-αSyn CAR construct and the FOXP3

transcription factor by viral transduction, either via co-delivery within a single vector or through independent transductions.

To facilitate the detection and selection of successfully transduced cells, modified nerve growth factor receptor (NGFR) sequences were incorporated into the constructs. This allowed us to both verify CAR expression on the cell surface and magnetically isolate $NGFR^+$ cells for downstream analyses. The resulting engineered populations were then characterized in terms of phenotype, transgene expression and functional responsiveness to disease-relevant antigens.

This engineering strategy addresses two translational bottlenecks: the scarcity of stable, antigen-specific Tregs obtainable from peripheral blood and the need to preserve suppressive function under pro-inflammatory stress. The combination of CAR specificity and FOXP3 overexpression is designed to ensure antigen-driven activation and resilience against lineage instability, even in pro-inflammatory environments typical of the PD brain.

2.2 In Vitro Functional Validation

To confirm the functionality of the engineered CAR Tregs, we performed *in vitro* assays to evaluate both their antigen-dependent activation and suppressive capacity.

CAR-expressing T cells were exposed to αSyn antigens such as pre-formed fibrils (PFF), oligomers and monomers to assess antigen-dependent activation. Quantification of activation dynamics was analyzed based on the proliferative response, measured through flow cytometric analysis of proliferation dyes, and IL-10 secretion upon activation of Tregs was measured trough enzyme-linked immunosorbent assay (ELISA).

To validate the FOXP3-driven suppressive program, we conducted Treg suppression assays, co-culturing CAR Tregs with responder Tconvs under both polyclonal stimulation and antigen-specific conditions. Suppression of responder T cells proliferation served as key readout of CAR Treg functionality. Together, these assays establish whether αSyn-specific CAR Tregs can simultaneously sense disease-relevant antigens and exert targeted immunomodulation.

2.3 In Vivo Preliminary Testing

The long-term goal of this project is to evaluate the immunomodulatory and neuroprotective potential of αSyn-specific CAR Tregs in a PD mouse model based on the overexpression of mutant human $SNCA^{A53T}$ by LV delivery.

To establish a suitable preclinical model, we initially optimized a model based on αSyn overexpression into the SN of non-humanized[1] NSG mice, recapitulating key features of αSyn accumulation and neurodegeneration. While this model enabled initial CAR Treg infusion experiments, its lack of a functional human immune system limits the assessment of immune cell interactions.

Therefore, further experiments will be performed to advance this platform by utilizing humanized NSG-SGM3 mice that, having a multi-lineage human immune system, can more effectively recapitulate human immune infiltration and enable relevant immune interactions. This model will facilitate evaluation of CAR Treg trafficking, persistence, and immunomodulatory efficacy in a clinically relevant context.

[1] In this thesis, "humanization" refers specifically to the engraftment and functional reconstitution of a human immune system in immunodeficient mice through transplantation of human hematopoietic stem cells. This term does not refer to genetically modified mouse strains such as NSG-SGM3, which express human cytokines but are not necessarily subjected to the immune reconstitution process.

3. Results

3.1. Murine T cells

3.1.1 Engineering CAR Treg cells

As a first step, we established a procedure for isolation of primary $CD4^+$ T cells from mouse spleens. The purity of the $CD4^+$ T cell suspension obtained was assessed by flow cytometry (fig. 3.1).

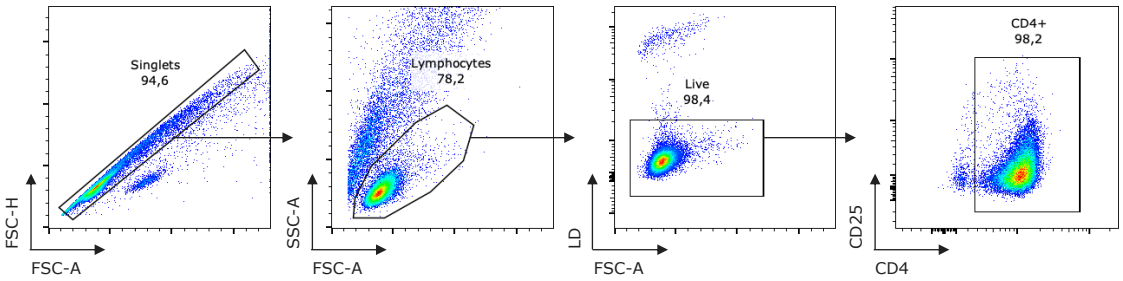

Figure 3.1. Primary $CD4^+$ T cell purity. *Flow cytometry analysis of the cell suspension obtained after $CD4^+$ isolation with magnetic beads. The gating strategy is based on single cells, lymphocytes, live cells and $CD4^+$ cells. FSC-A=Forward Scatter-Area, SSC-A=Side Scatter-Area, LD=live/dead staining.*

Then, it was essential to design constructs for the expression of the transgenes of interest: (I) *Foxp3* for the reprogramming of $CD4^+$ T cells into Tregs, (II) the anti-αSyn CAR to determine antigen specificity, and (III) NGFR as a marker of transduction. In particular, in this first part of the work we focused on a second-generation CAR embedding the NbSyn87 NB (Guilliams et al., 2013) (fig. 3.2 A).

The optimal strategy to deliver these transgenes would have been the use of a single retroviral vector (RV), therefore, we designed the construct RV *Foxp3*-PGK-CAR_NGFR (fig. 3.2 A) to enable their simultaneous expression. We exploited the 5' long terminal repeat (LTR) as a promoter driving the expression of *Foxp3* followed by a human phosphoglycerate kinase (PGK) promoter controlling the expression of a bicistronic element consisting of the CAR, P2A (porcine teschovirus-1 2A) self-cleaving peptide, and NGFR (CAR_NGFR). In order to test the functionality of the CAR alone, we also developed a vector RV CAR_NGFR (fig. 3.2 B) containing only the bicistronic element previously described.

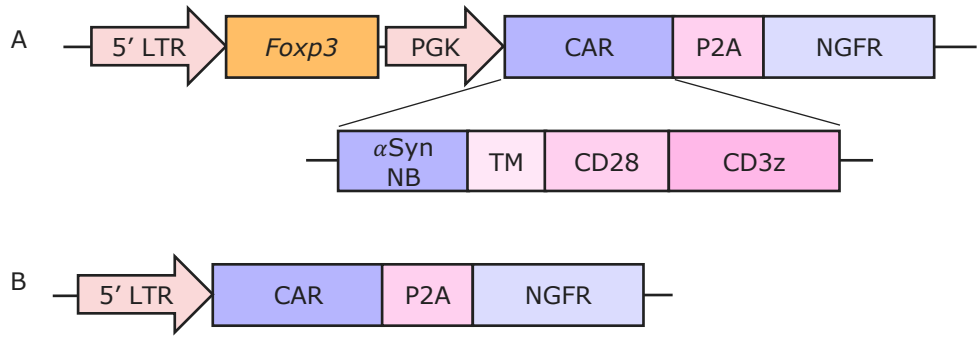

Figure 3.2. RV constructs. *Schematic representation of (A) RV Foxp3-PGK-CAR_NGFR with detail of CAR structure, and (B) RV CAR_NGFR.*

The production of RV particles and the transduction of primary murine T cells required several optimization steps. In particular, we tested different RV production methods, using either Phoenix-ECO or Plat-E cell lines, and compared transfection mediated by $CaCl_2$ or by Lipofectamine® LTX/PLUS™ (LF-LTX). Among these conditions, only Plat-E cells transfected with LF-LTX resulted in efficient RV production and, in turn, efficient $CD4^+$ T cell transduction.

Regarding $CD4^+$ T cells transduction, a step-wise optimization was performed, during which we implemented a series of adjustments to obtain efficient transduction. The final optimized process exploits double spinoculation on Retronectin®-coated plates using RV supernatant incubated with LF-LTX. In particular, Retronectin® interacts with both viral capsids and cell membranes, promoting close contact between RV and cells, while cationic lipid reagents as LF-LTX are known to enhance transduction efficiency by minimizing electrostatic repulsion between virions and negatively charged cell surfaces (Kaygisiz & Synatschke, 2020).

Transduction with RV *Foxp3*-PGK-CAR_NGFR did not determine the detection of $FOXP3^+NGFR^+$ double positive cells (fig. 3.3 A), but RV CAR_NGFR determined a transduction efficiency of 76,02 ± 6,82% based on the percentage of $NGFR^+$ cells detected by flow cytometry (fig. 3.3 B-C). To verify whether the RV *Foxp3*-PGK-CAR_NGFR construct could indeed be transcribed and expressed, we analyzed NGFR and FOXP3 expression in human embryonic kidney 293T cells (HEK293T) cells after LF-LTX-mediated transfection to deliver the RV plasmid, confirming the expression of both transgenes (fig. 3.3 D). Therefore, we attributed the lack of transgene expression to impaired RV packaging efficiency due to the construct's large size (>5000 bp), as inserts above 3000 bp are known to substantially reduce packaging performance despite an upper capacity of 8000 bp. We attempted to increase viral titer by concentrating the RV *Foxp3*-PGK-CAR_NGFR supernatant up to tenfold using RetroX™ Concentrator, but without observable improvement (fig. 3.3 A).

Therefore, we concluded that RV CAR_NGFR allows efficient T cell transduction and that achieving delivery of both CAR and FOXP3 transgenes would require an alternative strategy rather than a single construct.

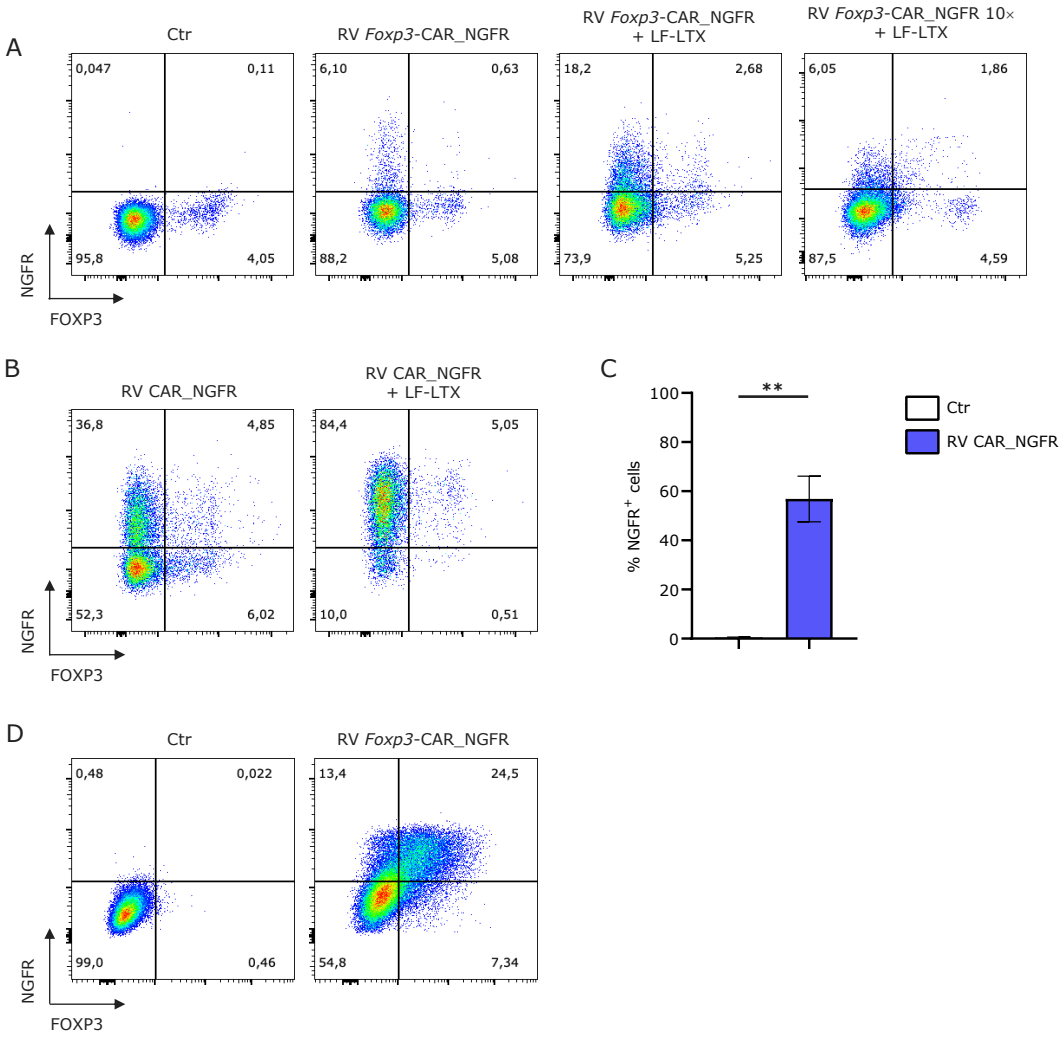

Figure 3.3. Murine T cells transduction. *(A-B) Levels of expression of FOXP3 and NGFR based on flow cytometry after RV transduction of CD4⁺ T cells with (A) RV Foxp3-PGK-CAR_NGFR alone, with LF-LTX or 10× concentrated; or (B) RV CAR_NGFR alone or with LF-LTX. (C) Quantification of NGFR⁺ cells following transfection with RV CAR_NGFR with the aid of LF-LTX. (D) Transgenes expression levels following LF-LTX-mediated transduction of HEK293T cells with RV Foxp3-PGK-CAR_NGFR compared to untransfected cells. Ctr=untransduced control. Statistical analysis with unpaired T test with Welch's correction method, **p-value = 0.008, n=5.*

3.1.2 CAR_NGFR-transduced cells respond to αSyn in vitro

Since optimal transduction was achieved with RV CAR_NGFR, before addressing the FOXP3-mediated reprogramming of CD4⁺ T cells into Tregs, we first tested the ability of our CAR to recognize αSyn. For doing so, we optimized an activation assay monitoring CAR T cells proliferation upon stimulation, using a fluorescent proliferation

dye as a readout and comparing their response to the one of untransduced cells. CAR T cells were exposed to different antigens and showed a significant ability to proliferate in response to αSyn preformed fibrils (PFFs), compared to conditions without stimuli or in presence of bovine serum albumin (BSA) as control unrelated antigen. No significant difference was observed in the comparison to the positive control, represented by cells cultured with a standard polyclonal stimulus consisting of anti-CD3 and anti-CD28 (αCD3/28) antibodies (fig. 3.4 A-B). Furthermore, control untransduced cells did not respond to PFFs. We also performed a dose-response analysis with serial dilution of PFFs. We observed that CAR T cells responded to all concentrations, although with reduced magnitude at 1nM PFFs (fig. 3.4 C-D).

These results demonstrate that this newly designed CAR confers αSyn specificity to engineered $CD4^+$ T cells and elicits a cellular response at nanomolar concentrations of PFFs.

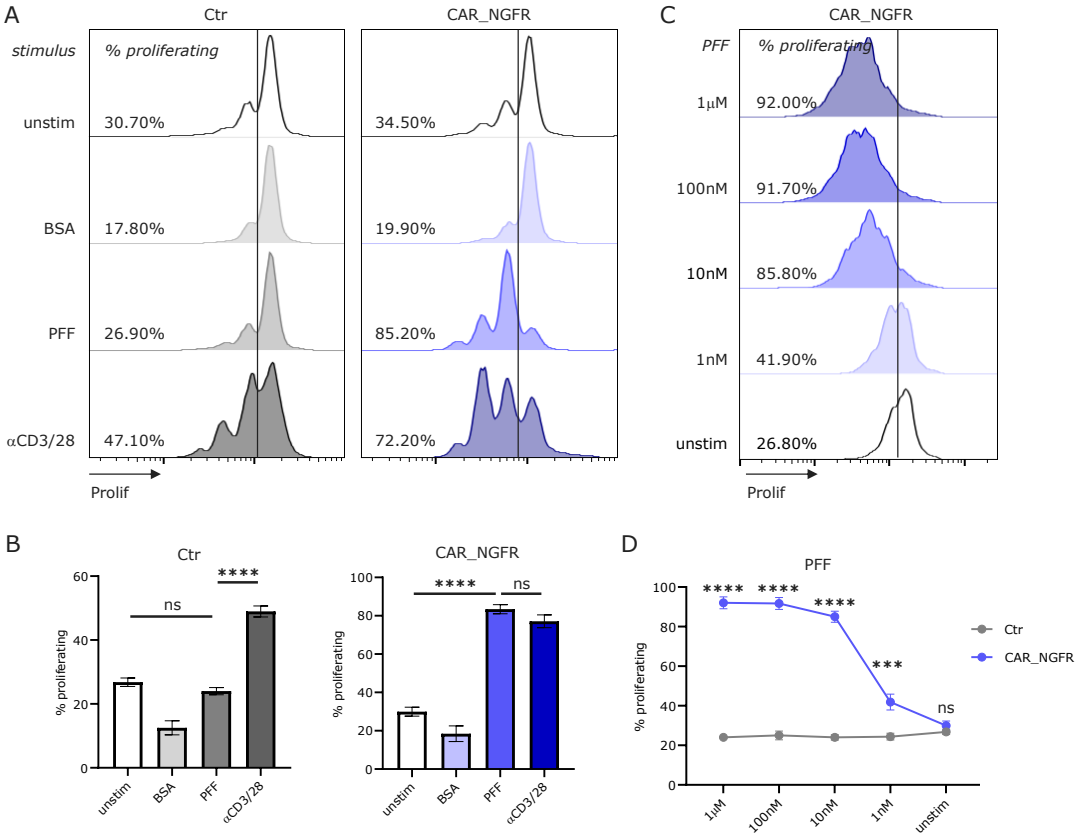

Figure 3.4. CAR-mediated activation. *(A-B) Activation assay of CAR T cells cultured in absence of stimulus and with BSA, PFFs or αCD3/28 compared to control untransduced cells. (A) Gating of proliferating cells based on proliferation dye fluorescence from flow cytometric analysis and (B) quantification of percentage of proliferating cells. Statistical analysis performed with ordinary one-way ANOVA and Tukey's multiple comparisons test, n=4. (C-D) Response of CAR T cells to different concentrations of PFFs in comparison to control untransduced cells (C) visualized as flow cytometry readout and (D) quantification of percentage of proliferating cells compared to untransduced control. Analyzed with two-way ANOVA and Sidak's multiple comparisons test; n=3. ***p-value < 0.001; ****p-value < 0.0001; Prolif=proliferation dye.*

3.1.3 In vitro suppression assays did not demonstrate functional suppression

To be able to transduce cells with both *Foxp3* and the CAR, we designed a vector carrying *Foxp3* alone (RV *Foxp3*) and determined its efficiency of transduction alone and in combination with RV CAR_NGFR using flow cytometry (fig. 3.5 A-B). We obtained 45.75 ± 3.21% of $FOXP3^+$ cells transduced with RV *Foxp3* alone, and 9.15 ± 3.77% of $NGFR^+FOXP3^+$ double positive cells with co-transduction. The dual infection resulted in a non-significant production of $NGFR^+FOXP3^+$ double-positive cells compared to untransduced controls (fig. 3.5 B).

The probabilistic nature of double infection already limits the frequency of double-positive cells relative to single infections, and this effect is further exacerbated by the constraints of RV transduction. In particular, because the procedure relies on using the supernatant from RV production and culture plates can accommodate only limited volumes, the amount of each viral preparation used for co-transduction is necessarily reduced to half of that used in single infections, substantially lowering the number of infectious viral units effectively used.

Since our objective was to obtain T cells that carry both transgenes, this result was not satisfactory. In particular, a low percentage of $FOXP3^+$ cells highlights the presence of non-reprogrammed Tconvs within the culture. This indicates that the cell population is heterogeneous and includes proinflammatory cells, which is not optimal for therapeutic purposes. Furthermore, under this experimental setting, we would have been able to isolate NGFR-transduced cells by magnetic selection, but not *Foxp3*-transduced cells, making this strategy irrelevant for addressing the issue.

To increase *Foxp3* transduction we once more utilized RetroX™ Concentrator to be able to use a higher RV titer for the double infection, but this did not determine a significant improvement in the number of double-positive cells. We also introduced an additional CMV promoter in the construct to boost the expression of *FoxP3*, but it determined an even lower expression of the protein (not shown).

We then produced another construct carrying a bicistronic element containing *Foxp3* and NGFR separated by a P2A element (RV *Foxp3*_NGFR), and obtained 34.86 ± 10.97% $NGFR^+FOXP3^+$ cells after transduction (fig. 3.5 C). This strategy allows to magnetically select $NGFR^+$ cells to isolate transduced cells and obtain the highest amount of $FOXP3^+$ cells.

The development of this construct allows us to adopt an approach based on two separate vectors for *Foxp3* and the CAR, both containing NGFR. This strategy would enable enrichment of $FOXP3^+$ cells—crucial for achieving the desired regulatory phenotype—while inevitably also enriching the CAR^+FOXP3^- population. Although not an optimal configuration, it remains preferable to the previous approach, in which only the CAR construct carried NGFR, thereby preventing any enrichment of $FOXP3^+$ cells. Therefore, we decided to proceed with a preliminary assessment of FOXP3-mediated reprogramming while continuing to search for a more effective solution for co-delivery.

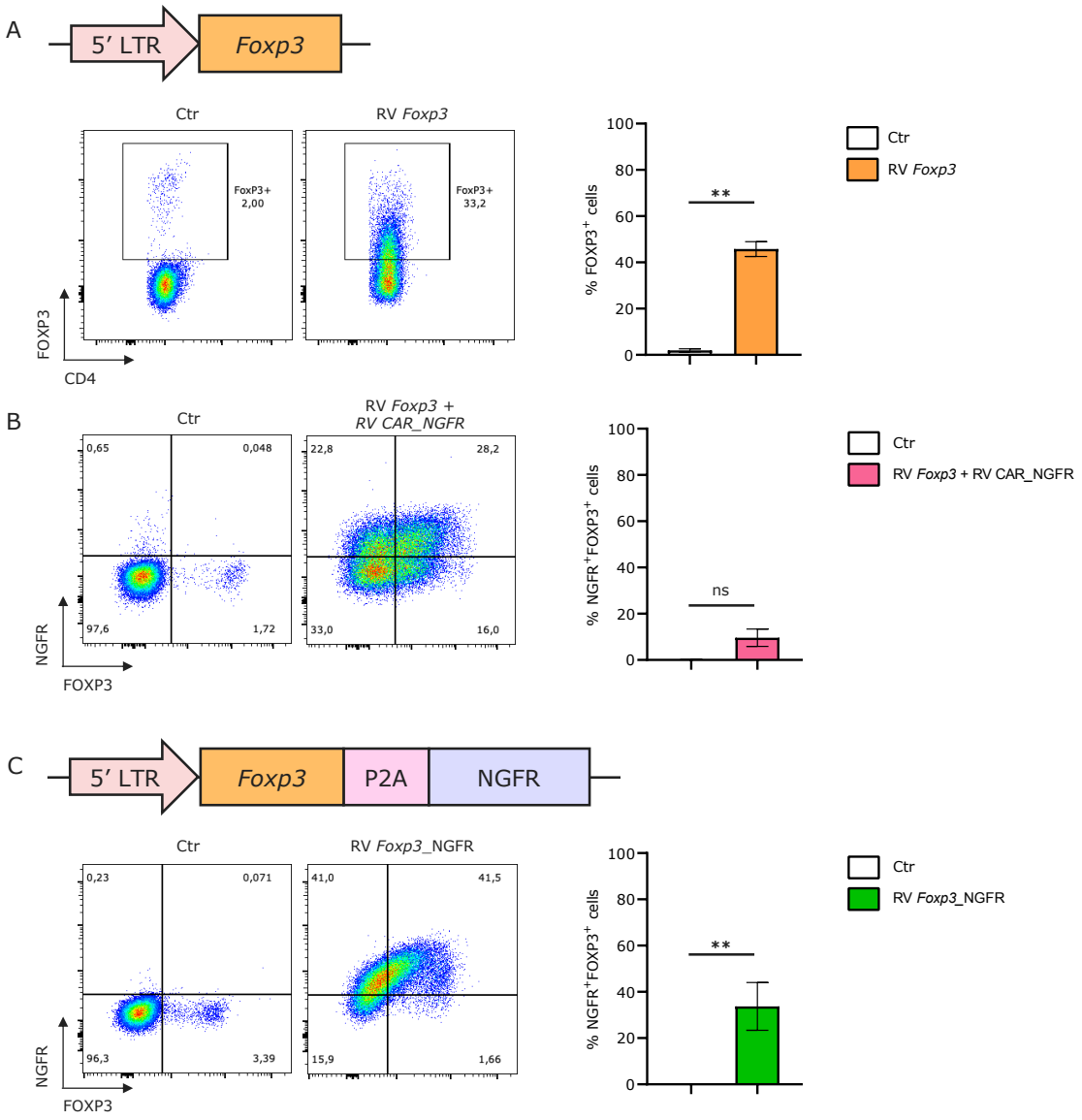

Figure 3.5. Transduction with Foxp3. *(A) Schematic representation of the RV Foxp3 construct and transduction efficiency assessed by flow cytometry. (B) Quantification of NGFR⁺FOXP3⁺ double-positive cells following co-transduction with RV Foxp3 and RV CAR_NGFR. (C) Schematic representation of the RV Foxp3_NGFR construct and corresponding transduction efficiency. Statistical analyses were performed using unpaired T test with Welch's correction, **p-value<0.01, n=3.*

3.1.4 Reprogrammed Tregs fail to exhibit functional suppressive activity in vitro

Obtaining Tregs through FOXP3-mediated reprogramming represents a central aspect of our approach, therefore, we analyzed the suppressive phenotype of cells transduced with either RV Foxp3 or RV Foxp3_NGFR. In this phase, we intentionally focused on Foxp3 transduction alone, both to characterize the effects of this single manipulation and to avoid complications associated with dual infections.

The regulatory capacity of FOXP3$^+$ cells toward Tconvs was assessed through suppression assays, in which Tregs and Tconvs were co-cultured at different ratios and Tconvs proliferation was measured using a proliferation dye. Since not all cells within the Treg cell suspension were successfully transduced and some thus retained a Tconv phenotype, higher Treg:Tconv ratios (2:1 or even 4:1) were occasionally employed to ensure an adequate proportion of functional Tregs in the co-culture.

We performed several assay optimizations but were unable to obtain conclusive results. Nevertheless, some of the optimization trials are reported, as they contributed to a better understanding of the technical aspects and challenges of this complex assay.

One assay with Tregs transduced with RV *Foxp3* (53% FOXP3$^+$), co-cultured with Tconvs under αCD3/28 stimulation and IL-2 supplementation did not result in reduced Tconvs proliferation in presence of Tregs. There was rather an opposite trend, with Tconvs proliferating more in presence of more Tregs (fig. 3.6 A).

Since one mechanism by which Tregs exert suppression is through competition with Tconvs for IL-2, we next tested the assay in the absence of IL-2 supplementation. For the same assay, we also modified Tregs culture conditions prior to the assay to enhance reprogramming. In particular, we cultured Tregs with higher IL-2 concentrations and added rapamycin to favor Tregs selection (Battaglia et al., 2005). Using RV *FoxP3*_NGFR transduced cells (FOXP3$^+$ 60% before, 83% after NGFR selection), we observed again no suppression of Tconvs in function of the amount of Tregs but rather an opposite trend, with higher proliferation in presence of increasing numbers of Tregs (fig. 3.6 B). However, the analysis was limited, as the proliferation dye-negative Treg population overlapped with Tconvs, preventing clear discrimination of Tconvs population in order to analyze its proliferation.

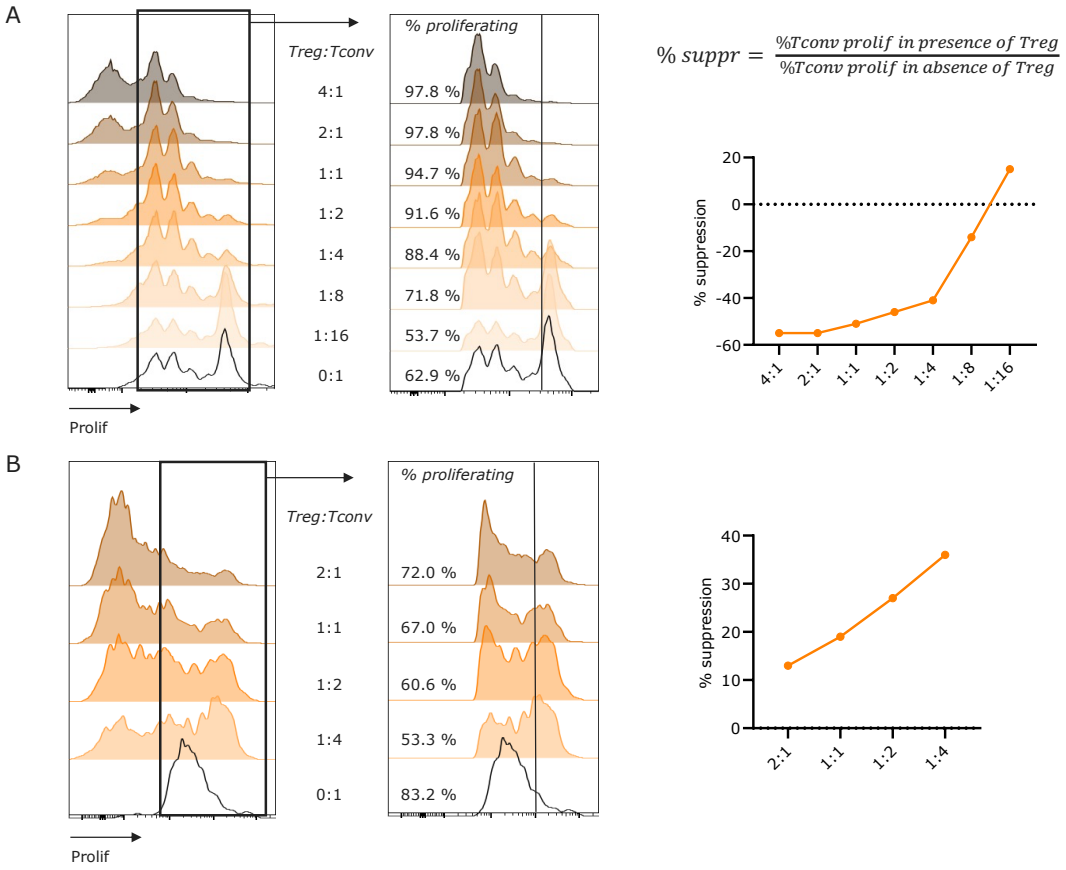

Figure 3.6. Single proliferation dye–based suppression assays. *(A) Analysis of Tconv proliferation using a fluorescent proliferation dye. Left: gating strategy identifying Tconvs while excluding unstained Tregs; center: Tconv proliferation with annotated percentages of dividing cells; right: formula used to calculate the percentage of suppression (% suppr) and the corresponding plot for different Treg:Tconv ratios. (B) Tconv proliferation following co-culture with Tregs pre-treated with high IL-2 and rapamycin. Left: Tconv gating; center: percentage of proliferating Tconvs; right: percentage suppression. Each condition represents n = 1.*

Next, we implemented a second proliferation dye to better separate Tregs from Tconvs. This allowed a more precise isolation of the Tconv population for proliferation analysis (fig. 3.7 B); however, we again did not observe a clear suppressive capacity of Tregs (fig. 3.7 A-C). Activating Tregs before co-culture, to ensure readiness for suppression, also failed to yield significant inhibitory effects (fig. 3.7 D).

To verify the validity of the assay, since reprogrammed Tregs did not yield functional results, we next tested cells with confirmed suppressive capacity by sorting natural Tregs as $CD4^{+}CD25^{+}$ double positive cells (Battaglia et al., 2005). The results were again inconclusive, as Tconvs showed higher proliferation in the presence of natural Tregs than when cultured alone (fig. 3.7 E). It was not possible to test the assay with pre-activated sorted natural Tregs, since after overnight activation the

sorted cells exhibited high mortality and were not suitable to perform the assay, probably due to the stress they were subjected to during the sorting.

These results indicate that the *in vitro* suppression assay used was insufficient to reliably detect suppression even in cells known to be suppressive. Consequently, the lack of observed suppression cannot be attributed solely to low FOXP3 expression in reprogrammed cells, but rather highlights intrinsic limitations of the suppression assay employed in this murine system.

We concluded that efficient transduction of murine $CD4^+$ T cells was achieved using CAR_NGFR vectors, while FOXP3 expression remains challenging. Functional assays showed responsiveness to αSyn antigen but failed to demonstrate suppressive capacity even in sorted natural Tregs, highlighting biological and technical barriers in murine models.

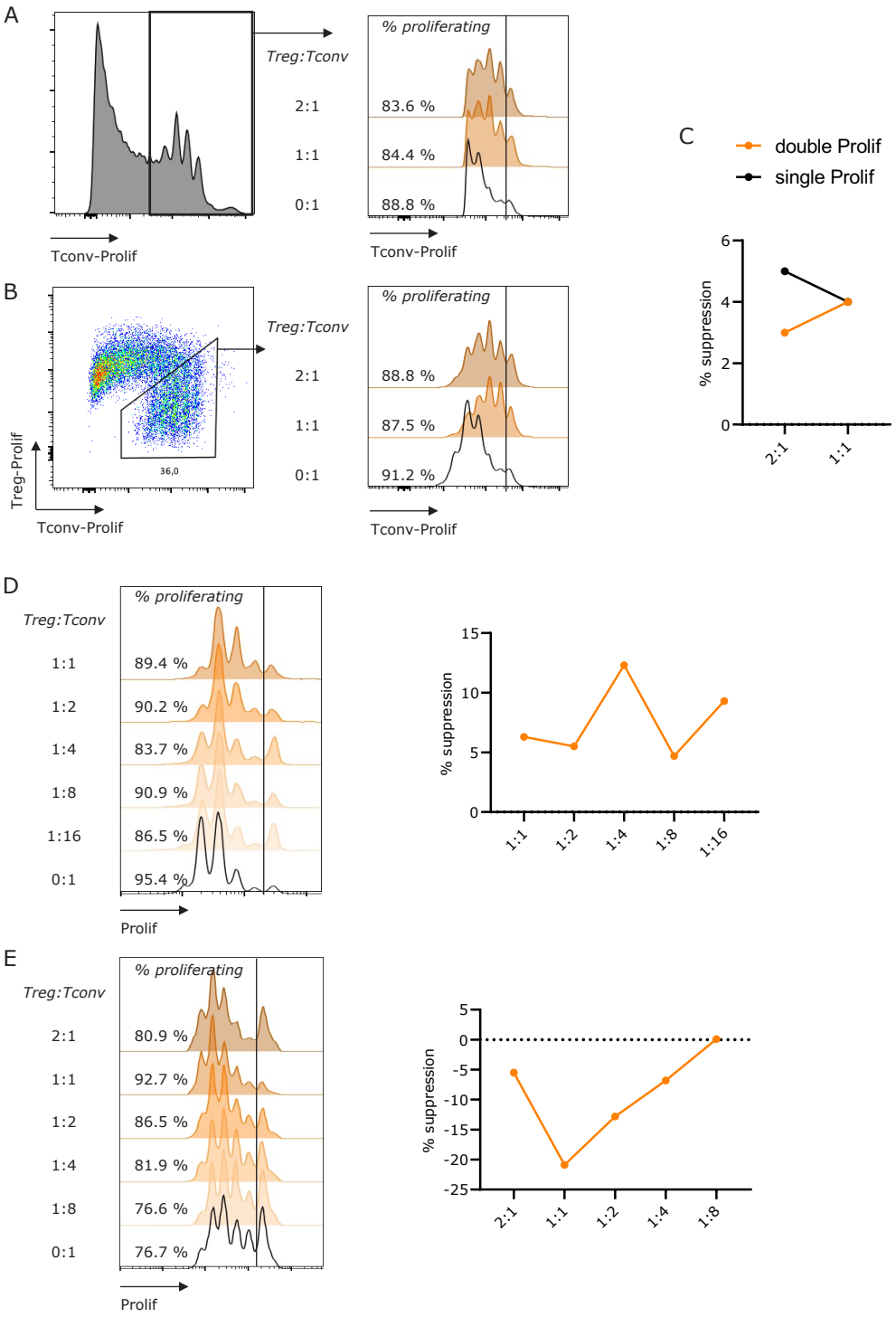

Figure 3.7. Double proliferation dye-based suppression assays. *Comparison of gating strategy and Tconvs proliferation analysis in (A) single proliferation dye-based and (B) double proliferation-dye based suppression assays with high IL-2 and rapamycin pre-treated Tregs. (C) Percentage of suppression in the two approaches. (D-E) Tconvs proliferation analysis and percentage of suppression determined by (D) pre-activated Tregs that were cultured with high IL-2 and rapamycin and (E) sorted natural Tregs. Each condition represents n=1.*

3.1.5 Limited in vivo persistence of murine Tregs highlights model constraints

Given the challenges determined by the low vitality of cultured murine T cells and the technical difficulties associated with suppression assays, we decided to characterize the effect of CAR Treg cells in a murine model of PD. In particular, we implied a mouse model based on αSyn overexpression, generated by intranigral injection of LV $SNCA^{A53T}$.

We isolated GFP^+ natural Treg cells from transgenic mice to enable straightforward identification of transplanted cells by immunofluorescence (fig. 3.8 A). To verify the purity of $CD4^+CD25^+$ sorted natural Tregs, expression of FOXP3 was evaluated and confronted to the $CD4^+$ population, confirming robust FOXP3 expression in natural Tregs (fig. 3.8 B). Then, we intracerebrally (i.c.) injected freshly sorted GFP^+ Tregs into the SN of mice overexpressing αSyn, 6 weeks after injection of LV $SNCA^{A53T}$. We euthanized mice after one week and proceeded to perform immunofluorescence analysis for GFP, αSyn monomeric form, to visualize the area in which it accumulates, and tyrosine hydroxylase (TH) staining to visualize the dopaminergic neurons of the SN (fig 3.8 C). Very few GFP^+ cells were visible one week after infusion and their morphology suggested that these cells were not lymphocytes but glial cells, characterized by a stellate shape.

We hypothesize that most of the transplanted Treg cells did not survive and that GFP was phagocyted by glial cells in the process of cleaning cellular debris, rendering them GFP-positive (fig. 3.8). This result further highlighted the challenges of working with murine T cells and led us to focus on human T cells, which are not only more reliable and resistant to manipulation, but also represent a more translationally relevant model.

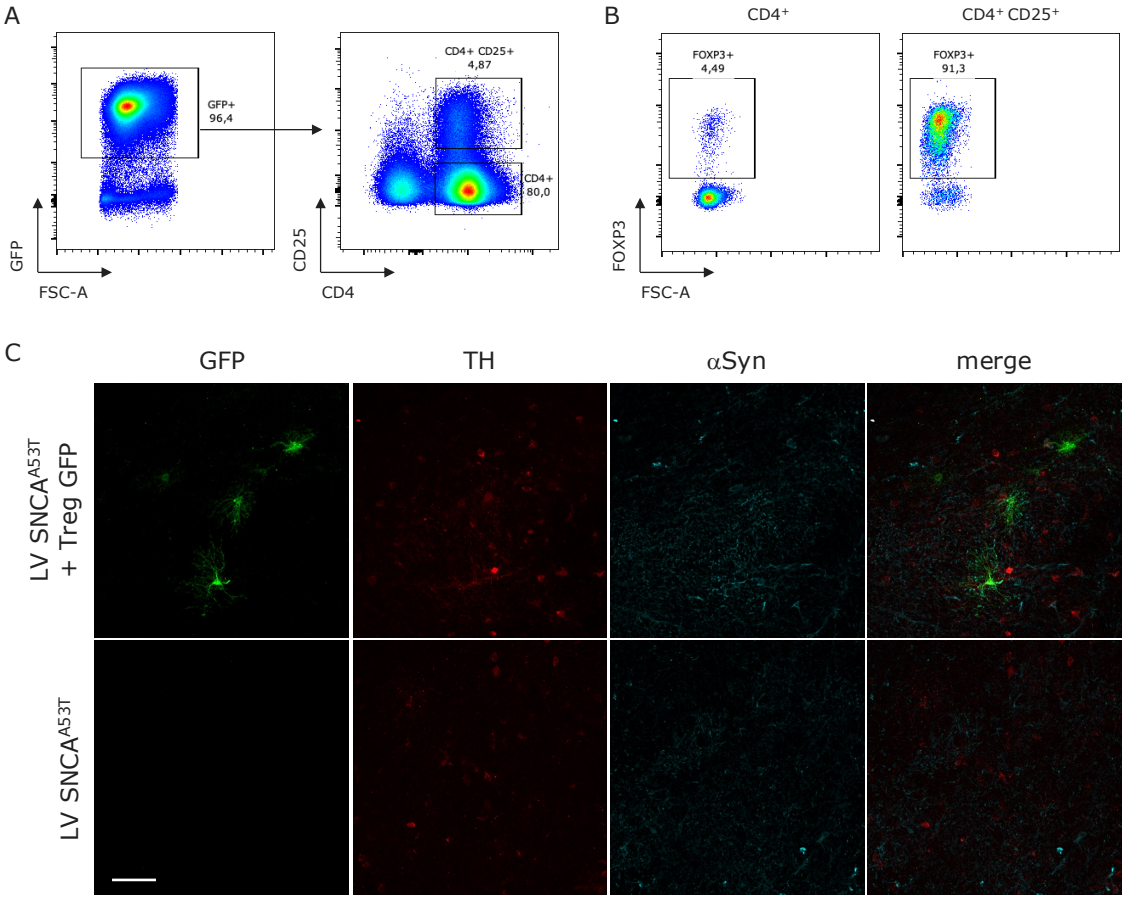

Figure 3.8. GFP⁺ transplanted Tregs cells in C57B/6 PD mouse model. *(A) Representative flow cytometry approach for sorting of GFP⁺ natural Tregs as CD4⁺CD25⁺ population and (B) flow cytometry analysis of expression of FOXP3 in CD4⁺CD25⁺ compared to CD4⁺ cells. (C) Immunofluorescence analysis of GFP⁺ cells (green), TH (red) and monomeric αSyn (cyan).*

3.2. Human T cells

3.2.1 Engineering CAR T cells

After establishing a procedure to isolate primary CD4⁺ human T cells from buffy coat, the purity of the isolated cell suspension was assessed by flow cytometry analysis, which showed a high percentage of CD4⁺ cells in the isolated population compared to the total buffy coat (fig. 3.9).

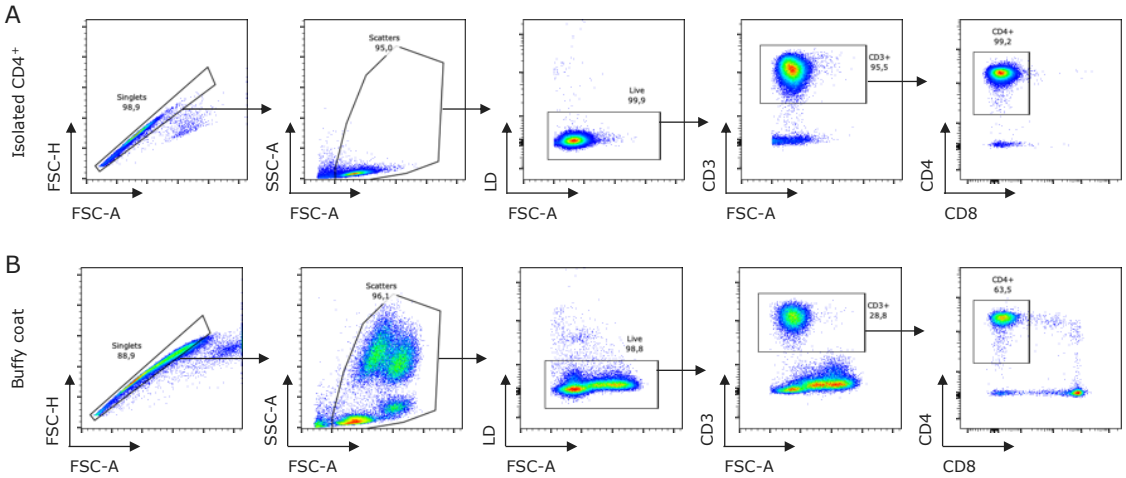

Figure 3.9. Purity of isolated cell fraction. *Flow cytometry analysis of (A) CD4⁺ isolated fraction compared to (B) total buffy coat.*

In order to deliver the two transgenes of interest to human CD4⁺ T cells, we cloned a bidirectional LV construct "LV bid *FOXP3*-CAR_NGFR" containing human *FOXP3* and the CAR_NGFR bicistronic element, respectively under a CMV promoter and PGK promoter (fig. 3.10 A). We analyzed the expression of NGFR and FOXP3 by flow cytometry and observed that the construct did not induce detectable increase of FOXP3 expression (fig. 3.10 B), which was confirmed by the same analysis after LF-LTX-mediated transfection of HEK293T cells (fig. 3.10 C).

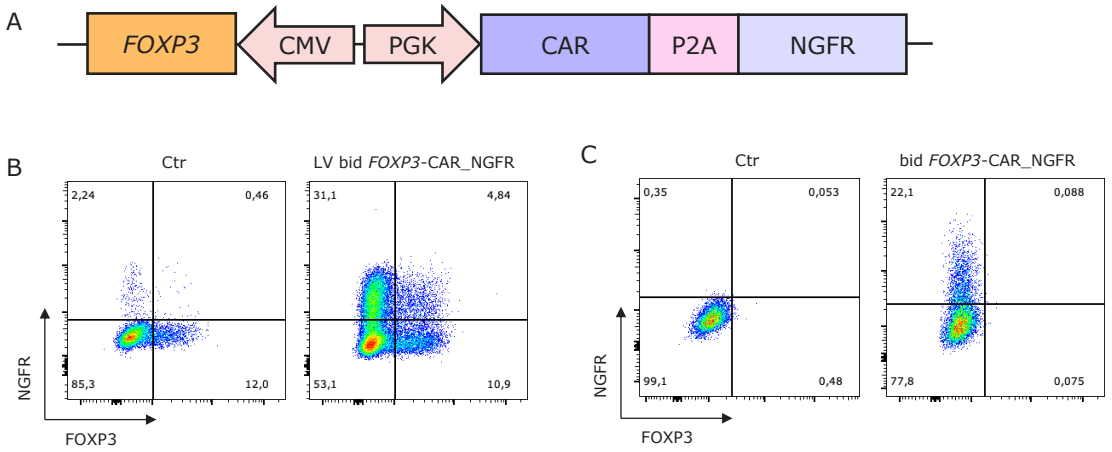

Figure 3.10. FOXP3-CAR bidirectional vector. *(A) Schematic representation of LV bid FOXP3-CAR_NGFR. Flow cytometry analysis of LV bid FOXP3-CAR_NGFR transduced (B) CD4+ T cells and (C) HEK293T cells, compared to untransduced cells.*

Therefore, we next tested the transduction of both transgenes separately, pairing each of them with the NGFR selection marker. Following the same rationale adopted for murine cells, this approach was expected to allow enrichment of FOXP3⁺ cells

while still resulting in some CAR^+FOXP3^- cells, representing a suboptimal yet more advantageous configuration compared to strategies in which only the CAR construct carries NGFR. We thus designed the LV CAR_NGFR and LV *FOXP3*_NGFR vectors, both driven by PGK-mediated expression (fig. 3.11 A-B).

Transduction with LV CAR_NGFR resulted in an efficiency of $73.43 \pm 4.462\%$ based on the percentage of $NGFR^+$ cells detected by flow cytometry (fig. 3.11 C-D). LV *FOXP3*_NGFR yielded $8.37 \pm 1.57\%$ $FOXP3^+$ cells, showing no significant increase compared to the baseline $FOXP3^+$ population in untransduced cells (fig. 3.11 C and E). However, $NGFR^+$ cells were detected after LV *FOXP3*_NGFR transduction, indicating that the LV production and LV-mediated transduction were effective, but only NGFR was efficiently expressed by the construct and not FOXP3.

Since FOXP3 overexpression had not been successfully achieved at this stage, we proceeded to test the functionality of the αSyn CAR in human T cells before addressing FOXP3-mediated reprogramming.

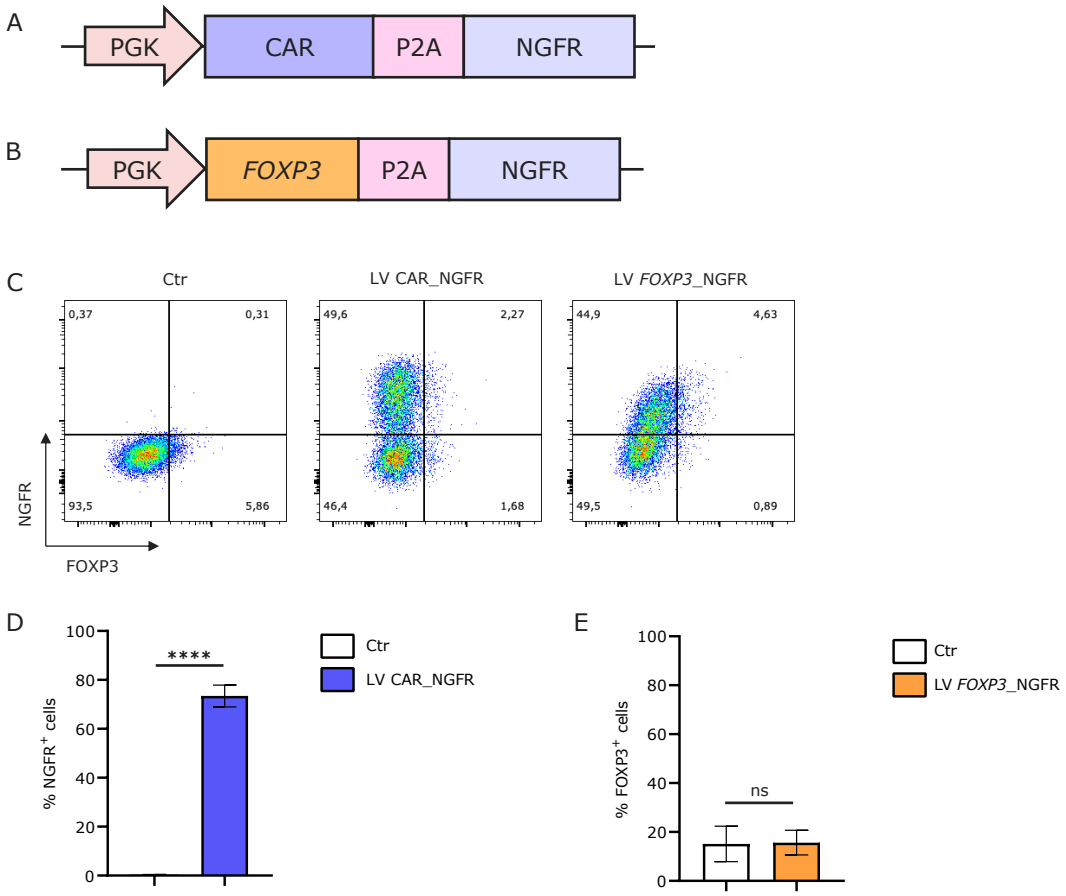

Figure 3.11. Separate vectors. *Schematic representation of (A) LV CAR_NGFR and (B) LV FOXP3_NGFR. (C) Flow cytometry analysis of LV CAR_NGFR and LV FOXP3_NGFR transduced cells compared to control untransduced cells. (D) Quantification of the percentage of NGFR⁺ cells following LV CAR_NGFR transduction. Analyzed with unpaired T test with Welch's correction, ****p-value<0.0001, n=8. (E) Quantification of the percentage of FOXP3⁺ cells following LV FOXP3_NGFR transduction. Analyzed with paired T test, n=4.*

3.2.2 αSyn CAR elicits a response to αSyn in T cells

To assess the ability of the CAR construct to activate human T cells, we transduced total CD4⁺ cells with LV CAR_NGFR and performed activation assays analogous to those used for murine cells. Cells were incubated either without stimuli, with BSA as control protein antigen, with αCD3/28 polyclonal stimulus or different forms of αSyn: monomers, oligomers or PFFs. CAR-transduced T cells exposed to PFFs showed a significant activation, whereas monomers and oligomers did not elicit a comparable response (Fig. 3.12A–B). Untransduced control cells did not respond to any form of αSyn.

This *in vitro* assays indicate that the αSyn CAR selectively responds to highly aggregated forms of αSyn, but not to lower-order species such as oligomers or monomers, supporting its suitability for targeting pathogenic αSyn aggregates in PD.

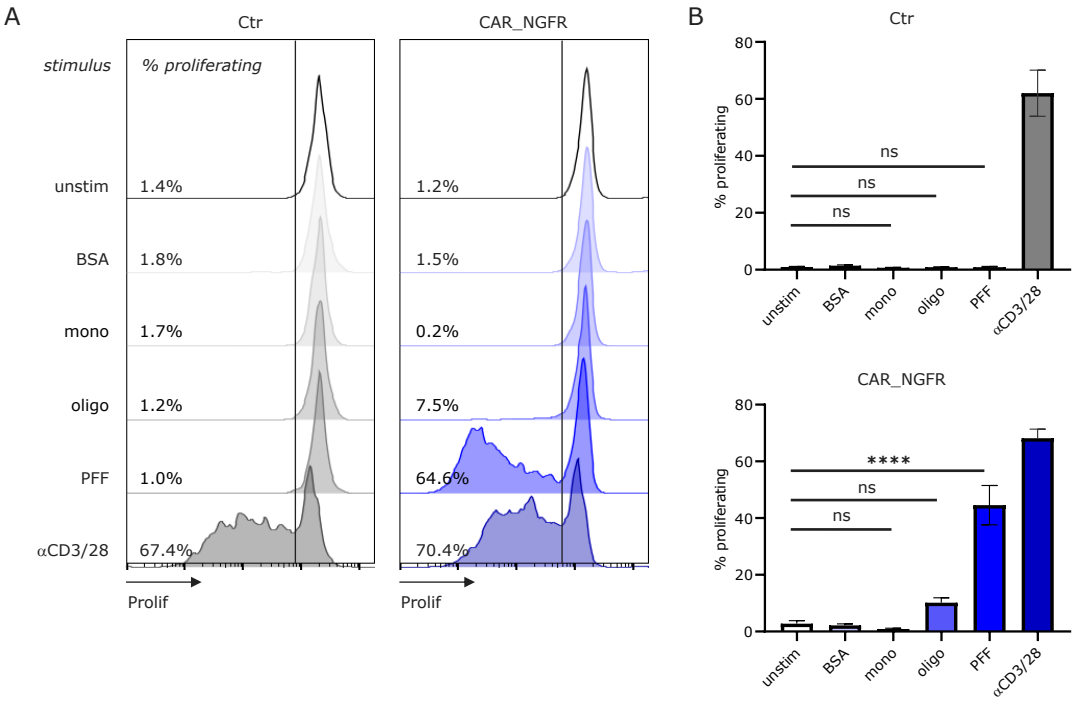

Figure 3.12. Activation assay on CAR T cells. *Activation assay of CAR T cells cultured in absence of stimulus and with BSA, monomeric αSyn, oligomeric αSyn, PFFs or αCD3/28 compared to control untransduced cells. (A) Proliferation dye–based gating strategy in flow cytometry and (B) corresponding quantification of proliferating cells for control untransduced cells and CAR_NGFR-transduced cells. Analyzed with ordinary one-way ANOVA and Tukey's multiple comparisons test, ****p-value < 0.0001, n=4. Mono = monomeric αSyn; oligo = oligomeric αSyn.*

3.2.3 FOXP3_CAR constructs efficiently generate CAR⁺FOXP3⁺ cells

After several failed attempts to express transgenic *FOXP3* into $CD4^+$ cells, we decided to rely on a construct shared by our collaborators. In particular, we modified LV *FOXP3*_CD19 described by Doglio and colleagues, which is a LV carrying a bicistronic element containing *FOXP3* and an anti-CD19 CAR with a NGFR-modified spacer for direct CAR detection (Doglio et al., 2024). We substituted the antigen binding domain with the anti-αSyn NB in LV *FOXP3*_αSyn-NB, or with a newly designed anti-αSyn scFv in LV *FOXP3*_αSyn-scFv (fig. 3.13 A). In this setting, we exploited LV *FOXP3*_CD19 as a control, as it allowed us to obtain FOXP3-reprogrammed Tregs expressing an unrelated CAR.

All the constructs determined a consistent efficiency of transduction, assessed by flow cytometry analysis of CAR^+FOXP3^+ double positive cells. In particular, the percentage of double positive cells was 76.93 ± 2.99% with LV *FOXP3*_αSyn-NB, 62.45 ± 4.96% with LV *FOXP3*_αSyn-scFv and 76.53 ± 2.86% with LV *FOXP3*_CD19, determining no significant difference between efficiencies of transduction among the different vectors (fig. 3.13 B-C). Therefore, all the newly applied vectors efficiently

determined overexpression of the transgenes of interest for CAR Treg cells engineering.

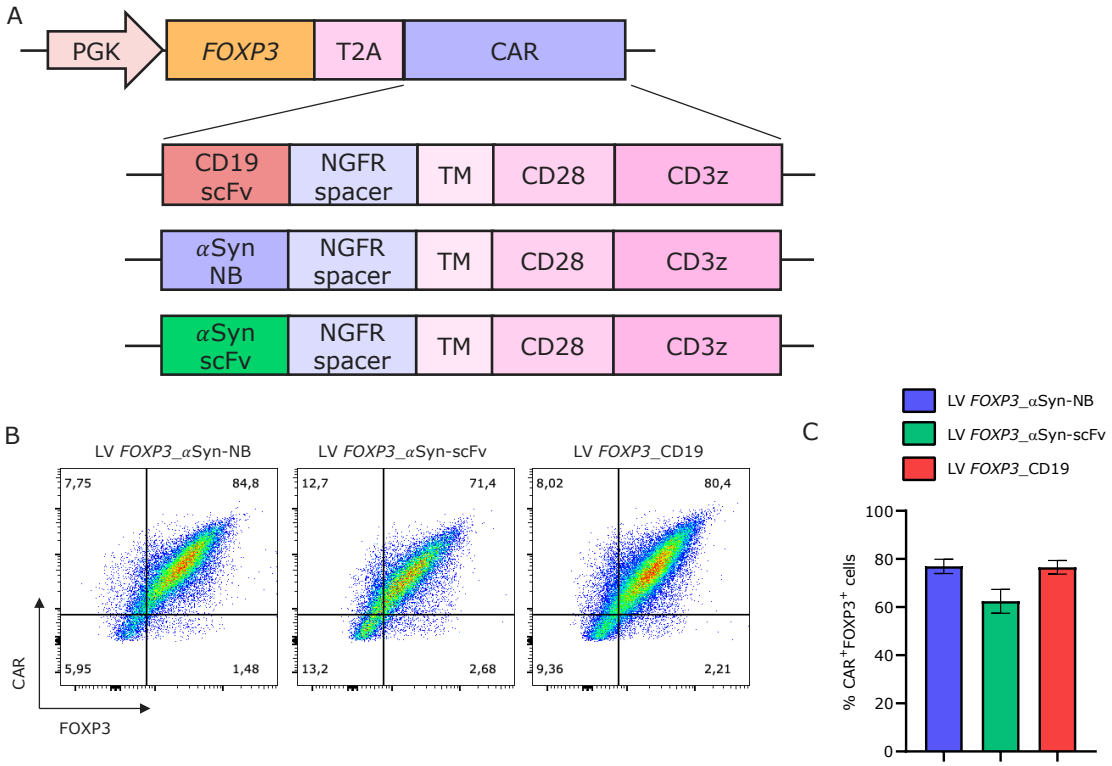

Figure 3.13. FOXP3_CAR vectors. *(A) schematic representation of LV FOXP3_CAR structure, with detail of CAR domains in LV FOXP3_CD19, LV FOXP3_αSyn-NB and LV FOXP3_αSyn-scFv. (B) Representative flow cytometry readout following transduction and (C) quantification of efficiency of transduction, n=5.*

3.2.4 αSyn-binding domains bind to αSyn in brain slices

In order to test the ability of the newly designed αSyn-scFv to bind αSyn, we generated monoclonal antibodies carrying the antigen binding domain of αSyn-scFv CAR and the one of αSyn-NB CAR as a control. We performed immunofluorescence analysis on brain slices of mice overexpressing αSyn at 8 weeks post injection of a LV SNCA^{A53T} (fig. 3.14). αSyn phosphorylated on serine 129 (P-αSyn) was stained to visualize aggregated αSyn together with the monomeric form. We observed a selective and specific signal in tissue overexpressing αSyn, indicating that both NB and scFv αSyn-binding domains are specific for αSyn.

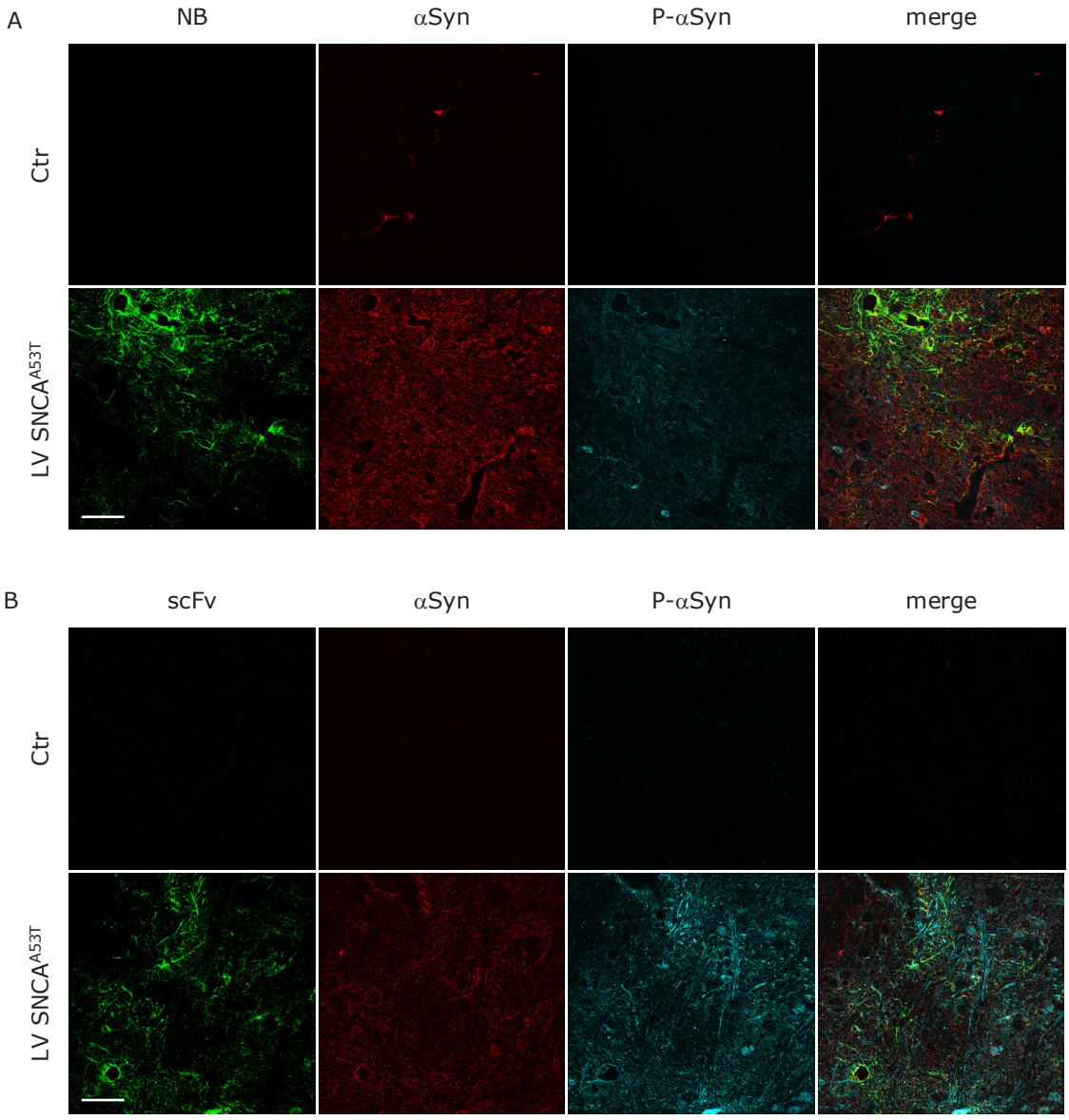

Figure 3.14. Validation of antigen binding domains. *Immunofluorescent staining of monomeric αSyn, P-αSyn and (A) NB or (B) scFv antigen binding domains on mouse brain slices overexpressing αSyn. αSyn = monomeric αSyn. Scale bar 50μm.*

3.2.5 Antigen specific activation of αSyn-NB CAR Tregs and tonic signaling of αSyn-scFv CAR Tregs

In order to test the response of the newly generated CAR Treg cells to αSyn, we performed activation assay with exposure to PFFs. The assay was conducted by culturing cells without stimuli to identify the non-proliferating peak, or with different stimuli in presence of IL-2, in particular BSA as control protein antigen, PFFs or αCD3/28 polyclonal stimulus (fig. 3.15 A-B). As expected, αSyn-NB CAR induced activation of CAR Treg cells in response to αSyn and αCD3/28 but not in control conditions. αSyn-scFv CAR did not elicit a statistically significant activation in the

presence of PFFs. Crucially, a similar trend was also evident under control conditions. Since we demonstrated the specificity of the binding, these results suggests that αSyn-scFv CAR Treg cells may undergo constitutive activation in the presence of IL-2, indicating potential tonic signaling. This phenomenon, previously reported for some CAR designs, is associated with spontaneous receptor clustering and constitutive signaling in the absence of antigen (Long et al., Nat Med, 2015).

Furthermore, preliminary experiments analyzed IL-10 production by activated CAR Tregs as readout for functional activation in response to αSyn. Both αSyn-specific CARs determined IL-10 secretion by CAR Tregs in response to PFFs and not in the negative controls (fig. 3.15 C). The αSyn-NB CAR demonstrated coherent antigen-specific activation with robust IL-10 secretion in response to αSyn aggregates, indicating a functional activation consistent with proliferative readouts. Regarding scFv-CAR cells, while IL-10 levels after stimulation with PFFs were statistically significant compared to the negative control, IL-10 production in presence of αSyn was low and did not correspond proportionally to proliferative signals. This result might reflect the low number of replicates of this preliminary experiment.

Overall, these findings highlight that the αSyn-NB CAR reliably mediates antigen-dependent activation characterized by concordant proliferation and IL-10 production, reflecting balanced functional competence. Conversely, the αSyn-scFv CAR apparent tonic signaling, evidenced by antigen-independent proliferation and discordant IL-10 responses, points to an intrinsic design limitation that may impact its functional relevance and downstream immunomodulatory capacity, therefore the functionality of αSyn-scFv CAR should be further investigated.

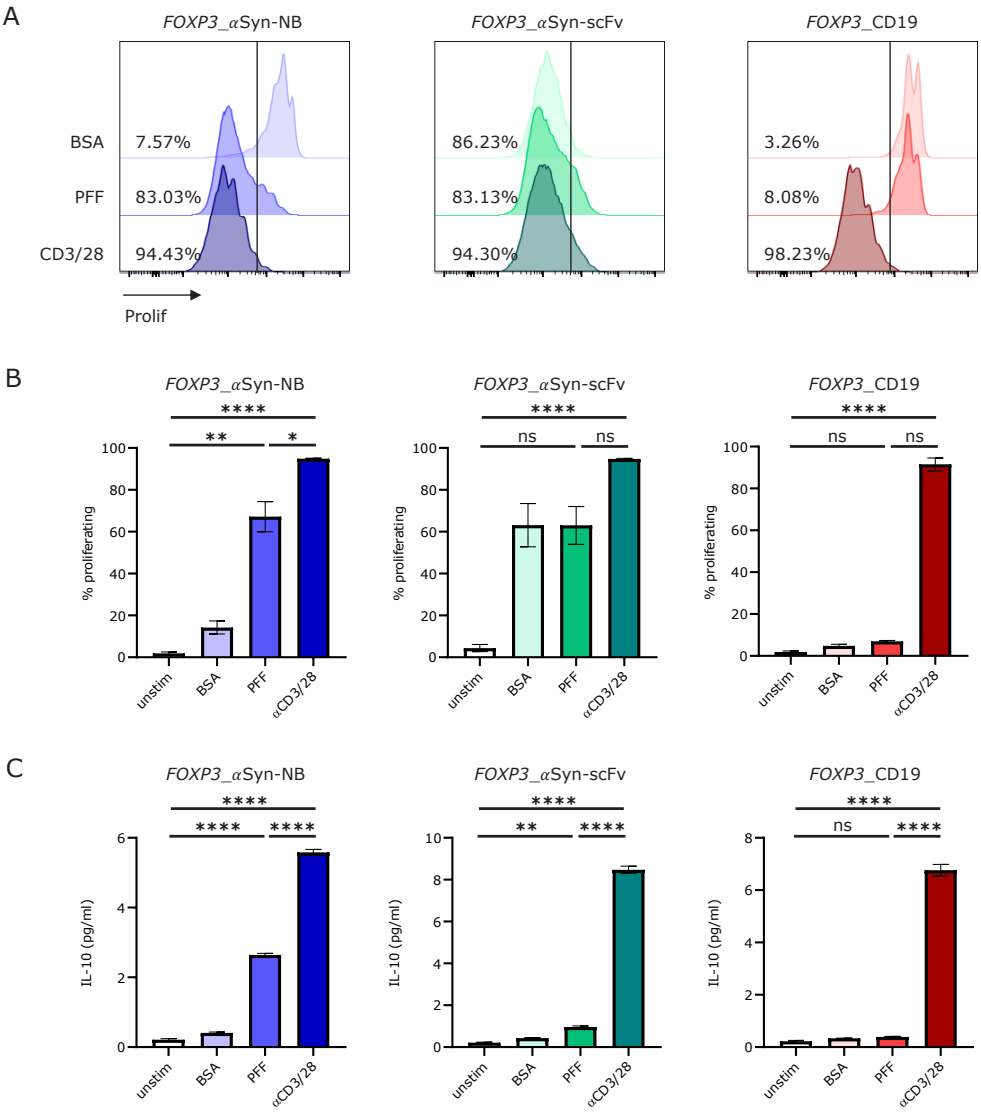

Figure 3.15. Activation assay on CAR Tregs. *(A) Proliferation dye–based gating strategy in flow cytometry and (B) corresponding quantification of proliferating cells, analyzed with the Kruskal–Wallis test followed by Dunn's multiple comparisons test, n = 6. (C) IL-10 production measured by ELISA and analyzed using one-way ANOVA with Tukey's multiple comparisons test , n = 3. * p < 0.05; ** p < 0.01; *** p < 0.001; **** p < 0.0001.*

3.2.6 CAR molecules evenly distribute on cell surface

We then assessed the surface distribution of the CAR molecule with immunofluorescence analysis, following the approach described by Long and colleagues to evaluate the presence of spontaneous receptor clustering (fig. 3.16 A). The inclusion of an NGFR-derived spacer within the CAR design allowed direct detection of surface-expressed CARs. Confocal imaging revealed that all CAR constructs displayed a membrane distribution comparable to that of CD3 counterstaining, indicating a homogeneous localization pattern and absence of detectable clustering phenomena (fig. 3.16 B). Therefore, the observed trend of

constitutive activation in the αSyn-scFv CAR cannot be attributed to spontaneous receptor clustering, as described by Long et al. This suggests that the trend in tonic signaling in the αSyn-scFv CAR likely arises from alternative mechanisms independent of receptor spatial aggregation.

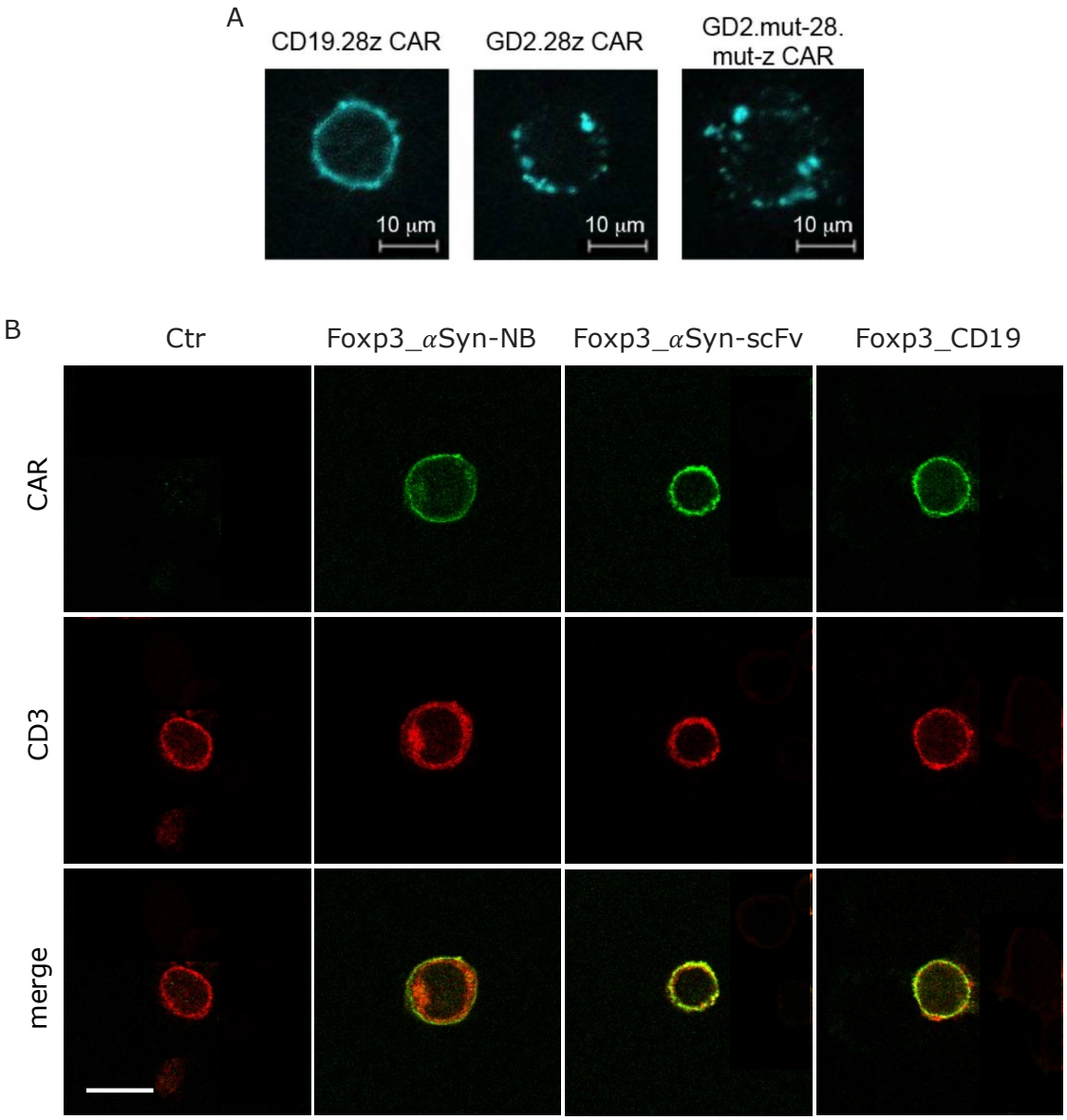

Figure 3.16. CAR distribution on cell surface. *(A) Immunofluorescence analysis reported by Lang and colleagues (Long et al., 2015) (B) Immunofluorescence showing CD3 and CAR molecules distribution on cell surface. Scale bar 10μm.*

3.2.7 Reprogrammed CAR Tregs have a suppressive phenotype

To test the suppressive phenotype of reprogrammed CAR Treg cells, we performed polyclonal suppression assay by co-culturing CAR Tregs and Tconvs in presence of an αCD3/28 stimulus and analyzed the proliferation of Tconvs in presence of increasing

numbers of Treg cells. Given that the suppressive capacity of *FOXP3*_CD19 cells was previously characterized by our collaborators, we used *FOXP3*_CD19 as positive control to verify that the newly designed CAR molecules did not interfere with suppressive function of Tregs (fig. 3.17). While a significant inter-group difference was observed, the effectiveness of the suppressive capacity was preserved by the introduction of the new CAR constructs.

These findings indicate that FOXP3-mediated reprogramming was efficient with all constructs and incorporation of the new CAR designs did not impair the intrinsic regulatory function of reprogrammed Tregs, confirming that their suppressive activity was effectively preserved.

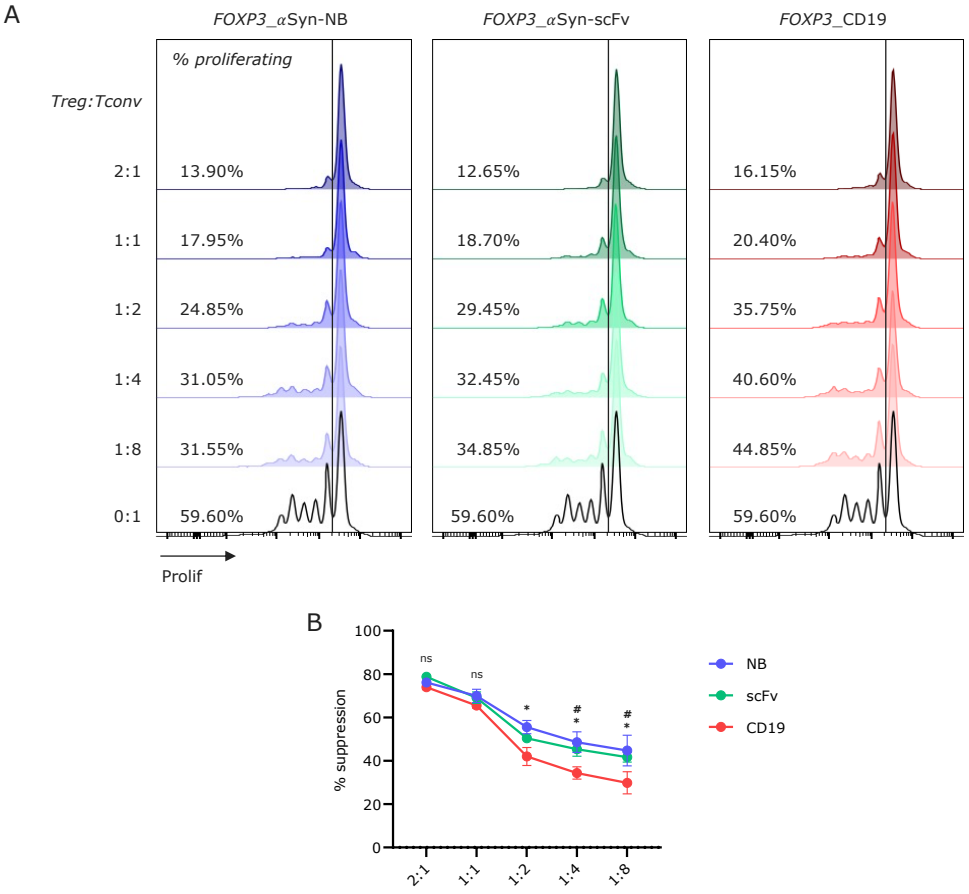

Figure 3.17. Polyclonal suppression assay on CAR Tregs. *(A) Proliferation dye–based gating strategy of Tconvs in flow cytometry and (B) corresponding quantification of proliferating cells. Analyzed with two-way ANOVA with multiple comparisons; *p-value < 0.05 for FOXP3_αSyn-NB vs FOXP3_CD19; # p-value < 0.05 for FOXP3_αSyn-scFv vs FOXP3_CD19; n=3.*

3.2.8 αSyn-NB CAR Treg cells determine antigen-specific suppression

In order to determine the ability of the CAR to stimulate the suppressive ability of CAR Tregs in response to αSyn, we performed antigen specific suppression assays. In particular, we pre-stimulated Treg and Tconv cells separately in order to avoid exposure of Treg to αCD3/28. Tconvs responder cells were stimulated with αCD3/28, while *FOXP3*_αSyn-NB, *FOXP3*_αSyn-scFv and *FOXP3*_CD19 CAR Treg cells were stimulated with PFFs. After stimulation, cells were cocultured at different Treg:Tconv ratios to perform the assay (fig. 3.18). As a negative control, Tregs were also cultured in absence of stimuli, while *FOXP3*_CD19 cells were stimulated with αCD3/28 as positive control for suppression. *FOXP3*_αSyn-NB CAR Tregs determined a significant suppression of Tconvs after αSyn stimulation compared to unstimulated Tregs (fig. 3.18 C). *FOXP3*_αSyn-scFv cells confirmed to be constitutively active, determining the same suppression level with or without previous stimulation (fig. 3.18 D). Finally, as expected, control *FOXP3*_CD19 cells showed suppressive ability in the positive control condition, but not in negative control or with αSyn exposure (fig. 3.18 E).

Therefore, *FOXP3*_αSyn-scFv cells confirmed to be active independently from the presence of αSyn antigen, rendering them unsuitable for our purpose, while *FOXP3*_αSyn-NB cells can elicit a selective antigen-specific suppression.Considering the *in vitro* results, we concluded that human $CD4^+$ T cells were successfully engineered to express CAR and FOXP3 and *FOXP3*_αSyn-NB-engineered CAR Tregs demonstrated antigen-specific activation and efficient immune suppression in response to aggregated human αSyn *in vitro*. These findings support the feasibility of generating functional αSyn-targeted CAR Tregs in a human system. Therefore, we decided to proceed to test whether *FOXP3*_αSyn-NB CAR Tregs would be an efficient tool for targeting neuroinflammation in a PD mouse model.

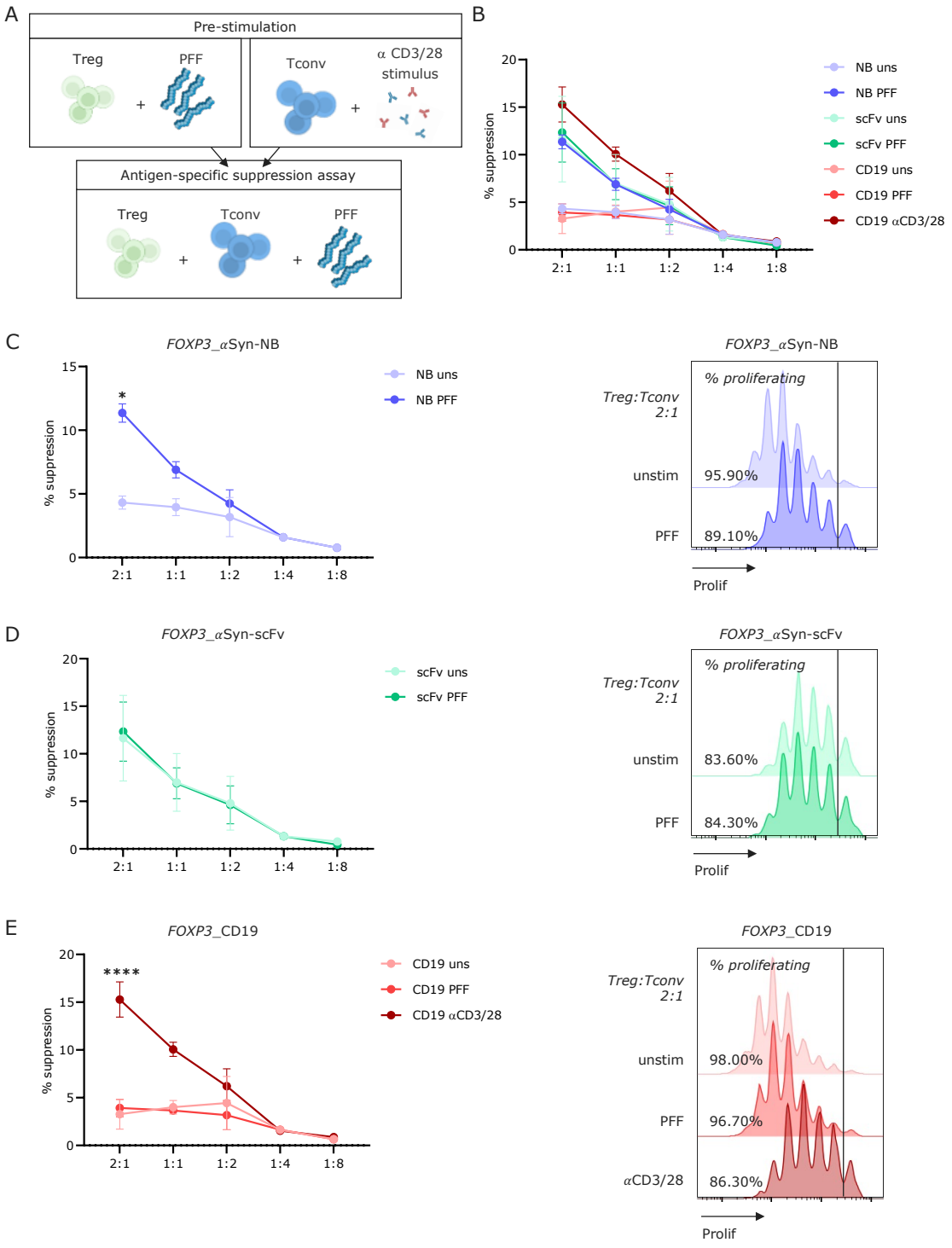

Figure 3.18. Antigen specific suppression assays. *(A) Schematic representation workflow with separate stimulation of cells preceding assay setup. Image created with Biorender. (B) Results showing the percentage of suppression exerted in all analyzed conditions, including different CAR Tregs and their differential stimulation. (C-E) Detailed results including percentage of suppression and proliferation dye flow cytometry analysis at 2:1 Treg:Tconv ratio of (C) FOXP3_NB, (D) FOXP3_scFv and (E) FOXP3_CD19 CAR Treg cells. Statistical analysis performed with two-way ANOVA and Tukey's multiple comparisons test; *p-value < 0.05; ****p-value < 0.0001; n=3.*

3.3 In vivo preliminary testing

3.3.1 NSG-SGM3 humanized PD mouse model generation

In order to test the *in vivo* protective role of our CAR Tregs, we first needed to characterize a suitable mouse model, as our established model of αSyn overexpression was based on immunocompetent C57BL/6 mice. To enable the infusion of human CAR Tregs without triggering rejection by the host immune system, we opted to use NSG-SGM3 immunocompromised mice, specifically NOD-scid IL2Rg^{null} (NSG), that lack B, T and NK cells, genetically modified to express human IL-3, granulocyte-macrophage colony-stimulating factor (GM-CSF) and stem cell factor (SCF). The introduction of these human cytokine genes favors the humanization of the mice, in particular supporting the engraftment, survival, and function of human hematopoietic and immune cells within the murine environment by providing essential human-specific growth factors and signaling cues that are otherwise absent in regular mice. This allows efficient humanization of the mice, which is critical to establish a physiologically relevant model for studying human immune cell therapies. In particular, we reconstituted the human immune compartment in these mice by infusion of human CD34^{+} hematopoietic stem cells (hHSCs), which engraft and differentiate over time to yield a multi-lineage human immune system. Myeloid lineage cells are the first to robustly reconstitute, followed by B cells and then T cells, which repopulate more slowly. Because B cell expansion can become excessive and lead to fatality, we administered human T cells into the model to achieve a balanced immune reconstitution (fig. 3.19). In this humanized NSG-SGM3 platform with a reconstituted human immune system, we induced αSyn pathology by LV SNCA^{A53T} i.c. delivery, aiming to provide a model with clinically relevant environment combining human immune components with αSyn-driven neurodegeneration, enabling in vivo evaluation of the trafficking, persistence, and neuroprotective efficacy of human αSyn-specific CAR Tregs.

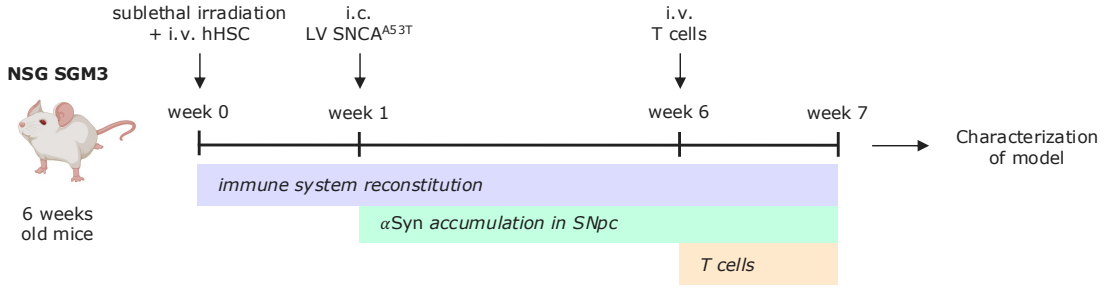

Figure 3.19. NSG-SGM3 humanized PD model generation. *Schematic representation of procedures carried on NSG-SGM3 mice including sublethal irradiation, hHSCs transplant, i.c. injection of LV SNCA^{A53T} and i.v. T cell infusion. Image created with Biorender.*

In particular, we characterized human immune repopulation by flow cytometry analysis of peripheral blood (Fig. 3.20). We observed a robust myeloid cell repopulation at week 2, followed by a contraction of this population from week 4 onward. As anticipated, B cells progressively expanded over time, and T cells were first detectable at week 7, one week after i.v. infusion. Therefore, peripheral human immune repopulation in NSG-SGM3 mice was confirmed and followed the expected time course.

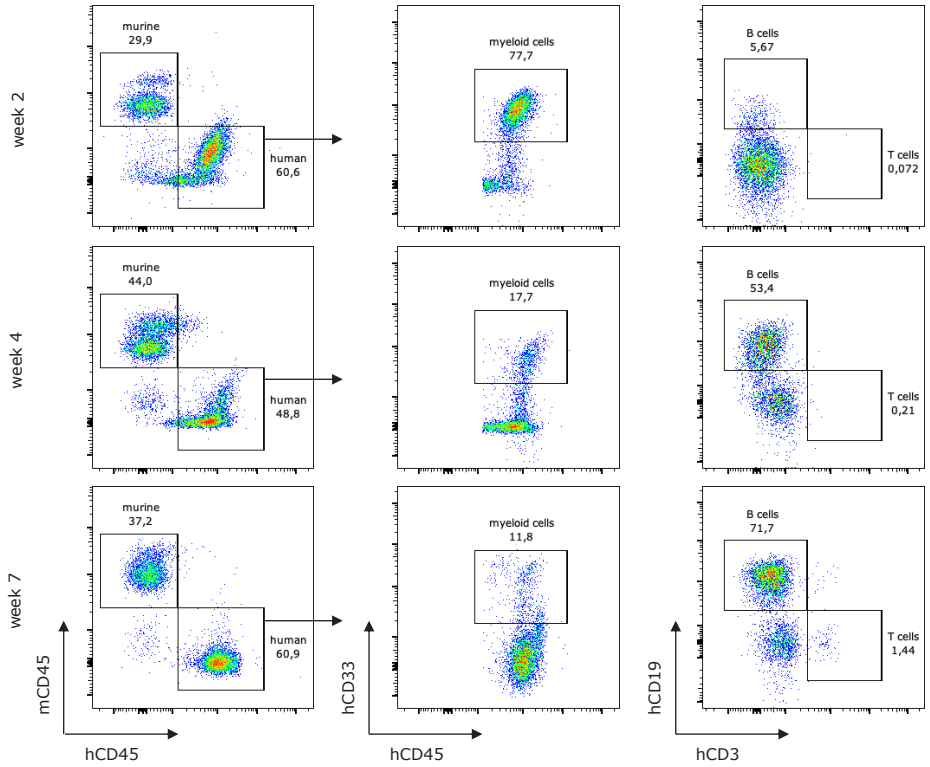

Figure 3.20. Human immune compartment repopulation in NSG-SGM3 mice. *Flow cytometry analysis of cell populations in peripheral blood at 2, 4 and 7 weeks after hHSCs infusion.*

3.3.2 NSG-SGM3 humanized PD mouse model shows immune infiltration

The first step for characterization of the model involved analyzing αSyn accumulation in the SN, dopaminergic neurodegeneration and local neuroinflammation. However, we noted that the initial intracranial injections in NSG-SGM3 mice did not reach the SN. This was not due to a technical error, but rather to anatomical differences: the larger cranial and brain dimensions of NSG-SGM3 mice caused injections performed using standard C57BL/6 coordinates to target the thalamic region instead of the SN (fig. 3.21 A). Therefore, we were only able to verify the presence immune infiltration from the reconstituted human immune compartment in response to αSyn accumulation, but not the specific effect within the SN. In particular, we performed immunofluorescence staining for human nuclei and ionized calcium-binding adapter molecule 1 (IBA1). IBA1 is a well-established marker that labels both microglia and infiltrating macrophages, as it is expressed broadly by cells of monocytic lineage. Therefore, its expression robustly identifies microglia and macrophages infiltration in neuroinflammatory contexts. The detection of double-positive cells for human nuclei and IBA1 specifically in areas with αSyn overexpression, but not in other regions, indicates the presence of infiltrating human macrophages in response to αSyn accumulation (Fig. 3.21B). Stainings for detection of T cells were not conclusive, but further optimizations will be performed.

After this single experiment the NSG-SGM3 mouse colony was exterminated due to a contamination and it was impossible to this day to reproduce the experiment with correct stereotaxic coordinates. Therefore we proceeded using conventional NSG mice.

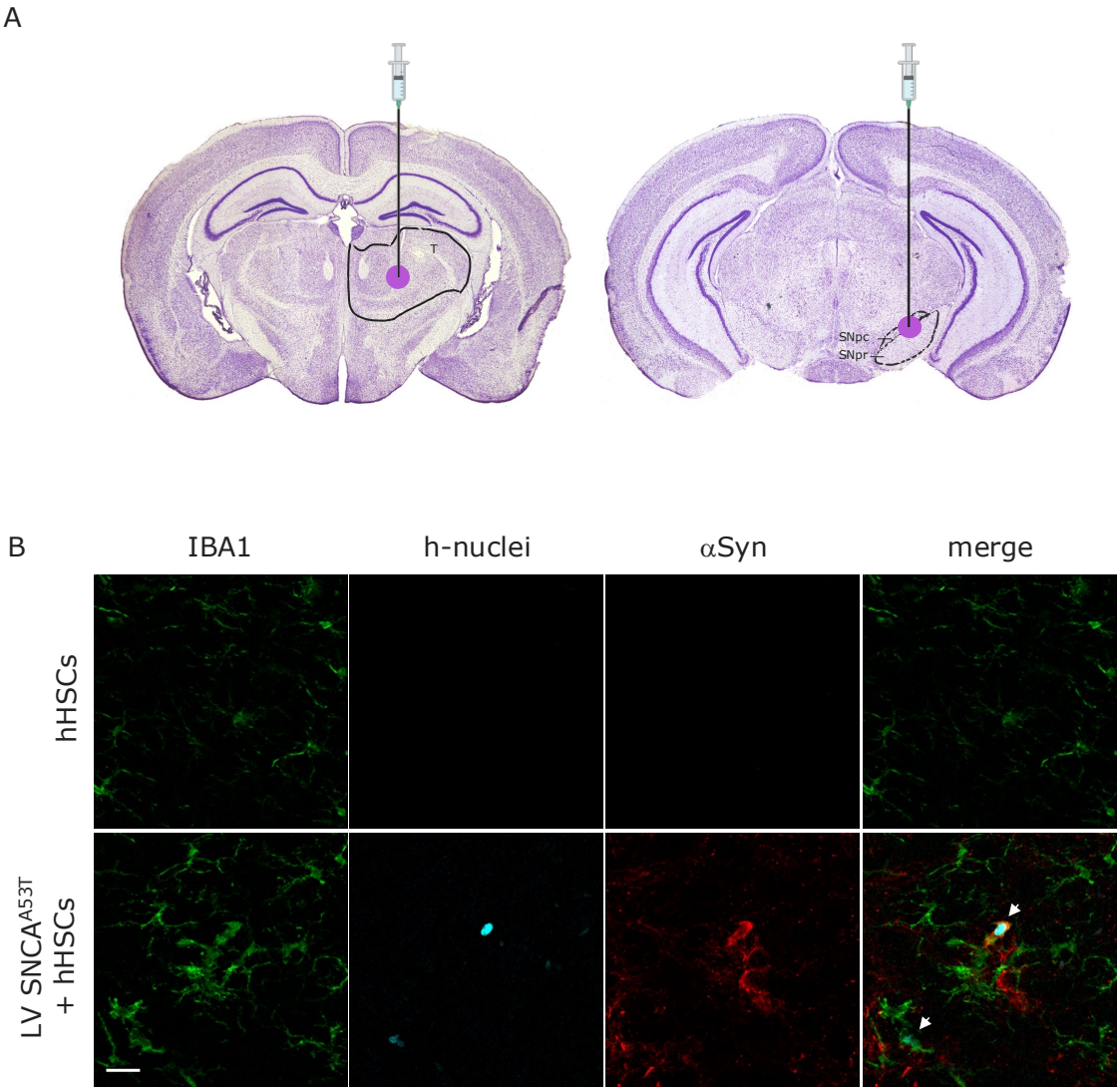

Figure 3.21. NSG-SGM3 αSyn overexpression and human immune infiltrate. *(A) Schematic representation of incorrect thalamic injection performed in NSG-SGM3 mice (left) and ideal SN targeting (right). Images adapted from Paxinos & Franklin, 2001. (B) Immunofluorescence analysis of IBA1 (green), human nuclei (cyan) and monomeric αSyn (red) in humanized NSG-SGM3 mice injected with LV SNCA^{A53T} or control. Arrows pointing at IBA1^{+}h-nuclei^{+} infiltrating cells. Scale bar 25μm.*

3.3.3 Stereotaxic injection coordinates optimization in NSG mice

After suppression of the NSG-SGM3 colony we were able to have access to a limited number of non-humanized NSG mice. Therefore, we were able to After suppression of the NSG-SGM3 colony we were able to have access to a limited number of non-humanized NSG mice. Therefore, we were able to perform an optimization of stereotaxic injection coordinates using a LV GFP and obtained optimal targeting of the SN as shown in double immunofluorescence staining of GFP and TH (fig. 3.22 A). Furthermore, we tested the effective overexpression of αSyn at 6 weeks post injection of LV SNCA^{A53T}. Monomeric αSyn was efficiently expressed, however,

the aggregated form of αSyn, visualized as P-αSyn, was not considerably spreading across the SN (fig. 3.22 B).

Therefore, we obtained efficient targeting of the SN with LV i.c. delivery and proceeded to characterize a model of αSyn overexpression in non-humanized NGS mice.

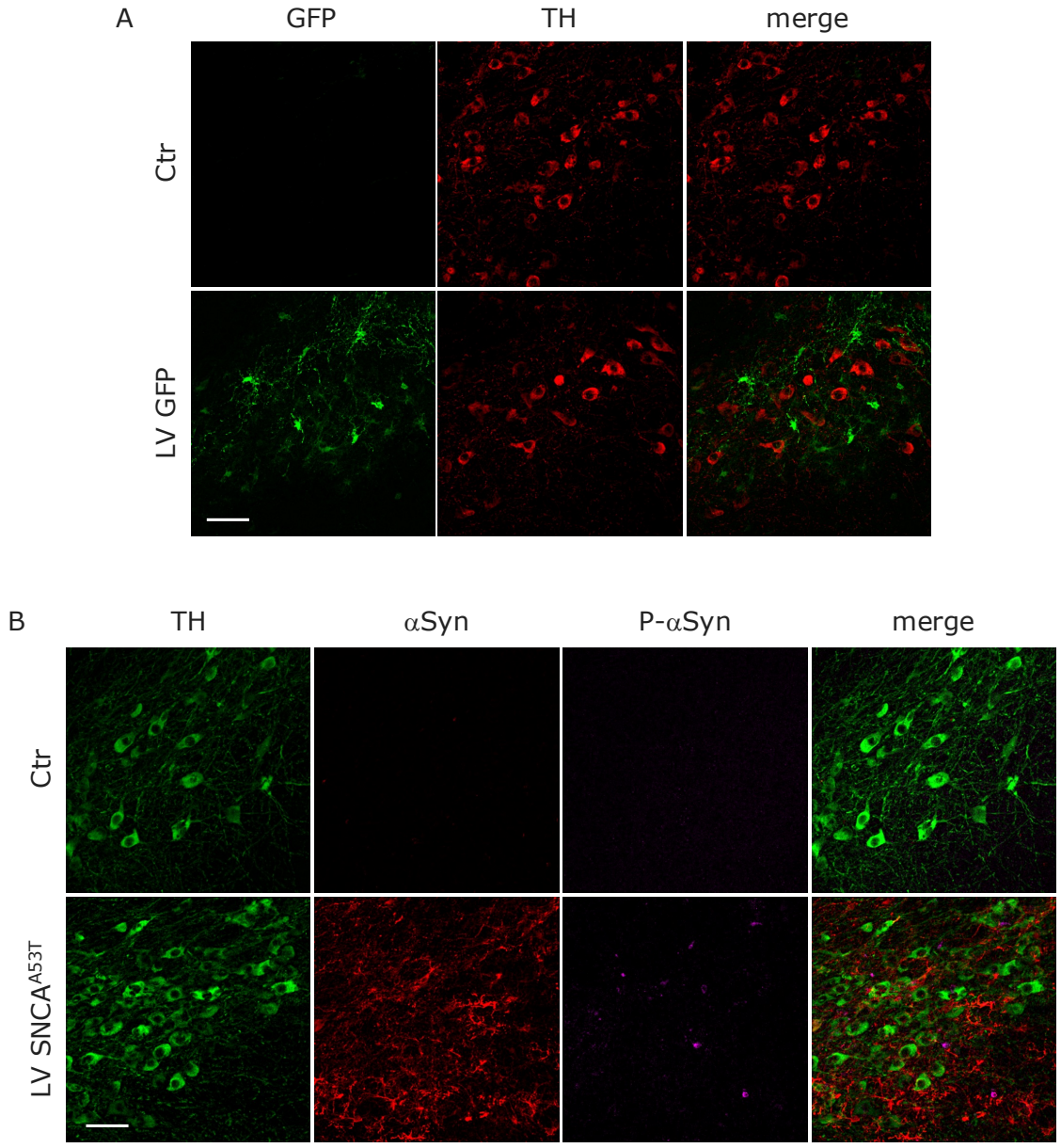

Figure 3.22. Stereotaxic injections targeting the SN. *Immunofluorescence analysis of (A) LV GFP and (B) LV SNCA^{A53T} stereotaxic injections showing efficient targeting of a TH^{+} area. Scale bar 50μm.*

3.3.4 NSG PD model shows neurodegeneration and neuroinflammation

In order to obtain a more robust aggregation of αSyn, we characterized protein accumulation at 10 weeks post injection, highlighting a significant accumulation of P-αSyn into the SN by immunofluorescence analysis (fig. 3.23 A). Interestingly, we observed intracellular accumulation of P-αSyn into dopaminergic neurons, which is consistent with observations of PD brains (Poewe et al., 2017). Therefore, we proceeded to characterize dopaminergic neuronal loss by stereological counting based on TH immunohistochemistry and we observed 39.3 ± 5.0% loss of dopaminergic neurons in association with αSyn overexpression compared to control condition (fig. 3.23 B).

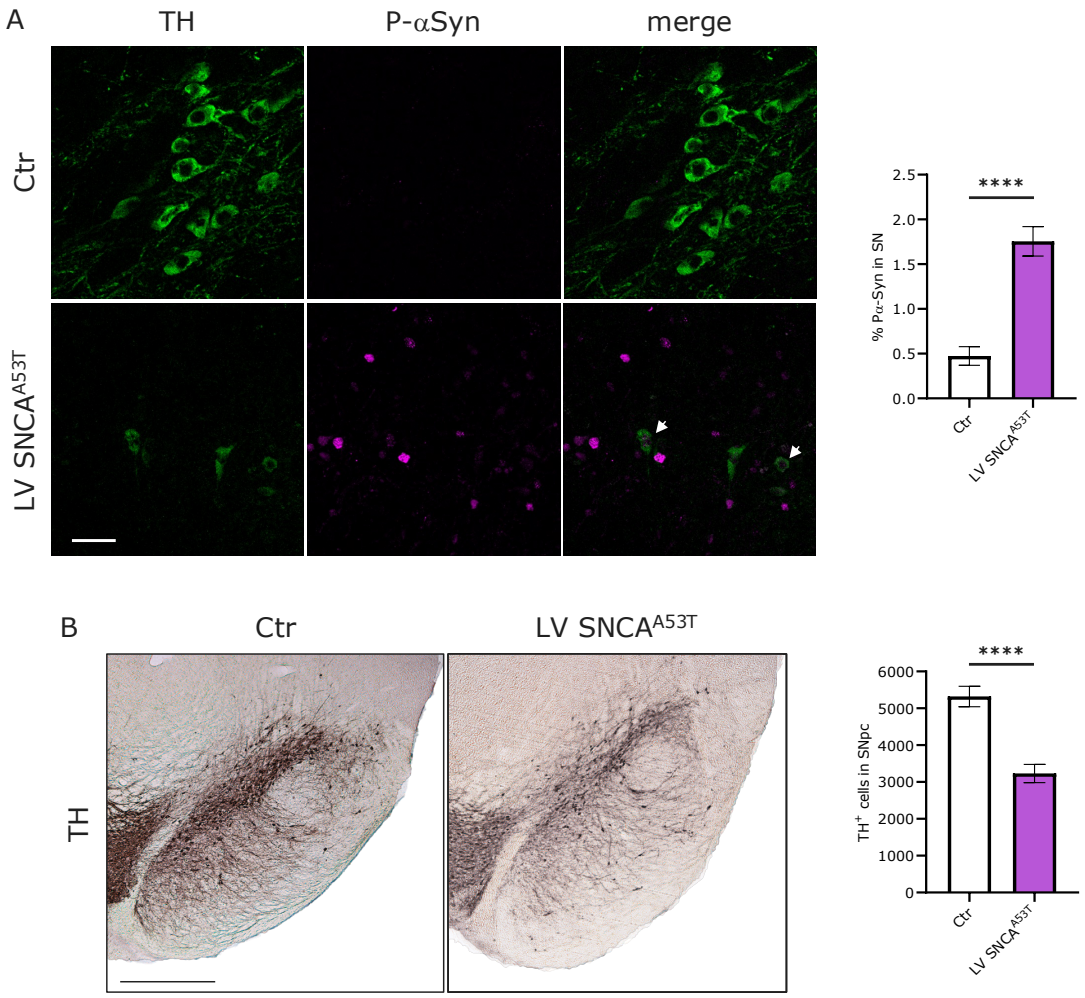

Figure 3.23. Accumulation of αSyn leads to neurodegeneration. *(A) Immunofluorescence staining and quantification of P-αSyn into the SN. Arrows pointing to TH⁺ neurons containing P-αSyn. Scale bar 25μm. Statistical analysis performed with Mann-Whitney test; ****p-value < 0.0001; n=6. (B) immunohistochemical analysis and counts of TH⁺ cell of the SN. Statistical analysis performed with unpaired T test; ****p-value < 0.0001; n=6. Scale bar 300μm.*

Furthermore, we characterized neuroinflammation in the presence of αSyn aggregates by evaluating activation of microglia and astrocytes by immunohistochemical staining for IBA1 and glial fibrillary acidic protein (GFAP), respectively. Both markers are characteristic of these cell types and are upregulated in response to activated states of microgliosis and astrocytosis. Importantly, increased IBA1 and GFAP stainings indicate cellular activation rather than an increase in cell number in presence of neuroinflammation (Norden et al., 2016). We observed a significant increase in IBA1⁺ area (+58.6 ± 18.1%) and GFAP⁺ area (+81.5 ± 30.9%) in presence of αSyn aggregation (fig. 3.24), reflecting enhanced glial activation.

CD68, a lysosomal protein expressed in microglia, is commonly used as a marker for phagocytic activity (Bido et al., 2024). Although we expected increased microglial phagocytosis in response to αSyn accumulation, $CD68^+$ area quantification did not reveal significant differences, suggesting that phagocytic activity was not markedly elevated under our conditions. This highlights the complexity of microglial responses, where activation as indicated by IBA1 upregulation may not always coincide with increased phagocytosis.

We concluded that the NSG PD model effectively recapitulates key pathological features of PD such as αSyn aggregation, dopaminergic neuron loss, and glial activation. However, its intrinsic lack of a human immune system, in particular T cells, limits its ability to model the full spectrum of neuroinflammatory responses critical to disease progression. This limitation underscores the need to investigate cellular immunotherapies within a humanized and more immunocompetent context in the future.

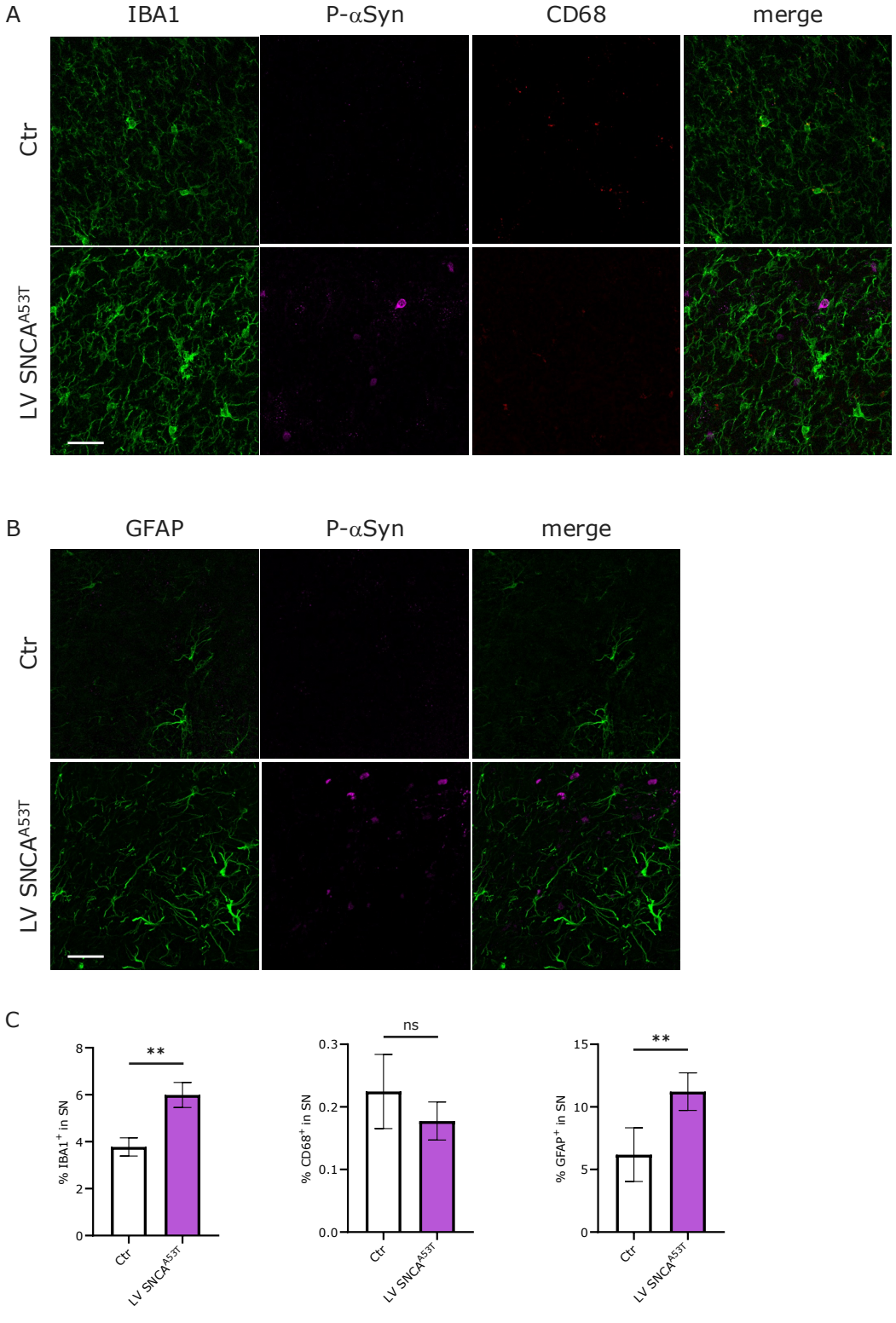

Figure 3.24. Microglial and astrocytic activation in presence of αSyn aggregation. *(A-B) Immunofluorescence analysis of (A) IBA1, CD68 and (B) GFAP in presence of αSyn accumulation compared to control condition. (C) Quantification of the area from the immunofluorescence. Statistical analysis of IBA1⁺ area with Unpaired T test and CD68⁺ and GFAP⁺ area with Mann-Whitney test. **p-value < 0.001; n=6. Scale bar 25μm.*

3.3.5 CAR Treg cell administration into NSG PD model

Building upon the pathological characterization of the NSG PD model, we next aimed to preliminarily evaluate the therapeutic potential of αSyn-specific CAR Tregs within this system. To this end, engineered FOXP3_aSyn-NB CAR Tregs were administered via intravenous (i.v.) and i.c. routes to assess their localization, persistence, and functionality in vivo (fig. 3.25).

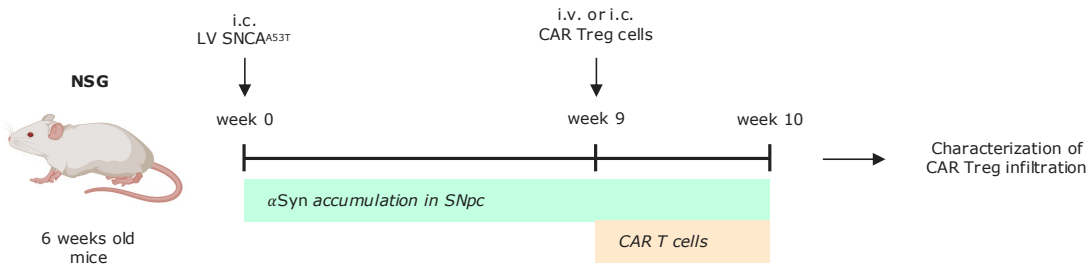

Figure 3.25. CAR Treg infusion in NSG PD mice. *Schematic representation of CAR Treg treatment of NSG PD model with 10 weeks of αSyn accumulation.*

We collected peripheral blood and brain tissue one week post-administration to evaluate CAR Treg presence. Given that this model lacks a human immune compartment, blood samples were analyzed to distinguish between murine and human CD45$^+$ hematopoietic cells. We detected human CD45$^+$ cells in mice after i.v. CAR Treg infusion but not after i.c. administration (fig. 3.26). Further gating confirmed that all hCD45$^+$ cells were CD4$^+$, indicating peripheral persistence of CAR Tregs at one week post-i.v. infusion.

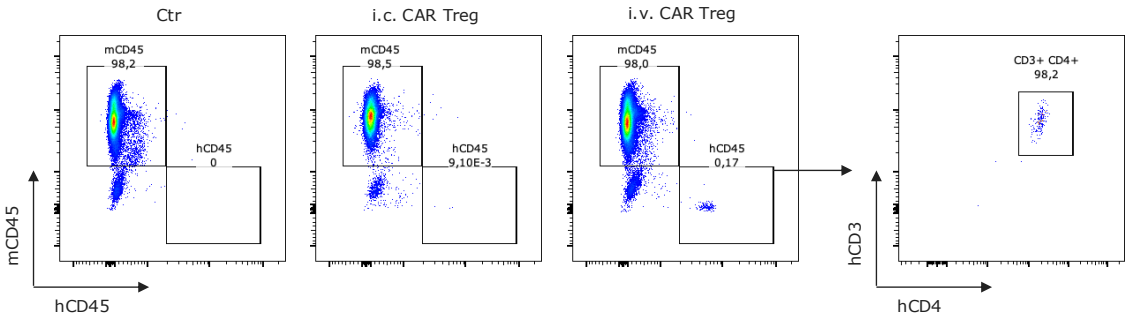

Figure 3.26. Permanence of CAR Tregs in the blood. *Flow cytometry analyses of hCD45$^+$ cells in the blood of CAR Treg-injected NSG PD mice. Gating on hCD45 population in i.v. injected animals shows a hCD3$^+$hCD4$^+$ population.*

CAR Tregs were not detected in brain tissue by flow cytometry or immunofluorescence after either administration route. We hypothesize that technical challenges with brain dissociation or immunofluorescence staining may have hindered

CD4+ T cell detection. Therefore, alternative methods such as bioluminescence imaging (BLI) with an in vivo imaging system (IVIS) are planned for improved cell trafficking and persistence analysis. Another aspect to investigate is whether CNS engraftment actually occurred. The absence of trophic factors and cytokines beneficial to cross-talk with human cells may be a factor, especially since the brain environment is deficient of IL-2, and murine and human interleukins show only partial cross-reactivity.

Based on these preliminary *in vivo* experiments, we conclude that lentiviral delivery of LV SNCA^{A53T} in NSG mice replicates previous data on immunocompetent mice regarding αSyn aggregation, dopaminergic neuron loss, and neuroinflammation. CAR Treg infusion showed short term peripheral persistence but failed to engraft in the CNS, guiding future strategy modifications. We will focus on the NSG-SGM3 humanized PD mouse model incorporating precise stereotaxic delivery and IVIS-based visualization. We hypothesize that, in this model, the presence of human immune infiltrate in response to αSyn accumulation could better replicate the complex inflammatory milieu of PD, favoring CAR Treg recruitment and persistence.

4. Materials and methods

4.1 Viral vectors

Anti-αSyn CAR constructs

Several CARs were designed during this project. All constructs are based on a second-generation CAR containing a CD28 transmembrane domain and intracellular CD28 and CD3ζ signaling domains. The first construct (CAR_NGFR) contains an antigen-binding domain derived from the NbSyn87 NB, which binds both aggregated and monomeric forms of αSyn, as described by Guilliams and colleagues (Guilliams et al., 2013). Two following constructs were based on a second-generation CAR embedding a long spacer derived from the wild-type NGFR, engineered by Casucci and colleagues (Casucci et al., 2018) to enable direct detection of the molecule and to optimize delivery. We generated a NB-based CAR (αSyn-NB) and a scFv-based CAR (αSyn-scFv) containing this spacer. The anti-αSyn scFv was derived from the variable heavy (V_H) and variable light (V_L) domains of the anti-αSyn antibody 306C7B3 described by Düchs and colleagues (Düchs et al., 2023), connected by the Whitlow spacer sequence (Whitlow et al., 1993).

Retroviral vectors design

Plasmids based on murine embryonic stem cell virus (MESV) were used to clone RV constructs. 5' long terminal repeat (LTR) was exploited as a promoter for transgene expression in all the described constructs. We designed RV *Foxp3*-PGK-CAR_NGFR carrying murine *Foxp3* followed by a human phosphoglycerate kinase promoter (PGK) controlling the expression of a bicistronic element consisting of the first NB-based CAR, P2A (porcine teschovirus-1 2A) self-cleaving peptide and a truncated form of nerve growth factor receptor (NGFR) lacking cytoplasmic signaling domains to act as a surface marker.

RV CAR_NGFR contains only the bicistronic element previously described, controlled by the 5' LTR promoter region. With the same logic RV *Foxp3* and RV *Foxp3*_NGFR were cloned.

Retroviral vector production

The ecotropic Platinum-E Retroviral Packaging Cell Line (Plat-E)(RV-101, Cell Biolabs) was maintained as manufacturer's instructions and RV production was based on manufacturer's instructions with additional modifications adapted from Eremenko and colleagues (Eremenko et al., 2021). A 100mm tissue culture dish was coated with 50μg/mL poly D-lysine (P6407-5MG, Sigma-Aldrich) for 30min at room

temperature. After washing with Dulbecco's Phosphate Buffered Saline (PBS), 8×10^6 Plat-E cells were plated to obtain an 80-90% confluency. After 8 hours a DNA-lipid complex was prepared using LF-LTX (15338-100, Invitrogen). Scaling up following manufacturer's instruction, 500μL of Optimem were mixed separately with 60μL LF-LTX or 20μg DNA and 20μl Plus Reagent. The two solutions were mixed and added dropwise to the cells after a 20min incubation at room temperature. After 16 hours the media was changed to 10mL of supplemented RPMI suitable for murine T cell culture (RPMI, FBS 10%, pen/strep 1%, Glutamine 1%, Non-essential amino acids 1%, Sodium-Pyruvate 1%, β-mercaptoethanol 0,05mM, HEPES 20mM). After 30 hours medium was collected and filtered through a 0,45μm PVDF membrane and stored at -80°C.

Lentiviral vectors design

For the transduction of human T cells, we first developed a bidirectional LV carrying a PGK promoter driving the expression of the NB-based CAR within the CAR_NGFR bicistronic element, and Cytomegalovirus (CMV) promoter controlling the expression of human Foxp3 (LV CMV-Foxp3 PGK-CAR_NGFR). For the expression of CAR_NGFR (LV CAR_NGFR) or Foxp3_NGFR (LV Foxp3_NGFR) single vectors with PGK promoter were used.

Furthermore, new constructs were generated by modifying a vector containing the PGK promoter driving human Foxp3 and an anti-CD19 scFv-based second-generation CAR incorporating a modified NGFR spacer together with CD3ζ and CD28 signaling domains (LV Foxp3_CD19 CAR). The two transgenes are separated by thosea asigna virus 2A (T2A) self-cleaving peptide. This construct was also used as an unrelated control CAR. For the generation of LV Foxp3_αSyn-NB-CAR and LV Foxp3_αSyn-scFV-CAR, the anti-CD19 scFv was replaced by the previously described anti-αSyn NB and scFv sequences.

Lentiviral vector production

Lentiviral replication-incompetent VSVg-coated lentiviral particles were packaged in 293T cells following a standard procedure in our laboratory (Bido et al., 2024). 7.5×10^6 HEK293T cells were plated in a 150mm dish the day before transfection. A conventional $CaCl_2$ transfection protocol was used. After 30h, medium was collected, filtered through a 0,22μm cellulose acetate membrane and centrifuged at 50'000×g for 2h at room temperature to concentrate the virus. The result of two dishes was resuspended in 80μL of PBS and stored at -80°C. The viral titer quantification was

performed using a qPCR-based lentivirus titer kit (LV900, Applied Biological Materials Inc) following manufacturer's instruction.

Antigen binding domain validation

The anti-αSyn NB selected and the newly designed anti-αSyn scFv were tested for antigen recognition on brain slices overexpressing αSyn. In order to detect the antigen binding domains in immunofluorescence, each domain was synthetized as a fusion protein together with a human IgG fragment crystallizable region (Fc). Stable cell lines were established for production of the humanized antibodies. LVs carrying each humanized antibody coding sequence and puromycin resistance were used to transduce HEK293T cells. Cells were expanded under puromycin selection for one week. Production of humanized antibodies was performed in PRO293a serum-free medium (BEBP12-764Q, Lonza). The supernatant containing the soluble humanized antibodies was collected and filtered after 72h. Supernatant from the production was used in place of primary antibody mix after supplementation with 3% BSA and 0.3% Tween and other primary antibodies.

4.2 Murine CD4+ T cells

Isolation

We obtained murine $CD4^+$ T cells from freshly harvested spleens of WT mice. We used the $CD4^+$ T Cell Isolation Kit mouse (130-104-454, Miltenyi Biotech) that isolates untouched $CD4^+$ T cells exploiting a cocktail of biotinylated antibodies (against CD8a, CD11b, CD19, CD45R, CD49b, CD105, MHC-class II, Ter-119 and TCRγ/δ) and Anti-Biotin MicroBeads. The procedure was performed following manufacturer's instructions. Briefly, we obtained a single cell suspension from spleens by dissociating the tissue by pressing with a 1mL syringe plunger trough a 70μm Nylon cell strainer (Falcon). After one wash in PBS, red blood cell lysis was performed with 1min incubation in ACK lysing buffer (Ammonium chloride 150mM, Potassium bicarbonate 10mM, Disodium EDTA 0.1mM) and then washed with PBS. Up to 1×10^7 cells were resuspended in 40μL MACS buffer (PBS, BSA 2,5%, EDTA 2mM) and 10μL of Antibody cocktail and incubated for 5min at 4°C. Then, 30μL of MACS buffer and 20μL of Anti-Biotin MicroBeads were added and incubated for 10min at 4°C. To proceed with the separation, LS MACS columns with Pre-Separation Filters (30μm) were mounted on a magnetic stand. After rinsing the columns with 3mL MACS buffer, the cell suspension was added to the column and $CD4^+$ T cells were collected

as the unlabeled population passing through, while tagged cells were retained in the column by the magnetic beads. Following, isolated cells were seeded for culturing.

Culturing and Transduction

After isolation, murine $CD4^+$ T cells were maintained in RPMI 1640 medium (Gibco) supplemented with 10% FBS, 1% pen/strep, 1% glutamine, 1% non-essential amino acids, 1% sodium-pyruvate, β-mercaptoethanol 0,05mM, HEPES 20mM. In order to maintain in culture and transduce the cells, they were activated with αCD3/28 polyclonal stimulus and murine interleukin-2 (IL-2). To do so, 24-well tissue culture plates were coated with 1μg/mL of anti-CD3 (555273, BD Pharmigen) at 37°C for 1h. After one wash with PBS, 1×10^6 cells per well were seeded in complete RPMI with 1μg/mL anti-CD28 (553295, BD Pharmigen) and 100U/mL mIL-2 (11271164001, Roche).

In order to obtain fully cycling cells for optimal transduction, cells were activated for two days prior to transduction. Then, RV-mediated transduction was performed through spinoculation. 24-well plates were prepared with 4°C O/N coating with 30μg/mL RetroNectin® (T100A, Takara) followed by blocking for 30min at room temperature with BSA 1% in PBS. In parallel to BSA blocking, 1mL of RV supernatant for each well was incubated with 10μL PLUS™ Reagent and 10μL LF-LTX for 30min at room temperature in gentle agitation. Then, 1×10^6 cells were resuspended in RV supernatant and added to the plate. Consequently, spinoculation was performed by centrifuging the plates at 2000×g for 1h30min at 37°C. Cells were then incubated at 37°C O/N and the spinoculation was repeated the following day adding new RV supernatant. The day after the second spinoculation, the cells were moved from the coated plate and maintained without stimulation with fresh RPMI supplemented medium with mIL-2. Cells were maintained either with 20U/mL mIL-2 in case of CAR transduction, while for reprogramming with FoxP3 the mIL-2 concentration was progressively increased to 100U/mL. Rapamycin was used to boost the Treg phenotype and added at a concentration of 100nM. On day 7 after isolation cells were used to carry out assays (fig. 4.1).

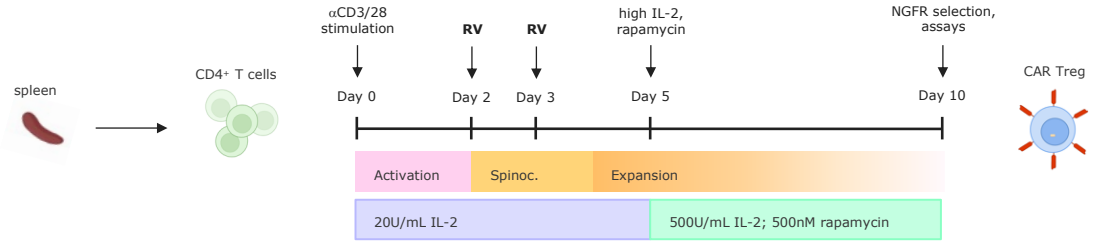

Figure 4.1. Timeline of murine CD4⁺ T cell engineering. *Overview of the experimental workflow used for activation, transduction, and expansion of primary CD4⁺ T cells prior to functional assays. Spinoc. = spinoculations.*

Flow cytometry

To evaluate efficiency transduction, cells were fluorescently labeled and analyzed with flow cytometry. Cells were collected, washed with PBS and incubated for 15min at room temperature with Live/Dead staining. After washing, cells were incubated with surface-staining antibodies for 10min at 4°C. Consequently, cells were permeabilized using FOXP3 Transcription Factor Staining Buffer Set (00-5523-00, Invitrogen) using manufacturer's instructions. Briefly, Permeabilization buffer was used to wash cells in between incubations with Fixation Buffer (15min), Permeabilization Buffer (10min) and intracellular-staining mix with Permeabilization buffer and anti-FOXP3 antibody (30min). Stained cells were consequently analyzed with BD FACS Canto II cytometer (Becton Dickinson) in the FRACTAL cytometry facility of San Raffaele Scientific institute. Dyes and antibodies used are listed in table 4.1.

Staining	Fluorophore	Dilution	Catalog #	Manufacturer
Live/Dead	APC Cy7	1:2000	L34975	Invitrogen
CD4	VioGreen	1:100	130-118-693	Miltenyi Biotec
CD25	PE Vio770	1:100	130-123-893	Miltenyi Biotec
NGFR	Vio Bright 423	1:25	130-131-824	Miltenyi Biotec
FOXP3	APC	1:50	17-5773-82	Invitrogen

Table 4.1. Flow cytometry dyes and antibodies.

NGFR magnetic selection

In order to isolate transduced cells, MACSelect™ LNGFR MicroBeads (130-091-330, Miltenyi Biotec) were used to perform magnetic positive selection of NGFR⁺ cells following manufacturer's instructions. Cultured cells were collected and washed with PBS, then resuspended in 320μL MACS buffer with 80μL beads per 4×10^7 total cells

and incubated for 15min on ice. After washing LS columns and Pre-Separation Filters with 3mL MACS buffer, the cell suspension was added to the column. 3 washes with 3 mL MACS buffer were performed to elute the negative population. The columns were removed from the magnetic stand to allow to retrieve the $NGFR^+$ magnetically-labeled cells by flushing with 5mL MACS buffer, then counted and reseeded used for assays.

In vitro assays

Both activation and suppression assays required the staining of cells with proliferation dyes to assess the proliferative activity of different cell populations. In particular, we used proliferation dyes that bind to cellular proteins and are distributed equally between daughter cells upon division, determining the halving of the fluorescence intensity with each generation and allowing identification of the first peak on the right as undivided cells, with successive divisions forming consecutive peaks toward the left (fig. 4.2).

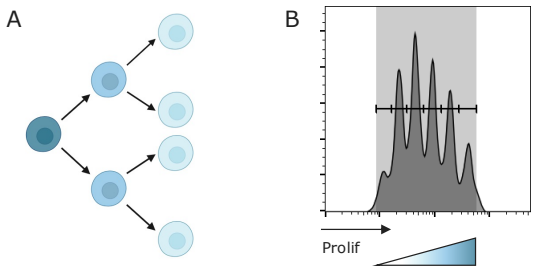

Figure 4.2. Proliferation dye principle. *Schematic representation illustrating (A) how proliferation dye fluorescence intensity is halved in daughter cells after each division and (B) how successive generations appear as discrete peaks in the flow cytometry profile. Image created with Biorender.*

We used eFluor™ 450 and eFluor™ 670 Cell Proliferation Dyes (65-0842-85 and 65-0840-85, Thermo Fisher Scientific) following manufacturer's instructions. Briefly, cells were collected and washed with PBS to remove FBS, resuspended in 500μL PBS. A solution of proliferation dye 1:500 in PBS was added while vortexing and the mixture was incubated for 10min at 37°C in the dark. After adding 5 mL of cold complete medium, the cell suspension was kept on ice for 5 min, then washed three times and counted before assay setup. At the end of each assay, cells were washed, stained with live/dead viability dye and fixed. Flow cytometric acquisition was performed using a Cytoflex S cytometer (Beckman Coulter) in the FRACTAL cytometry facility of San Raffaele Scientific institute.

Activation assay

After proliferation dye staining and counting, 50×10^3 cells were seeded in 96-well round-bottom tissue culture-treated plates in a volume of 100μL supplemented RPMI. Different stimuli were then added in fresh supplemented RPMI to reach the final volume of 200μL. For αCD3/28 stimulation, wells were pre-coated with 1μg/mL of anti-CD3 antibody, while 1μg/mL anti-CD28 antibody was added to the culture medium. BSA was used at a final concentration of 1%, while PFF were used at 1μM for standard assay and in serial 1:10 dilutions for dose-response analysis. Unstimulated conditions did not receive any antigen. All cultures were supplemented with 200U/mL recombinant mIL-2.

Polyclonal suppression assay

Freshly isolated $CD4^+$ T cells were used as Tconv. After labeling Tregs and Tconvs with distinct proliferation dyes, cells were counted and seeded in 96-well round-bottom tissue culture-treated plates pre-coated with 1μg/mL anti-CD3 antibody. For assays with a 2:1 maximum Treg:Tconv ratio, 2×10^5 Tregs in 200μL fresh RPMI were plated in the first well and serial 1:2 dilutions were performed by transferring 100 μL of the cell suspension into the following wells containing an equal volume of medium. For assays with a 4:1 maximum ratio, 4×10^5 Tregs were used in the initial suspension. Subsequently, 5×10^4 Tconv in 50μL were added to each well and the remaining 50 μL were used to add anti-CD28 antibody (1μg/mL). Control conditions included Tregs and Tconvs cultured separately, with or without αCD3/28 stimulation.

4.3 Human $CD4^+$ T cells

Isolation

Primary human $CD4^+$ T cells were isolated from buffy coat collected from healthy donors, after written informed consent, according to the San Raffaele Scientific Institutional Ethical Committee guidelines. We used RosetteSep™ Human $CD4^+$ T Cell Enrichment Cocktail (#15022, STEMCELL Technologies), that allows to obtain untouched $CD4^+$ T cells by negative selection. This reagent contains an antibody cocktail that binds unwanted cells to multiple red blood cells, forming immunorosettes whose higher density enables their separation using a density gradient medium. The kit was used following manufacturer's instructions. Briefly, the buffy coat was mixed with RosetteSep™ reagent (50μL reagent per 1mL buffy coat) and incubated for 20min at RT. The sample was then diluted using an equal volume of PBS with 10%

FBS and layered on Histopaque®-1077 Hybri-Max™ density gradient medium (H8889, Sigma-Aldrich). After centrifuging at 1200×g for 20min without brake, the enriched cell layer was collected and washed twice with PBS with 10% FBS. The isolated cell suspension was counted and either seeded for culturing or frozen for -80°C storage.

Culturing and transduction

Primary CD4⁺ T cells were cultured in X-VIVO™ 15 Hematopoietic Serum-Free Medium (BW04-418Q, Lonza) supplemented with 10% FBS and 100 μg/ml Primocin (ant-pm-1, InvivoGen). Cells were activated using Dynabeads™ Human T-Activator CD3/CD28 for T Cell Expansion and Activation (11131D, Gibco) and 200U/mL human IL-2 for two days prior to transduction. LV-mediated transduction was performed in reduced culture volume and 24h after fresh media was added to stop the process. Three days after transfection the culture conditions were adjusted to 1000U/mL human IL-2 and 500nM rapamycin to promote Treg cell survival. On day 9 post-isolation, cells were restimulated with αCD3/28 beads to promote expansion. On day 14 the beads were removed to induce a resting state and the cells were subsequently frozen on day 21 (fig. 4.3). Cells were stored at -80°C until use.

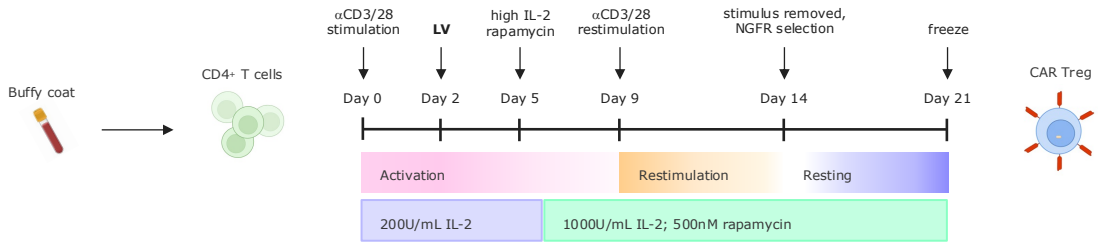

Figure 4.3. Timeline of human CD4⁺ T cell engineering. *Schematic representation of the experimental workflow used for activation, transduction, and expansion of primary CD4⁺ T cells prior to functional assays. Image created with Biorender.*

Flow cytometry

Efficiency of transduction was evaluated based on flow cytometry analysis following the same procedure as murine cells using antibodies listed in table 4.2.

Staining	Fluorophore	Dilution	Catalog #	Manufacturer
Live/Dead	APC Cy7	1:2000	L34975	Invitrogen
CD4	VioBright V423	1:200	130-126-322	Miltenyi Biotec
CD25	VioBright B515	1:100	130-113-849	Miltenyi Biotec
NGFR	PE	1:100	130-113-849	Miltenyi Biotec
FOXP3	APC	1:50	17-5773-82	Invitrogen

Table 4.2. Flow cytometry antibodies and dyes.

In vitro assays

In vitro assays were performed following the same general protocols used for murine T cells. The same proliferation dyes were employed and both activation and suppression assays were conducted according to the procedures established for murine cells, with minor adjustments reflecting human T-cell culture requirements. Specifically, X-VIVO 15 medium was used as the culturing medium, together with recombinant hIL-2 and αCD3/28 activation beads. CAR_NGFR $CD4^+$ T cells were activated in presence of 200U/mL hIL-2, while CAR Tregs were stimulated with 1000U/mL hIL-2. For both activation and polyclonal suppression assay αCD3/28 activation beads were used at a 1:1 bead-to-cell ratio. αSyn antigens such as PFF, oligomers and monomers were used at a concentration of 1μM.

Antigen specific suppression assay

In order to test αSyn-mediated suppression by CAR Tregs, Foxp3_αSyn-NB, Foxp3_αSyn-scFv and Foxp3_CD19 cells were pre-stimulated separately from Tconv. Tconv were stimulated with αCD3/28 beads using a 1:1 bead-to-cell ratio and 200U/mL IL-2, while Tregs were stimulated with 1000U/mL IL-2 with PFF. Control conditions included Tregs pre-incubated without stimuli or with αCD3/28 beads as negative and positive controls for suppression, respectively. After 48h of pre-stimulation, beads were magnetically removed and cells were washed and counted prior to seeding. Similarly to polyclonal suppression assays, Tregs were seeded in serial dilutions, Tconvs were added and finally PFF were added for the conditions involving Tregs stimulated with αSyn.

ELISA

Supernatants from activation and suppression assay wells were collected for ELISA analysis. Specifically, IL-10 production by CAR Tregs in activation assays was measured using a human IL-10 ELISA kit (EHIL10, Invitrogen), following the

manufacturer's instructions. Samples and standards were incubated for 2 hours at room temperature in plates pre-coated with capture antibody provided by the kit. After incubation, plates were washed five times. A detection antibody conjugated with horseradish peroxidase (HRP) was then added and incubated for 1 hour at room temperature, followed by three washes. Subsequently, a substrate solution containing tetramethylbenzidine (TMB) and hydrogen peroxide was added and incubated for 10 minutes in the dark at room temperature. The reaction was stopped using stop solution. Absorbance was measured at 450 nm and 550 nm, and the 550 nm reading was subtracted from the 450 nm value. IL-10 concentrations were calculated using linear regression based on the standard curve.

Cellular immunostaining analysis

In order to perform immunofluorescence on $CD4^+$ T cells, cells were collected and 15×10^4 cells were resuspended in 100μL in order to perform cytocentrifugation using Cytospin 4 (Thermo Fisher Scientific) and obtain a single cell layer on glass slides. Cells were fixed with 4% PFA, blocked for 1h at room temperature in PBS with 3% BSA, 0.3% Tween and consequently stained for immunofluorescence. Antibody mix (PBS with 1% BSA, 0.1% Tween) with primary antibodies was incubated at 4°C overnight. After 3 washes with PBS, the antibody mix with secondary antibodies and Hoechst nucleic acid stain was incubated for 1h at room temperature. After three washes in PBS, coverslips were mounted using fluorescence mounting medium (S3023, Dako). Images were acquired with Leica SP8 confocal microscope in the ALEMBIC imaging facility of San Raffaele Scientific Institute. Antibodies used are listed in table 4.3.

Primary antibody	Host	Dilution	Catalog #	Manufacturer
CD3	Rat	1:100	MCA1477	Bio-Rad
NGFR	Rabbit	1:1000	8238T	Cell Signaling

Secondary antibody	Fluorescence	Dilution	Catalog #	Manufacturer
Anti-Rabbit	488	1:500	A21206	Thermo F. S.
Anti-Rat	546	1:500	A11081	Thermo F. S.

Table 4.3. Primary and secondary antibodies for cellular immunofluorescence.

4.4 *In vivo* experiments

Animals

Wild type (WT) C57BL/6j mice and NOD.Cg-*Prkdc*^{scid} *Il2rg*^{tm1Wjl}/SzJ (NSG) mice were purchased from Jackson Laboratories and housed in the San Raffaele Hospital animal Facility. The mice were raised under a 12h dark-light cycle, with controlled temperature (25°C) and relative humidity (50-60%) and had free access to food and water. All experiments were performed in accordance with protocols approved by internal Institutional Animal Care and Use Committee (IACUC 1142, 1351, 1360 and 1514 Ospedale San Raffaele, Milan, Italy) and reported to the Italian Ministry of Health according to the European Commission Council Directive 2010/63/EU.

Stereotaxic injections

To perform surgical procedures isoflurane anesthetization was used. During the procedure oxygen and isoflurane levels were regulated based on the mouse health state. Stereotaxic injections were used to administer LVs or T cells in the SNpc. LVs were injected at a 2×10^9 UI/mL concentration using a 34-gauge needle, and control animals received a mock LV preparation consisting of empty viral capsids. For T cell injections, 5×10^4 cells were delivered with a 26-gauge needle at a higher dorso-ventral coordinate to prevent disruption of the tissue by the bigger needle, and an equivalent volume of PBS was administered in control conditions. The standard volume injected was 1,5μL at a 0,25 L/min flow rate at different coordinates from the skull, based on the mice strain (table 4.4).

Strain	LV	cells
C57B/6	AP = −2,9; ML = ±1,2; DV = −4,4	AP = −2,9; ML = ±1,2; DV = −4,2
NSG	AP = −3,9; ML = ±1,9; DV = −4,9	AP = −3,9; ML = ±1,9; DV = −4,7

Table 4.4. Stereotaxic injection coordinates from skull. *AP=Antero-Posterior, ML=Medio-Lateral, DV=Dorso-Ventral.*

Humanized NSG-SGM3 mice

The experiment using humanized NSG-SGM3 mice was conducted in collaboration with the Innovative Immunotherapies Unit at the San Raffaele Scientific Institute. The mice underwent sublethal irradiation followed by transplantation with hHSCs. Specifically, intravenous infusion of 1×10^5 $CD34^+$ hHSCs cells was performed to establish humanization of the immune compartment. Humanization was monitored weekly via flow cytometric analysis of peripheral blood. Since initial repopulation is predominantly myeloid, followed later by B cells with slow T cell repopulation, 1×10^6

T cell receptor knockout (TCR-KO) T cells were intravenously administered 6 weeks post-irradiation to enhance T cell repopulation before high B cell expansion could affect survival. TCR-KO T cells were used to prevent adverse reactions with non-autologous hHSCs.

To generate a Parkinson's disease model in this murine system, we performed bilateral intracranial injections of LV SNCA^{A53T}, that expresses the transgene under a constitutive Ef1a promoter (fig. 4.4). Injections were performed using stereotactic coordinates conventionally used for C57BL/6 mice.

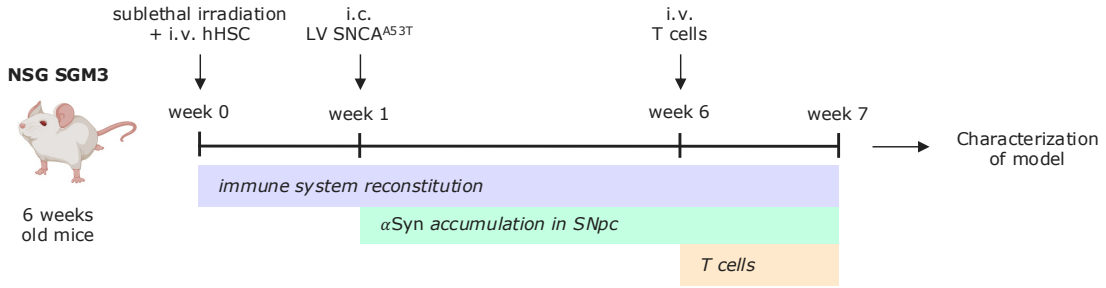

Figure 4.4. NSG-SGM3 mouse model. *Schematic representation of the treatments administered to NSG-SGM3 mice. Image created with Biorender.*

NSG PD mouse model

Non-humanized NSG mice were used to optimize stereotaxic injection coordinates and to develop an αSyn overexpression model. Initial optimization involved stereotaxic administration of a lentiviral vector expressing GFP under the constitutive Ef1a promoter (LV GFP). Mice were euthanized 72 hours post-injection to proceed with immunofluorescence analysis to determine the precise point of injection to target the SNpc.

For model generation, i.c. injections of LV SNCA^{A53T} were performed using the optimized NSG stereotaxic coordinates (Fig. 4.5). Mice were sacrificed at 10 weeks post-injection for characterization of αSyn accumulation, neurodegeneration, and neuroinflammation into the SN. To assess CAR Treg persistence and localization, engineered CAR Tregs were infused either in i.c. (5×10^4 cells) or i.v. (1×10^6 cells) at 9 weeks post-LV injection, with animals sacrificed after one week and collection of peripheral blood and brain tissue.

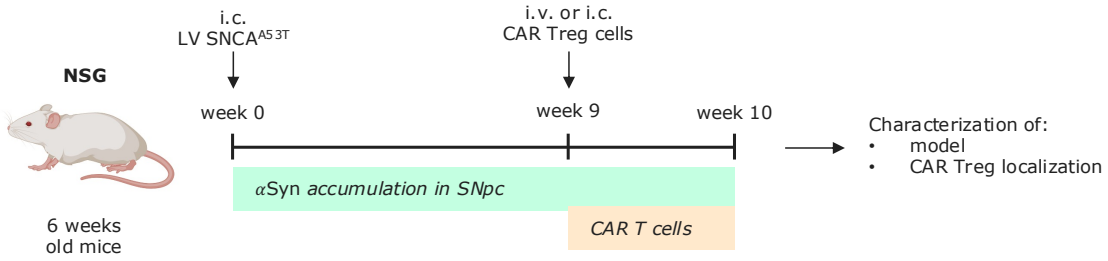

Figure 4.5. NSG mouse model. *Schematic representation of the timeline used for NSG PD mouse model. Image created with Biorender.*

Immunofluorescence and immunohistochemistry analysis

Animals were perfused with saline solution followed by 4% PFA. Brains were collected and immersed overnight in PFA 4% and then in PBS with 20% sucrose cryopreserving solution for one day. The tissue was consequently flash frozen and conserved at -80°C until cut into 50μm slices with a cryostat.

For immunofluorescence, free floating slices were incubated in PBS with 3% H_2O_2, 10% methanol for 10min and then permeabilized in PBS with Triton 2% for 20min. After 2 washes in PBS immunofluorescence staining was performed with the process previously indicated for single cell layer on glass slide.

For immunohistochemistry, brain slices were incubated in PBS with 3% H_2O_2 for 10min and then blocked for 1h at room temperature in PBS with 3% BSA, 0.3% Triton. Antibody mix (PBS with 1% BSA, 1% Triton) with primary antibodies was incubated at 4°C overnight. After incubating in in PBS with 3% H_2O_2 for 10min and 3 washes with PBS, the antibody mix with secondary biotinylated antibodies was incubated for 1h at room temperature. Following four washes in PBS, slices were incubated in ABC solution (Vector Labs), which contains HRP conjugated with avidin and biotin. HRP catalyzes the subsequent reaction with DAB solution (Vector Labs), producing a brown precipitate that visualizes antigen localization. After DAB revelation and four washes, brain slices were mounted on agar-coated glass slides and allowed to dry at 36°C for 20 minutes. The tissue was dehydrated overnight in chloroform-ethanol followed by 1 hour in xylene. Coverslips were mounted with Eukitt mounting medium (03989, Sigma-Aldrich). Antibodies used are listed in table 4.5.

Primary antibody	Host	Dilution	Catalog #	Manufacturer
αSyn	Mouse	1:100	180215	Thermo F. S.
Phosphorylated-αSyn	Rabbit	1:1000	ab51253	Abcam
CD68	Rat	1:1000	ab53444	Abcam
GFP	Chicken	1:500	A10262	Thermo F. S.
GFAP	Chicken	1:1000	ab4674	Abcam
Human Nuclear Ag.	Rabbit	1:100	RBM-346-P1	Thermo F. S.
Iba1	Chicken	1:1000	234009	DBA
TH	Chicken	1:1000	AB-10312	Immuno-Sci
TH	Mouse	1:1000	MAB318	Millipore

Secondary antibody	Conjugated	Dilution	Catalog #	Manufacturer
Anti-chicken	488	1:500	A11039	Thermo F. S.
Anti-chicken	647	1:500	A21449	Thermo F. S.
Anti-chicken	Biotinylated	1:300	BA-9010	Vector Labs
Anti-human	488	1:100	A55747	Invitrogen
Anti-mouse	488	1:500	A21202	Thermo F. S.
Anti-mouse	546	1:500	A10036	Thermo F. S.
Anti-mouse	647	1:500	A31571	Thermo F. S.
Anti-rabbit	488	1:500	A21206	Thermo F. S.
Anti-rabbit	546	1:500	A10040	Thermo F. S.
Anti-rat	546	1:500	A11081	Thermo F. S.

Table 4.5. Primary and secondary antibodies for immunofluorescence and immunohistochemistry.

Stereological cell count

In order to estimate the number of dopaminergic neurons in the SN and evaluate the extent of neurodegeneration, unbiased stereological counting was performed using the optical fractionator method. After performing TH immunohistochemistry, five coronal brain sections per animal, spaced 200 μm apart and covering the rostro-caudal extent of the SN, were selected for analysis. A Leica DM4000B motorized microscope equipped with Stereo Investigator software (MBF Bioscience) was used at 40x magnification.

After manually delineating the boundaries of the SN under low magnification, the software applied a systematic random sampling grid to select counting frames within

the traced area. TH^+ cell bodies were then counted manually within each frame using optical fractionation parameters. The software output provided an estimated total number of dopaminergic neurons per SN for each animal.

4.5 Graphs and statistical analysis

Flow cytometry data were analyzed using FlowJo software v10.10.0 (Becton Dickinson). All statistical analyses and graph generation were performed in GraphPad Prism v10.0.0 (GraphPad Software). Data are expressed as mean ± SEM unless otherwise specified. Comparisons between two groups were performed using unpaired t-tests and multiple comparisons were analyzed using one-way or two-way ANOVA followed by appropriate post hoc tests. P-values < 0.05 were considered statistically significant.

5. Discussion

This study aimed to engineer αSyn-specific CAR Tregs as a novel immunotherapy for PD, with a primary goal to provide antigen-specific and durable immunomodulation of neuroinflammation. A systematic and stepwise approach was employed, involving both murine and human $CD4^+$ T cells for *in vitro* evaluation, alongside the establishment of relevant *in vivo* preclinical models to assess therapeutic efficacy and translational feasibility.

Initial in vitro experiments with murine T cells provided essential proof-of-concept for CAR expression and antigen-dependent functionality. Efficient lentiviral transduction yielded robust CAR expression in murine $CD4^+$ T cells, which exhibited selective proliferative responses to pathological αSyn aggregates, confirming the construct's antigen specificity. However, critical limitations emerged, including compromised viability and technical difficulties to evaluate suppressive capacity *in vitro*, as well as limited *in vivo* persistence following adoptive transfer. These challenges led to a strategic shift towards human T cells, which are inherently more robust in *ex vivo* manipulation and provide a more translationally relevant model to evaluate human-specific CAR Treg constructs.

In human $CD4^+$ T cells, LV delivery of CAR and FOXP3 constructs was optimized. An initial vector containing a *FOXP3* sequence available in-house failed to produce reliable FOXP3 expression, while a construct provided by collaborators with a different *FOXP3* sequence and bicistronic architecture yielded robust and stable FOXP3 expression. We attribute this improved expression and phenotypic stability primarily to the optimized *FOXP3* sequence and vector design, emphasizing the necessity of construct optimization in generating functional CAR Tregs. Moreover, this construct enabled delivery of both *FOXP3* and the NGFR spacer-embedded CAR in a single vector, optimizing simultaneous transgene expression and facilitating direct detection of the CAR molecule. This direct detection allowed us to qualitatively analyze CAR distribution on the cell surface, confirming the absence of spontaneous clustering that could cause detrimental constitutive activation (Long et al., 2015).

In this optimized setting involving human αSyn CAR Tregs engineered with a single LV vector, FOXP3 overexpression determined an efficient reprogramming of $CD4^+$ T cells into Tregs, showing consistent Tconv suppression in polyclonal suppression assays. We employed two different αSyn CARs, comparing their functionality in different assays. Both antigen binding domains demonstrated selective localization to αSyn burdened tissue, confirming their specificity. However, the αSyn-NB CAR demonstrated superior functional features: it elicited antigen-dependent proliferation

and suppression, whereas the scFv-based CAR showed antigen-independent activation suggestive of tonic signaling. The structural simplicity of NB-based CARs, consisting of a single-domain nanobody, reduces aggregation propensity and homomeric interactions that underlie tonic signaling, thereby enhancing functional stability and precision of activation (Safarzadeh Kozani et al., 2022). This mechanistic advantage positions the NB-CAR as a more selective and potentially safer therapeutic platform for PD.

The selection of the NB-based CAR was a critical strategic decision supported by multiple key findings in our *in vitro* analyses. A particularly noteworthy aspect is its selectivity for aggregated αSyn conformers: human CAR_NGFR cells responded selectively to highly aggregated αSyn forms with minimal or no activation by monomeric or oligomeric αSyn species. This selective responsiveness is especially important given the physiological diversity the physiological diversity and compartmentalization of αSyn. Even though monomeric αSyn is primarily intracellular and not readily accessible for CAR interaction, the ability to specifically target pathological extracellular aggregates optimizes therapeutic precision. By focusing CAR Tregs on aggregated αSyn fibrils concentrated within affected brain regions, this strategy enhances immunomodulation precisely where neuroinflammation and neurodegeneration are most pronounced, while sparing physiological monomeric αSyn found systemically. This reduces the likelihood of off-target immunosuppression and preserves normal αSyn functions.

We hypothesize that although the nanobody embedded in the CAR can bind all conformers of αSyn (Guilliams et al., 2013), the deployment within the CAR context inherently favors recognition of aggregated forms. This is likely due to the multivalent pattern of antigen presentation on fibrils, which allows for crosslinking and clustering of CAR molecules on the T cell surface. Such multivalent crosslinking is a well-established mechanism of receptor activation in CAR T cells, requiring simultaneous engagement of multiple CARs by repetitive antigen epitopes to trigger robust downstream signaling and avoid activation by monomeric species that provide insufficient avidity (Wu et al., 2020).

The validation of these promising functional characteristics with CAR_NGFR variants lays a solid foundation for advancing the FOXP3_NB-CAR constructs, wherein FOXP3-driven regulatory stability will be combined with highly specific antigen targeting. The critical next step is to ensure that FOXP3 co-expression preserves the NB-CAR's selectivity and dose responsiveness while conferring durable suppressive function.

For *in vivo* validation, immunodeficient mouse models were developed. Humanized NSG-SGM3 mice, reconstituted with human hematopoietic components and transduced with LV SNCA^{A53T}, were intended to recapitulate PD pathology including αSyn aggregation and neuroinflammation. However, technical challenges with stereotaxic injection led to mistargeting outside the SN, preventing evaluation of neurodegeneration and neuroinflammation at the intended site. Nevertheless, presence of human myeloid infiltration alongside αSyn accumulation was documented. Unexpectedly, lymphocytic infiltration was not observed, potentially due to technical detection limitations or reagent differences, as previous studies mainly profiled murine immune cells (Bido et al., 2021, 2024; Williams et al., 2021).

Non-humanized NSG mice were subsequently employed for optimization of injections and induction of PD-like pathology. These mice exhibited robust αSyn aggregation into the SN, dopaminergic neuron loss and gliosis consistent with preclinical models (Bido et al., 2021, 2024; Williams et al., 2021).

Human CAR Tregs infused into this model persisted in peripheral blood but were undetectable in the CNS. This likely reflects technical detection limits or, importantly, the absence of a human immune microenvironment necessary for Treg survival, providing critical antigen-presenting cell interactions and human cytokines like IL-2, which conventional NSG mice lack (Olson et al., 2023).

Experiments on non-humanized NSG mice highlighted that absence of human immune components restricts the model's capacity to reproduce full immune infiltration and neuroinflammation. Therefore, future *in vivo* studies will prioritize humanized mouse models with comprehensive immune reconstitution to accurately capture the full neuroinflammatory milieu observed in PD, enabling rigorous assessment of CAR Treg engraftment, persistence, CNS homing and functionality, focusing on migration to sites of αSyn accumulation and exploring their potential to moderate lymphocytic infiltration and neuroinflammatory pathology. State-of-the-art imaging techniques, including BLI using IVIS, will track CAR Treg biodistribution and dynamics *in vivo*, facilitating a nuanced understanding of their therapeutic potential.

To overcome the limitations related to rodent models, future studies may explore the application of αSyn-expressing human organoid platforms obtained from patient-derived iPSCs, which offer a compelling human-specific testing ground for this CAR Treg system. In particular, midbrain-like organoids harboring functional dopaminergic neurons overexpressing αSyn (Jo et al., 2016) can integrate iPSC-derived microglia (Zhang et al., 2023) and primary human T cells (Gerasimova et al., 2025), recapitulating PD hallmarks like αSyn aggregation, neuronal vulnerability and neuroinflammation. Previous studies on organoids co-cultured with CAR T cells

demonstrate how these platforms enable evaluation of CAR T cell migration and activation (Jassin et al., 2025). Therefore, neuroimmune organoids modeling PD could enable detailed evaluation of αSyn CAR Treg migration, antigen recognition and immunomodulatory effects on glial and T cell responses. Moreover, organoid-based systems support high-resolution imaging of CAR Treg infiltration, persistence and spatial engagement with αSyn pathology, offering mechanistic insights challenging to obtain *in vivo*. Although organoids cannot fully recapitulate the complexity of the intact immune system or CNS vasculature, their use as an intermediate translational model would strengthen preclinical validation of αSyn CAR Tregs.

In summary, this study establishes a robust platform for generating functional αSyn-specific CAR Tregs with precise antigen selectivity and durable suppressive capacity, and highlights essential considerations for their translational application in PD. The integration of human immune cells, optimized genetic engineering, and physiologically relevant models offers a clear path toward clinical development of next-generation antigen-specific immunotherapies for PD.

Bibliography

1. Aarts-Riemens, T., Emmelot, M. E., Verdonck, L. F., & Mutis, T. (2008). Forced overexpression of either of the two common human Foxp3 isoforms can iduce regulatory T cells from CD4+CD25- cells. *European Journal of Immunology*, *38*(5), 1381–1390. https://doi.org/10.1002/eji.200737590

2. Alfaidi, M., Barker, R. A., & Kuan, W. L. (2025). An update on immune-based alpha-synuclein trials in Parkinson's disease. *Journal of Neurology*, *272*(1). https://doi.org/10.1007/s00415-024-12770-x

3. Allan, S. E., Alstad, A. N., Merindol, N., Crellin, N. K., Amendola, M., Bacchetta, R., Naldini, L., Roncarolo, M. G., Soudeyns, H., & Levings, M. K. (2008). Generation of potent and stable human CD4+ T regulatory cells by activation-independent expression of FOXP3. *Molecular Therapy*, *16*(1), 194–202. https://doi.org/10.1038/sj.mt.6300341

4. Arjomandnejad, M., Kopec, A. L., & Keeler, A. M. (2022). CAR-T Regulatory (CAR-Treg) Cells: Engineering and Applications. *Biomedicines*, *10*(2). https://doi.org/10.3390/biomedicines10020287

5. Bacchetta, R., Roncarolo, M. G., Sato, Y., Naldini, L., & Passerini, L. (2020). *WO2020247805A1 - FOXP3 Engineered CD4+ T Cells for use in Treg-Based Immunotherapy*. World Intellectual Property Organization.

6. Badr, M., McFleder, R. L., Wu, J., Knorr, S., Koprich, J. B., Hünig, T., Brotchie, J. M., Volkmann, J., Lutz, M. B., & Ip, C. W. (2022). Expansion of regulatory T cells by CD28 superagonistic antibodies attenuates neurodegeneration in A53T-α-synuclein Parkinson's disease mice. *Journal of Neuroinflammation*, *19*(1), 319. https://doi.org/10.1186/s12974-022-02685-7

7. Battaglia, M., Stabilini, A., & Roncarolo, M. G. (2005). Rapamycin selectively expands CD4+CD25+FoxP3+ regulatory T cells. *Blood*, *105*(12), 4743–4748. https://doi.org/10.1182/BLOOD-2004-10-3932

8. Bido, S., Muggeo, S., Massimino, L., Marzi, M. J., Giannelli, S. G., Melacini, E., Nannoni, M., Gambarè, D., Bellini, E., Ordazzo, G., Rossi,

G., Maffezzini, C., Iannelli, A., Luoni, M., Bagicaluppi, M., Gregori, S., Nicassio, F., & Broccoli, V. (2021). Microglia-specific overexpression of α-synuclein leads to severe dopaminergic neurodegeneration by phagocytic exhaustion and oxidative toxicity. *Nature Communications 2021 12:1*, *12*(1), 1–15. https://doi.org/10.1038/s41467-021-26519-x

9. Bido, S., Nannoni, M., Muggeo, S., Gambarè, D., Ruffini, G., Bellini, E., Passeri, L., Iaia, S., Luoni, M., Provinciali, M., Giannelli, S. G., Giannese, F., Lazarevic, D., Gregori, S., & Broccoli, V. (2024). Microglia-specific IL-10 gene delivery inhibits neuroinflammation and neurodegeneration in a mouse model of Parkinson's disease. *Sci. Transl. Med*, *16*, 8563. https://www.science.org

10. Bloem, B. R., Okun, M. S., & Klein, C. (2021). Parkinson's disease. In *The Lancet* (Vol. 397, Issue 10291, pp. 2284–2303). Elsevier B.V. https://doi.org/10.1016/S0140-6736(21)00218-X

11. Boroughs, A. C., Larson, R. C., Choi, B. D., Bouffard, A. A., Riley, L. S., Schiferle, E., Kulkarni, A. S., Cetrulo, C. L., Ting, D., Blazar, B. R., Demehri, S., & Maus, M. V. (2019). Chimeric antigen receptor costimulation domains modulate human regulatory T cell function. *JCI Insight*, *4*(8). https://doi.org/10.1172/jci.insight.126194

12. Braak, H., Del Tredici, K., Rüb, U., De Vos, R. A. I., Jansen Steur, E. N. H., & Braak, E. (2003). Staging of brain pathology related to sporadic Parkinson's disease. *Neurobiology of Aging*, *24*(2), 197–211. https://doi.org/10.1016/S0197-4580(02)00065-9

13. Casucci, M., Falcone, L., Camisa, B., Norelli, M., Porcellini, S., Stornaiuolo, A., Ciceri, F., Traversari, C., Bordignon, C., Bonini, C., & Bondanza, A. (2018). Extracellular NGFR spacers allow efficient tracking and enrichment of fully functional car-t cells co-expressing a suicide gene. *Frontiers in Immunology*, *9*(MAR). https://doi.org/10.3389/fimmu.2018.00507

14. De, A., Pohl, P., Schmidt, A., Zhang, A.-H., Maldonado, T., Königs, C., & Scott, D. W. (2020). Engineered regulatory T cells expressing myelin-specific chimeric antigen receptors suppress EAE progression. *Cellular*

Immunology, *358*, 104222. https://doi.org/10.1016/j.cellimm.2020.104222

15. Doglio, M., Ugolini, A., Bercher-Brayer, C., Camisa, B., Toma, C., Norata, R., Del Rosso, S., Greco, R., Ciceri, F., Sanvito, F., Casucci, M., Manfredi, A. A., & Bonini, C. (2024). Regulatory T cells expressing CD19-targeted chimeric antigen receptor restore homeostasis in Systemic Lupus Erythematosus. *Nature Communications*, *15*(1). https://doi.org/10.1038/s41467-024-46448-9

16. Domingues, R., Sant'Anna, R., da Fonseca, A. C. C., Robbs, B. K., Foguel, D., & Outeiro, T. F. (2022). Extracellular alpha-synuclein: Sensors, receptors, and responses. In *Neurobiology of Disease* (Vol. 168). Academic Press Inc. https://doi.org/10.1016/j.nbd.2022.105696

17. Düchs, M., Blazevic, D., Rechtsteiner, P., Kenny, C., Lamla, T., Low, S., Savistchenko, J., Neumann, M., Melki, R., Schönberger, T., Stierstorfer, B., Wyatt, D., Igney, F., & Ciossek, T. (2023). AAV-mediated expression of a new conformational anti-aggregated α-synuclein antibody prolongs survival in a genetic model of α-synucleinopathies. *Npj Parkinson's Disease*, *9*(1). https://doi.org/10.1038/s41531-023-00542-9

18. Eremenko, E., Taylor, Z. V, Khand, B., Zaccai, S., Porgador, A., & Monsonego, A. (2021). An optimized protocol for the retroviral transduction of mouse CD4 T cells. *STAR Protocols*, *2*, 100719. https://doi.org/10.1016/j.xpro.2021.100719

19. Fransson, M., Piras, E., Burman, J., Nilsson, B., Essand, M., Lu, B., Harris, R. A., Magnusson, P. U., Brittebo, E., & Loskog, A. S. (2012). *CAR/FoxP3-engineered T regulatory cells target the CNS and suppress EAE upon intranasal delivery*. https://doi.org/10.1186/1742-2094-9-112

20. Frikeche, J., David, M., Mouska, X., Treguer, D., Cui, Y., Rouquier, S., Lecorgne, E., Proics, E., Fall, P. B., Lafon, A., Lara, G., Menardi, A., Fenard, D., Abel, T., Gertner-Dardenne, J., de la Rosa, M., & Dumont, C. (2024). MOG-specific CAR Tregs: a novel approach to treat multiple sclerosis. *Journal of Neuroinflammation* , *21*(1). https://doi.org/10.1186/s12974-024-03262-w

21. Gerasimova, E., Beenen, A. C., Kachkin, D., Regensburger, M., Zundler, S., Blumenthal, D. B., Lutzny-Geier, G., Winner, B., & Prots, I. (2025). Novel co-culture model of T cells and midbrain organoids for investigating neurodegeneration in Parkinson's disease. *Npj Parkinson's Disease*, *11*(1). https://doi.org/10.1038/s41531-025-00882-8

22. Guilliams, T., El-Turk, F., Buell, A. K., O'Day, E. M., Aprile, F. A., Esbjörner, E. K., Vendruscolo, M., Cremades, N., Pardon, E., Wyns, L., Welland, M. E., Steyaert, J., Christodoulou, J., Dobson, C. M., & De Genst, E. (2013). Nanobodies raised against monomeric α-synuclein distinguish between fibrils at different maturation stages. *Journal of Molecular Biology*, *425*(14), 2397–2411. https://doi.org/10.1016/j.jmb.2013.01.040

23. Harms, A. S., Yang, Y.-T., & Gámez Tansey, M. (2023). *Central and peripheral innate and adaptive immunity in Parkinson's disease*. https://www.science.org

24. Hayes, M. T. (2019). Parkinson's Disease and Parkinsonism. In *American Journal of Medicine* (Vol. 132, Issue 7, pp. 802–807). Elsevier Inc. https://doi.org/10.1016/j.amjmed.2019.03.001

25. Henschel, P., Landwehr-Kenzel, S., Engels, N., Schienke, A., Kremer, J., Riet, T., Redel, N., Iordanidis, K., Saetzler, V., John, K., Heider, M., Hardtke-Wolenski, M., Wedemeyer, H., Jaeckel, E., & Noyan, F. (2023). Supraphysiological FOXP3 expression in human CAR-Tregs results in improved stability, efficacy, and safety of CAR-Treg products for clinical application. *Journal of Autoimmunity*, *138*. https://doi.org/10.1016/j.jaut.2023.103057

26. Huang, Y., Liu, Z., Cao, B. B., Qiu, Y. H., & Peng, Y. P. (2020). Treg Cells Attenuate Neuroinflammation and Protect Neurons in a Mouse Model of Parkinson's Disease. *Journal of Neuroimmune Pharmacology*, *15*(2), 224–237. https://doi.org/10.1007/s11481-019-09888-5

27. Jassin, M., Block, A., Désiront, L., Vrancken, L., Grégoire, C., Baron, F., Ehx, G., Nguyen, T. T., & Caers, J. (2025). From spheroids to organoids: next-generation models for CAR-T cell therapy research in solid tumors.

In *Frontiers in Immunology* (Vol. 16). Frontiers Media SA. https://doi.org/10.3389/fimmu.2025.1626369

28. Jiménez-Jiménez, F. J., Alonso-Navarro, H., García-Martín, E., Santos-García, D., Martínez-Valbuena, I., & Agúndez, J. A. G. (2023). Alpha-Synuclein in Peripheral Tissues as a Possible Marker for Neurological Diseases and Other Medical Conditions. In *Biomolecules* (Vol. 13, Issue 8). Multidisciplinary Digital Publishing Institute (MDPI). https://doi.org/10.3390/biom13081263

29. Jo, J., Xiao, Y., Sun, A. X., Cukuroglu, E., Tran, H. D., Göke, J., Tan, Z. Y., Saw, T. Y., Tan, C. P., Lokman, H., Lee, Y., Kim, D., Ko, H. S., Kim, S. O., Park, J. H., Cho, N. J., Hyde, T. M., Kleinman, J. E., Shin, J. H., … Ng, H. H. (2016). Midbrain-like Organoids from Human Pluripotent Stem Cells Contain Functional Dopaminergic and Neuromelanin-Producing Neurons. *Cell Stem Cell*, *19*(2), 248–257. https://doi.org/10.1016/j.stem.2016.07.005

30. Jordi Galiano-Landeira, Albert Torra, Miquel Vila, & Jordi Bové. (2020). CD8 T cell nigral infiltration precedes synucleinopathy in early stages of Parkinson's disease. In *Brain* (Vol. 143, Issue 12, pp. 3518–3521). Oxford University Press. https://doi.org/10.1093/brain/awaa390

31. Kalia, L. V., Kalia, S. K., McLean, P. J., Lozano, A. M., & Lang, A. E. (2013). α-synuclein oligomers and clinical implications for parkinson disease. *Annals of Neurology*, *73*(2), 155–169. https://doi.org/10.1002/ana.23746

32. Kaygisiz, K., & Synatschke, C. V. (2020). Materials promoting viral gene delivery. In *Biomaterials Science* (Vol. 8, Issue 22, pp. 6113–6156). Royal Society of Chemistry. https://doi.org/10.1039/d0bm01367f

33. Lee, J. K., Tran, T., & Tansey, M. G. (2009). Neuroinflammation in Parkinson's disease. In *Journal of Neuroimmune Pharmacology* (Vol. 4, Issue 4, pp. 419–429). https://doi.org/10.1007/s11481-009-9176-0

34. Li, W., Luo, Y., Xu, H., Ma, Q., & Yao, Q. (2021). Imbalance between T helper 1 and regulatory T cells plays a detrimental role in experimental

Parkinson's disease in mice. *Journal of International Medical Research*, *49*(4). https://doi.org/10.1177/0300060521998471

35. Lindestam Arlehamn, C. S., Dhanwani, R., Pham, J., Kuan, R., Frazier, A., Rezende Dutra, J., Phillips, E., Mallal, S., Roederer, M., Marder, K. S., Amara, A. W., Standaert, D. G., Goldman, J. G., Litvan, I., Peters, B., Sulzer, D., & Sette, A. (2020). α-Synuclein-specific T cell reactivity is associated with preclinical and early Parkinson's disease. *Nature Communications*, *11*(1). https://doi.org/10.1038/s41467-020-15626-w

36. Long, A. H., Haso, W. M., Shern, J. F., Wanhainen, K. M., Murgai, M., Ingaramo, M., Smith, J. P., Walker, A. J., Kohler, M. E., Venkateshwara, V. R., Kaplan, R. N., Patterson, G. H., Fry, T. J., Orentas, R. J., & Mackall, C. L. (2015). 4-1BB costimulation ameliorates T cell exhaustion induced by tonic signaling of chimeric antigen receptors. *Nature Medicine*, *21*(6), 581–590. https://doi.org/10.1038/nm.3838

37. Luo, Y., Qiao, L., Li, M., Wen, X., Zhang, W., & Li, X. (2024). Global, regional, national epidemiology and trends of Parkinson's disease from 1990 to 2021: findings from the Global Burden of Disease Study 2021. *Frontiers in Aging Neuroscience*, *16*. https://doi.org/10.3389/fnagi.2024.1498756

38. Markovic, M., Yeapuri, P., Namminga, K. L., Lu, Y., Saleh, M., Olson, K. E., Gendelman, H. E., & Mosley, R. L. (2022). Interleukin-2 expands neuroprotective regulatory T cells in Parkinson's disease. *NeuroImmune Pharmacology and Therapeutics*, *1*(1), 43–50. https://doi.org/10.1515/nipt-2022-0001

39. McGovern, J., Holler, A., Thomas, S., & Stauss, H. J. (2022). Forced Fox-P3 expression can improve the safety and antigen-specific function of engineered regulatory T cells. *Journal of Autoimmunity*, *132*. https://doi.org/10.1016/j.jaut.2022.102888

40. Moorman, C. D., Yu, S., Briseno, C. G., Phee, H., Sahoo, A., Ramrakhiani, A., & Chaudhry, A. (2023). CAR-T cells and CAR-Tregs targeting conventional type-1 dendritic cell suppress experimental autoimmune encephalomyelitis. *Frontiers in Immunology*, *14*. https://doi.org/10.3389/fimmu.2023.1235222

41. Morris, H. R., Spillantini, M. G., Sue, C. M., & Williams-Gray, C. H. (2024). The pathogenesis of Parkinson's disease. *The Lancet*, 293–304.

42. Norden, D. M., Trojanowski, P. J., Villanueva, E., Navarro, E., & Godbout, J. P. (2016). Sequential activation of microglia and astrocyte cytokine expression precedes increased iba-1 or GFAP immunoreactivity following systemic immune challenge. *GLIA*, *64*(2), 300–316. https://doi.org/10.1002/glia.22930

43. Olson, K. E., Mosley, R. L., & Gendelman, H. E. (2023). The potential for treg-enhancing therapies in nervous system pathologies. In *Clinical and Experimental Immunology* (Vol. 211, Issue 2, pp. 108–121). Oxford University Press. https://doi.org/10.1093/cei/uxac084

44. Park, S. Y., Yang, H. J., Kim, S., Yang, J., Go, H., & Bae, H. (2023). Alpha-Synuclein-Specific Regulatory T Cells Ameliorate Parkinson's Disease Progression in Mice. *International Journal of Molecular Sciences*, *24*(20). https://doi.org/10.3390/ijms242015237

45. Park, T. Y., Jeon, J., Lee, N., Kim, J., Song, B., Kim, J. H., Lee, S. K., Liu, D., Cha, Y., Kim, M., Leblanc, P., Herrington, T. M., Carter, B. S., Schweitzer, J. S., & Kim, K. S. (2023). Co-transplantation of autologous Treg cells in a cell therapy for Parkinson's disease. *Nature*, *619*(7970), 606–615. https://doi.org/10.1038/s41586-023-06300-4

46. Paxinos, George., & Franklin, K. B. J. . (2001). *The mouse brain in stereotaxic coordinates*. Academic Press.

47. Poewe, W., Seppi, K., Tanner, C. M., Halliday, G. M., Brundin, P., Volkmann, J., Schrag, A. E., & Lang, A. E. (2017). Parkinson disease. *Nature Reviews Disease Primers 2017 3:1*, *3*(1), 1–21. https://doi.org/10.1038/nrdp.2017.13

48. Reynolds, A. D., Banerjee, R., Liu, J., Gendelman, H. E., & Lee Mosley, R. (2007). Neuroprotective activities of CD4+CD25+ regulatory T cells in an animal model of Parkinson's disease. *Journal of Leukocyte Biology*, *82*(5), 1083–1094. https://doi.org/10.1189/jlb.0507296

49. Reynolds, A. D., Stone, D. K., Hutter, J. A. L., Benner, E. J., Mosley, R. L., & Gendelman, H. E. (2010). Regulatory T Cells Attenuate Th17 Cell-Mediated Nigrostriatal Dopaminergic Neurodegeneration in a Model of Parkinson's Disease. *The Journal of Immunology*, *184*(5), 2261–2271. https://doi.org/10.4049/jimmunol.0901852

50. Rietdijk, C. D., Perez-Pardo, P., Garssen, J., van Wezel, R. J. A., & Kraneveld, A. D. (2017). Exploring Braak's Hypothesis of Parkinson's Disease. *Frontiers in Neurology*, *8*(FEB), 37. https://doi.org/10.3389/FNEUR.2017.00037

51. Rocha, E. M., Keeney, M. T., Di Maio, R., De Miranda, B. R., & Greenamyre, J. T. (2022). LRRK2 and idiopathic Parkinson's disease. In *Trends in Neurosciences* (Vol. 45, Issue 3, pp. 224–236). Elsevier Ltd. https://doi.org/10.1016/j.tins.2021.12.002

52. Safarzadeh Kozani, P., Naseri, A., Mirarefin, S. M. J., Salem, F., Nikbakht, M., Evazi Bakhshi, S., & Safarzadeh Kozani, P. (2022). Nanobody-based CAR-T cells for cancer immunotherapy. In *Biomarker Research* (Vol. 10, Issue 1). BioMed Central Ltd. https://doi.org/10.1186/s40364-022-00371-7

53. Srinivasan, E., Chandrasekhar, G., Chandrasekar, P., Anbarasu, K., Vickram, A. S., Karunakaran, R., Rajasekaran, R., & Srikumar, P. S. (2021). Alpha-Synuclein Aggregation in Parkinson's Disease. *Frontiers in Medicine*, *8*. https://doi.org/10.3389/FMED.2021.736978/FULL

54. Su, D., Cui, Y., He, C., Yin, P., Bai, R., Zhu, J., Lam, J. S. T., Zhang, J., Yan, R., Zheng, X., Wu, J., Zhao, D., Wang, A., Zhou, M., & Feng, T. (2025). Projections for prevalence of Parkinson's disease and its driving factors in 195 countries and territories to 2050: modelling study of Global Burden of Disease Study 2021. *BMJ*, *388*. https://doi.org/10.1136/BMJ-2024-080952

55. Sulzer, D., Alcalay, R. N., Garretti, F., Cote, L., Kanter, E., Agin-Liebes, J., Liong, C., McMurtrey, C., Hildebrand, W. H., Mao, X., Dawson, V. L., Dawson, T. M., Oseroff, C., Pham, J., Sidney, J., Dillon, M. B., Carpenter, C., Weiskopf, D., Phillips, E., … Sette, A. (2017). T cells from patients

with Parkinson's disease recognize α-synuclein peptides. *Nature*, *546*(7660), 656–661. https://doi.org/10.1038/nature22815

56. Tanner, C. M., & Ostrem, J. L. (2024). Parkinson's Disease. *New England Journal of Medicine*, *391*(5), 442–452. https://doi.org/10.1056/NEJMra2401857

57. Tansey, M. G., Wallings, R. L., Houser, M. C., Herrick, M. K., Keating, C. E., & Joers, V. (2022). Inflammation and immune dysfunction in Parkinson disease. In *Nature Reviews Immunology* (Vol. 22, Issue 11, pp. 657–673). Nature Research. https://doi.org/10.1038/s41577-022-00684-6

58. Terkelsen, M. H., Klaestrup, I. H., Hvingelby, V., Lauritsen, J., Pavese, N., & Romero-Ramos, M. (2022). Neuroinflammation and Immune Changes in Prodromal Parkinson's Disease and Other Synucleinopathies. In *Journal of Parkinson's Disease* (Vol. 12, pp. S149–S163). IOS Press BV. https://doi.org/10.3233/JPD-223245

59. Thome, A. D., Atassi, F., Wang, J., Faridar, A., Zhao, W., Thonhoff, J. R., Beers, D. R., Lai, E. C., & Appel, S. H. (2021). Ex vivo expansion of dysfunctional regulatory T lymphocytes restores suppressive function in Parkinson's disease. *Npj Parkinson's Disease*, *7*(1). https://doi.org/10.1038/s41531-021-00188-5

60. Vega-Angeles, V. T., Morales-Ruiz, V., & Adalid-Peralta, L. V. (2024). Immunomodulation as a treatment for parkinson's disease in current trials: a systematic review and meta-analysis. *Revista de Investigacion Clinica; Organo Del Hospital de Enfermedades de La Nutricion*, *76*(3), 159–169. https://doi.org/10.24875/RIC.24000068

61. Vignali, D. A. A., Collison, L. W., & Workman, C. J. (2008). How regulatory T cells work. *Nature Reviews Immunology 2008 8:7*, *8*(7), 523–532. https://doi.org/10.1038/nri2343

62. Visanji, N. P., Brooks, P. L., Hazrati, L. N., & Lang, A. E. (2013). The prion hypothesis in Parkinson's disease: Braak to the future. *Acta Neuropathologica Communications*, *1*(1), 2. https://doi.org/10.1186/2051-5960-1-2

63. Wang, T., Sun, Y., & Dettmer, U. (2023). Astrocytes in Parkinson's Disease: From Role to Possible Intervention. *Cells*, *12*(19), 2336. https://doi.org/10.3390/CELLS12192336

64. Watanabe, H., Dijkstra, J. M., & Nagatsu, T. (2024). Parkinson's Disease: Cells Succumbing to Lifelong Dopamine-Related Oxidative Stress and Other Bioenergetic Challenges. In *International Journal of Molecular Sciences* (Vol. 25, Issue 4). Multidisciplinary Digital Publishing Institute (MDPI). https://doi.org/10.3390/ijms25042009

65. Whitlow, M., Bell, B. A., Feng, S.-L., Fupula, D., Hardman, K. D., Hubert, S. L., Rollence, M. L., Wood, J. F., Schott, M. E., Milenic, D. E., Yokota, T., & Schlom, J. (1993). An improved linker for single-chain Fv with reduced aggregation and enhanced proteolytic stability. In *Protein Engineering* (Vol. 6). https://academic.oup.com/peds/article/6/8/989/1559790

66. Williams, G. P., Schonhoff, A. M., Jurkuvenaite, A., Gallups, N. J., Standaert, D. G., & Harms, A. S. (2021). CD4 T cells mediate brain inflammation and neurodegeneration in a mouse model of Parkinson's disease. *Brain*, *144*(7), 2047–2059. https://doi.org/10.1093/brain/awab103

67. Wu, L., Wei, Q., Brzostek, J., & Gascoigne, N. R. J. (2020). Signaling from T cell receptors (TCRs) and chimeric antigen receptors (CARs) on T cells. In *Cellular and Molecular Immunology* (Vol. 17, Issue 6, pp. 600–612). Springer Nature. https://doi.org/10.1038/s41423-020-0470-3

68. Xiao, B., & Tan, E. K. (2025). Prasinezumab slows motor progression in Parkinsons disease: beyond the clinical data. *Npj Parkinson's Disease*, *11*(1). https://doi.org/10.1038/s41531-025-00886-4

69. Young, C. B., Reddy, V., & Sonne, J. (2023). *Neuroanatomy, Basal Ganglia*. StatPearls.

70. Zhang, W., Jiang, J., Xu, Z., Yan, H., Tang, B., Liu, C., Chen, C., & Meng, Q. (2023). Microglia-containing human brain organoids for the study of brain development and pathology. In *Molecular Psychiatry* (Vol. 28, Issue

1, pp. 96–107). Springer Nature. https://doi.org/10.1038/s41380-022-01892-1